IMPROVED RETRIEVAL OF WATER LEAVING REFLECTANCE AND CHLOROPHYLL IN COASTAL PRODUCTIVE WATERS

by

MARCO VARGAS

A dissertation submitted to the Graduate Faculty in Engineering in partial fulfillment of the requirements for the degree of Doctor of Philosophy

The City University of New York

2007

UMI Number: 3245087

ProQuest Information and Learning Company
300 North Zeeb Road
P.O. Box 1346
Ann Arbor, MI 48106-1346

This manuscript has been read and accepted for the
Graduate Faculty in Engineering in satisfaction of the
dissertation requirement for the degree of Doctor of Philosophy.

Barry Gross

Date — Chair of Examining Committee

Mumtaz K. Kassir

Date — Executive Officer

Samir Ahmed

Fred Moshary

Christopher Brown

Reza Khanbilvardi

Alex Gilerson
Supervisory Committee

THE CITY UNIVERSITY OF NEW YORK

Abstract

IMPROVED RETRIEVAL OF WATER LEAVING REFLECTANCE AND CHLOROPHYLL IN COASTAL PRODUCTIVE WATERS

by

Marco Vargas

Advisor: Professor Barry Gross

It is well known that retrieval of the water leaving signal in coastal waters is qualitatively different than the procedure for open oceans. In particular, the dark pixel assumptions in the typical NIR atmospheric correction channels do not apply due to high concentration of suspended solids and the water constituents no longer covary with CHL. Furthermore, the aerosol models used in the retrieval process must be modified to account for more relevant climatologies in coastal environments. In this thesis, we explore a variety of approaches in order to improve the retrieval of water leaving radiances and how these water leaving radiances can be used to extract biologically meaningful parameters such as CHL.

To my Parents

Acknowledgments

I want to express my most sincere gratitude and appreciation to my mentor Dr. Barry Gross for all his support, assistance, advice, patience, and time invested throughout my studies. I also extend my thanks to my committee members Drs. Fred Moshary, Samir Ahmed, Reza Khanbilvardi and Chris Brown for their guidance. Gratitude goes to all my colleagues at the Remote Sensing Laboratory of the City College of the City University of New York. Thanks to my parents and family members for their support and encouragement. Special thanks to my wife for her love, support and understanding during all these years. I would like to thank NOAA-CREST and NOAA/EPP/GSP for their support of my work and for the privilege of working with them. Many thanks to CICS/ESSIC/NOAA for providing me with a quiet, comfortable and convenient environment to finish this dissertation.

Table of Contents

List of Tables

Chapter 3

Chapter 4

Chapter 5

Chapter 6

List of Figures

Chapter 2

Chapter3

Chapter 4

Chapter 5

Chapter 6

Chapter 7

List of Acronyms

Acronym	Description
ADEOS	Advanced Earth Observation Satellite
AERONET	Aerosol Robotic Network
AOP	Apparent Optical Properties
CCNY	the City College of New York
CDOM	Chromophoric Dissolved Organic Matter
CHL	Chlorophyll
CICS	Cooperative Institute for Climate Studies
CMIS	Conical-Scanning Microwave Imager/Sounder
CREST	Cooperative Remote Sensing Science and Technology Center
CW	Coastal Water
CZCS	Coastal Zone Color Scanner
DLR	German Space Agency
EPP	Educational Partnership Program
ESSIC	Earth System Science Interdisciplinary Center
GOES	Geostationary Operational Environmental Satellites
GSP	Graduate Science Program
HES	Hyperspectral. Environmental Suite
HSI	Hyperspectral Imaging
IOCCG	International Ocean Colour Coordinating Group
IOP	Inherent Optical Properties

IR	Infra Red
LSQ	Least Squares
LUT	Look Up Table
MERIS	Medium Resolution Imaging Spectrometer
MODIS	Moderate Resolution Imaging Spectroradiometer
MSL12	Multi-Sensor Level-1 to Level-2 code
NASA	National Aeronautics and Space Administration
NASDA	National Space Development Agency of Japan
NEΔL	Noise Equivalent Delta Radiance
NEΔρ	Noise Equivalent Delta Reflectance
NESDIS	National Environmental Satellite, Data, & Information Service
NIR	Near Infrared
NOAA	National Oceanographic and Atmospheric Administration
NOMAD	the NASA bio-Optical Marine Algorithm Data set
NPOESS	National Polar-orbiting Operational Environmental Satellite System
NSMC	National Satellite Meteorological Center
OBPG	The Ocean Biology Processing Group
OCTS	Ocean Color and Temperature Sensor
OMI	Ozone Monitoring Instrument
ORA	Office of Research and Applications
SeaBAM	The SeaWiFS Bio-optical Algorithm Mini-Workshop
SEABASS	The SeaWIFS Bio-optical Archive and Storage System

SeaDAS	SeaWIFS data analysis system
SeaWIFS	Sea-viewing Wide Field-of-view Sensor
SHARM	Spherical Harmonics code
SNR	Signal to Noise Ratio
SPM	Suspended Particulate Material
SWIR	Short Wave Infra Red
TM	Thematic Mapper
TSS	Total Suspended Sediments
TOA	Top of the Atmosphere
VIIRS	Visible Infrared Imager Radiometer Suite
VIS	Visible
UV	Ultra Violet

Chapter 1 Introduction

Satellite ocean color sensors at the top of the atmosphere (TOA) measure the radiance or reflectance backscattered by the ocean-atmosphere system with the purpose of determining the water constituents of importance to oceanographers, biologists, habitat and resource specialists, coastal zone managers, environmental scientists, etc.

Monitoring the ecology and water quality of coastal zones and inland waters is a growing global concern. Coastal zones are an important part of the global oceanic environment for several reasons; a large percentage of global ocean primary productivity takes place in the coastal zone, due to increased nutrient availability either from terrestrial input (rivers) or from coastal upwelling systems. Estuarine areas provide nursery areas for larval fish and benthic fauna, and are important economically for seafood production, shipping, transportation, and recreation.

Satellite measurements in the visible and near infrared regions of the electromagnetic spectrum allow the determination of the oceanic chlorophyll-*a*, the principal photosynthetic pigment associated with oceanic plants. The presence of chlorophyll-*a* (and other pigments), in the water changes the color of the water, as seen from space usually from blue to green. Plankton are the most abundant life form in the world's oceans, both in terms of weight and of numbers. Phytoplankton are microscopic plants, while zooplankton are the microscopic animals that feed on the phytoplankton [1]. They are globally distributed, consist of thousands of species and make up about 25% of the total planetary vegetation [2]. Phytoplankton use photosynthesis to fix

inorganic carbon into organic forms of carbon such as carbohydrates. Phytoplankton produce chemical compounds that escape into the atmosphere and have a role in the formation of clouds. In growing they use carbon dioxide from the atmosphere that has been absorbed into the ocean, and when they die, some proportion of the plankton fall out of the upper layers of the ocean and become part of the seabed sediments, thus removing carbon from the system. Therefore, phytoplankton have a major role in the global carbon cycle. The preceding paragraph shows the importance of phytoplankton and why measuring them and their behavior is necessary. As noted above, phytoplankton are ubiquitous in the world's oceans, but the traditional ship-based methods of observation are unable to give a truly global view of the phytoplankton in the ocean. The data collected by satellite ocean color instruments provide scientists a synoptic view at the productivity and variability of the Earth's oceans and atmosphere on high-resolution temporal and spatial scales. Thus observations from space are the only means of obtaining a global view.

The connection between ocean color and the water constituents has been the topic of exploration both experimentally through extensive ship borne measurements and theoretically through radiative transfer modeling. This has led to a number of useful relationships or bio-optical models that connect the water leaving (Remote Sensing) reflectance to water components including CHL, suspended solids, colored dissolved organic matter etc. In chapter 2, these relationships are described and the fundamental definitions and phenomenon are discussed.

In chapter 3, we describe our experimental and numerical efforts to test a number of possible CHL retrieval schemes including simple band ratio algorithms in

the blue green used mostly for deep ocean water as well as NIR band ratio algorithms which are designed to avoid the problems associated with high CDOM absorption and particulate scattering. In particular, we confirm that the NIR two channel algorithms are superior to conventional blue-green algorithms and that they are more robust to atmospheric correction problems. Finally, we explored more complex multispectral algorithms in which several constituent parameters are retrieved simultaneously.

In Chapter 4, we briefly explored the information content in hyperspectral remote sensing measurements in comparison to traditional multispectral sensors such as MODIS and SeaWIFS. This comparison was motivated by NOAA's attempt to configure the most useful ocean observing instrument for the GOES-R Platform. Our analysis shows clearly that hyperspectral channels significantly improved the retrievals for water constituent parameters along with dramatic improvements for surface albedo and height. Unfortunately, since this study was concluded, the HES-CW instrument was decommissioned from GOES-R.

Finally, we also performed a consistency study to see how well the multicomponent bio-optical models can fit our in situ measurements and be used for the retrieval. In Chapter 3, we showed a LSQ multiparameter estimation approach should be superior to multiband methods in retrieving CHL concentrations, but we found in chapter 4 that for realistic field measurements, the systemic bias in the LSQ optimization resulted in poor retrieval of CHL and to the conclusion that the assumptions of the bio-optical model which assume a unique phytoplankton specific absorption is not suitable.

In the last 3 chapters, our work in atmospheric retrieval is presented and forms the core of our efforts. Successful remote sensing of water bodies relies on accurately separating the atmospheric contribution (path radiance) of the top of atmosphere signal from the water leaving radiance. Unfortunately, since the TOA signal is dominated by the atmospheric path radiance with the water leaving radiance comprising about 10% of the total radiance, a very accurate estimation of the atmosphere is needed. In particular, small errors in atmospheric correction can produce large errors in the retrieval of the water leaving radiance, leading to useless retrievals of chlorophyll concentration and other products.

The most successful ocean color observing system has been the SeaWIFS ocean color sensor due to the very good SNR and stable calibration. In analyzing the multiwavelength data on an operational global basis, an atmospheric correction scheme [3] was developed where the atmospheric contribution was estimated using TOA reflectances obtained from the SeaWIFS 765-865 (or MODIS 748-869) NIR channels where it is assumed that the water leaving radiance is negligible (black pixel approximation) due to the strong water absorption. This atmospheric correction algorithm works well in open ocean waters but, tends to over correct for the atmosphere in coastal waters because the black pixel assumption is no longer valid [4],[5]. During the atmospheric correction process the aerosol model is selected after evaluating the epsilon parameter which is defined as the ratio of the reflectance between the two NIR bands, and then, the aerosol contribution to the radiance is extrapolated to the visible bands. If the water leaving radiance is not negligible in the NIR bands which is a common condition of coastal turbid waters, the selected aerosol

model from the suite of aerosol models will be in error, and when these aerosol radiances are extrapolated to the visible bands and subtracted from the TOA reflectance, it can produce negative water leaving radiances [6],[7] which is commonly seen in the 412nm channel of the SeaDAS processed data.

To help overcome some of the problems associated with bright pixels, an attempt is made within the SeaDAS atmospheric correction algorithm scheme to estimate the water leaving radiance in the NIR through the use of regression relations between the VIS water leaving radiances and the NIR water leaving radiances [8],[9]. In this scheme, the dark pixel approximation is simply the first guess used to estimate the water leaving radiances in the VIS channels. From this estimate, a first correction to the NIR water leaving radiance can be obtained thereby allowing for an improved atmosphere estimation based on the NIR channels. This scheme may be continuously iterated in an attempt to further improve the retrieval. Unfortunately, these "closure" algorithms obviously depend on the quality of the regression relations which can significantly vary over diverse coastal waters.

In chapter 5, we showed that the traditional NIR iterative algorithms which use semi-empirical correction techniques to compensate for bright pixel contaminations would result in significant errors and these errors are greatly modified if the atmospheric aerosol is not contained within the database of aerosol models used in the atmospheric compensation algorithms.

For these reasons, we turned away from the NIR approaches and began a study of SWIR atmospheric corrections using the 1240-2130 channels of MODIS which may avoid these problems [10]. This approach is based on the fact that ocean

water absorbs strongly in this spectral region and the contributions of the in-water constituents are negligible and can safely be considered dark. However, the atmospheric reflectance at these long wavelengths was significantly weaker and spectral features due to absorbing aerosols or fine urban modes are particularly difficult to resolve at these longer wavelengths. Therefore, it was expected that the retrieval error for water leaving radiances in the VIS channels would be significantly larger in comparison to the conventional NIR channels given the pixels in the NIR were sufficiently dark.

However, we noted from our field measurements that in the productive waters of the Chesapeake Bay, where the 412nm water leaving reflectance is reduced through high CHL and CDOM absorption, the 412nm water leaving reflectance could be used as an additional atmospheric channel although the water leaving radiance would act as a noise source which would impose limits on the accuracy of the aerosol measurement.

In chapter 6, we explore the possibility of using the 412nm reflectance channel as a constraint for aerosol retrieval. While the 412 nm channel in turbid coastal waters can be a small component of the atmospheric signal and can help identify absorbing aerosols, the possibility of using the 412nm channel to help constrain the aerosol model has not been pursued for two main reasons. First, in situations where the pixels are sufficiently dark, the uncertainty in aerosol reflectance on the 412nm channel using the standard NIR algorithm is significantly smaller than the uncertainty of the water leaving signal. Second, in regions where the NIR pixels

are not dark, multiple false solutions could occur in the black pixel approximation when combining the VIS and NIR channel reflectances.

Recently, however, the use of the 412nm channel to help distinguish aerosol properties has been given some attention. For example, in reference [11], errors in the water reflectance due to absorbing aerosols can be compensated by comparing the initial retrievals based on conventional algorithms to a bio-optical model estimate based on remote sensing reflectance at higher wavelengths. If the measured water leaving reflectance after the conventional atmospheric correction is lower than the bio-optically estimated value, it may be assumed that the errors are due to an inherently absorbing aerosol feature and a correction based on in situ estimates of the correction factor can be applied. However, this technique was particularly suited for absorbing aerosols but fine mode aerosols with high epsilon (ε) parameter pose the reverse problem in which the atmospheric reflectance is underestimated leading to an overestimation of the water leaving reflectance. This dual problem cannot be solved using the correction scheme in [11]. It must further be emphasized that significant errors can occur in the bio-optical model estimator including errors in the CHL estimates and in the CDOM.

In another study [12], the 412 channel reflectance was assumed to be negligible. Using the 412 signal in combination with constraining the aerosol path reflectance spectral slope in the NIR bands (i.e., epsilon factor) $\frac{\rho_{aer}(\lambda = 765)}{\rho_{aer}(\lambda = 865)} \equiv \varepsilon(765,865) \approx 1$, an estimate of the NIR water leaving signals was obtained. Unfortunately, this study did not consider the error budget due to the non-

zero water leaving radiance or the sensitivity of the retrievals to the unphysical constraint $\varepsilon(765,865) \approx 1$.

Finally, it has recently been recognized that the aerosol models that are needed for coastal waters have greater variability than those used within the SeaDAS environment which are mainly oceanic in nature [13]. In particular, as mentioned above, there is a strong need to account for absorbing aerosols as well as fine non-absorbing urban aerosols such as those that can occur in the north east region of the US. The absorbing aerosols are characterized by a significant decrease in the aerosol reflectance in the short wavelength channels in contrast to the longer channels. This results in an effective absorbing epsilon factor which is less than the equivalent non-absorbing counterpart. $\varepsilon_{abs}(412,865) < \varepsilon_{non-abs}(412,865)$. In contrast, the urban fine-mode aerosols are distinguished by a significantly higher absorbing epsilon factor than the traditional large particle maritime modes. The result of these aerosol model categories is to significantly broaden the optical signatures of the aerosol reflectances used in the atmospheric LUT in the VIS bands relative to the NIR (and SWIR) bands thereby significantly increasing atmosphere reflectance retrieval error. In short, the inclusion of more realistic aerosol models which are needed in an urban coastal environment will result in an overall increase in uncertainty in the retrieval if additional constraints are not used.

Therefore, we were led to study and inter-compare in Chapter 6 the different approaches and soon found that for a more representative aerosol database which includes absorbing aerosols and small mode aerosols indicative of urban condition, the SWIR algorithm will give rise to unacceptable errors. On the other hand, we

realized that the water leaving reflectance at the 412 MODIS channel is nearly always small in the Chesapeake due to high CHL and CDOM absorption so that it looks like an effective dark pixel. In this case, we could use the 412nm aerosol channel to constrain (differentiate) the aerosols including absorbing aerosols.

This led us to a sensitivity study to determine the accuracy of the newly developed SWIR correction scheme which was designed to remove the bright pixel contamination which showed that significant retrieval errors in the blue wavelengths will occur if a more diverse atmospheric model set combining oceanic and local aerosol models are used. However, we found that the use of the 412nm sounding channel can significantly reduce retrieval errors for biologically productive waters such as the Chesapeake Bay in which the 412nm water leaving signal is significantly reduced through a combination of CDOM and CHL absorption providing a strong constraint on the aerosol models at 412nm. From our calculations, the tight constraints imposed make it possible for a more diverse and representative set of aerosol models based on global and local climatology to be incorporated.

Finally, in Chapter 7, we explored a different approach where absorbing aerosols were detected by use of a bio-optical estimator at 412nm. After testing the relative soundness of the approach using both measurement and synthetic data, we performed a sensitivity analysis comparing the approach to the simple threshold constraints we used and showed that no improvement will occur.

References Chapter 1

[1] Srokosz, M.A. Biological Oceanography by Remote Sensing. Encyclopedia of Analytical Chemistry. R.A. Meyers (Ed.) pp. 8506–8533, 2000

[2] Jeffrey, S. w., & Vesk,M. (1997). Introduction to marine phytoplankton and their pigment signatures. In Phytoplankton Pigments in Oceanography: Guidelines to Modem Methods, ed. S. W. Jeffrey, R. F. C. Mantoura & S. W. Wright, pp. 37-84. Paris: UNESCO Publishing.

[3] Gordon, H. R. and M. Wang, "Retrieval of water-leaving radiance and aerosol optical thickness over the oceans with SeaWiFS: A preliminary algorithm". Applied Optics, 33, 443–452. (1994)

[4] Darecki, M., and D. Stramski. "An evaluation of MODIS and SeaWiFS bio-optical algorithms in the Baltic Sea". Remote Sensing of Environment, 89, 326-350. (2004)

[5] K. G. Ruddick, F. Ovidio, and M. Rijkeboer, "Atmospheric Correction of SeaWiFS Imagery for Turbid Coastal and Inland Waters ," Appl. Opt. 39, 897-912 (2000)

[6] Lavender, S. J., Pinkerton, M. H., Moore, G. F., Aiken, J. & Blondeau-Patissier, D. "Modification to the atmospheric correction of SeaWiFS ocean colour images over turbid waters", Continental Shelf Research, 25, 539-555, 2005.

[7] Hu Chuanmin, Carder Kendall L, Muller Karger, Frank E. Atomospheric Correction of SeaWiFS Imagery over Turbid Coastal Waters: A practical method. Remote sensing of Environment, 74, 195-206. (2000)

[8] Stumpf, R. P., R. A. Arnone, R. W. Gould, P. M. Martinolich, and V. Ransibrahmanakul (2003), A Partially Coupled Ocean-Atmosphere Model for Retrieval of Water-Leaving Radiance From SeaWiFS in Coastal Waters, SeaWiFS Postlaunch Tech. Rep. Ser., vol. 22, NASA Tech. Memo. 2003-206892, edited by S. B. Hooker and E. R. Firestone, pp. 51– 59, NASA Goddard Space Flight Cent., Greenbelt, Md.

[9] D. A. Siegel, M. Wang, S. Maritorena, and W. Robinson, "Atmospheric Correction of Satellite Ocean Color Imagery: The Black Pixel Assumption ," Appl. Opt. 39, 3582-3591 (2000)

[10] M. Wang and W. Shi "Estimation of ocean contribution at the MODIS near-infrared wavelengths along the east coast of the U.S.: Two case studies" Geophys. Res. Lett, 32, L13606, doi:10.1029/2005GL022917, (2005)

[11] V. Ransibrahmanakul and R. P. Stumpf, 'Correcting ocean colour reflectance for absorbing aerosols", International Journal of Remote Sensing, 27, 1759 - 1774 , 2006

[12] HE Xianqiang, PAN Delu, MAO Zhihua "Atmospheric correction of SeaWiFS imagery for turbid coastal and inland waters" Acta Oceanologica Sinica,Vol. 23, No. 4, p.609-615, (2004)

[13] R. C. Levy, L. A. Remer, J. V. Martins, and Y. J. Kaufman," Evaluation of the MODIS Aerosol Retrievals over Ocean and Land during CLAMS", J. Atmos. Sci., 62**,** 974–992. (2005)

Chapter 2 Background

2.1 Definitions

Radiance $L(\theta,\phi,\lambda)$**:** radiant flux propagating toward or away from a surface in a specified direction within a solid angle direction. The radiance L has units of W m^{-2} sr^{-1}

Irradiance $E(\lambda)$: radiant flux per unit area that is incident on a unit surface area. The irradiance has units of W m^{-2}

Upwelling irradiance $E_u(\lambda)$: the upward directed radiant flux per unit area onto a downward facing horizontal surface.

Downwelling irradiance $E_d(\lambda)$: the downward directed radiant flux per unit area onto an upward facing horizontal surface.

Remote sensing reflectance $R_{RS}(\lambda)$: is defined as the ratio of the water leaving radiance $L_w(\lambda)$ to the downward irradiance measured just above the surface $E_d(\lambda,0_+)$

$$R_{RS}(\lambda)=\frac{L_w(\theta,\phi,\lambda)}{E_d(\lambda,0_+)} \tag{2.1}$$

The remote sensing reflectance specifies that portion of downward light incident on the water surface which is returned through the surface in the direction (θ,ϕ).

The water leaving radiance $L_w(\lambda)$: the water leaving radiance represents the light leaving the sea surface resulting from the absorption and scattering (by the water

itself and by in-water constituents such as phytoplankton) of light incident on the sea surface.

The diffuse attenuation coefficient (for downwelling irradiance) K_d: defines the rate of decrease of downwelling irradiance with depth. By definition,

$$\frac{dE_d(\lambda, z)}{E_d(\lambda, z)} = -K_d(\lambda)\, dz \tag{2.2}$$

The absorption coefficient $a(\lambda)$**:** is defined as the spectral absorptance per unit distance of photon travel in a dielectric medium.

The scattering coefficient $b(\lambda)$ **:** is defined as the spectral scatterance per unit distance of photon travel in a dielectric medium.

The spectral beam attenuation coefficient $c(\lambda)$**:** is defined as the sum of $a(\lambda)$ and $b(\lambda)$.

The volume scattering function $\beta(\theta, \lambda)$: is defined as the ratio of the scattered radiance to the incident irradiance per unit volume. Integrating $\beta(\theta, \lambda)$ over all directions gives the scattering coefficient. It can be expressed as:

$$b(\lambda) = 2\pi \int_0^{\pi} \beta(\theta, \lambda) \sin\theta \, d\theta \tag{2.3}$$

The forward spectral scattering coefficient $b_f(\lambda)$: relating to light scattered from the beam in a forward direction. It can be expressed as:

$$b_f(\lambda) = 2\pi \int_0^{\pi/2} \beta(\theta, \lambda) \sin\theta \, d\theta \tag{2.4}$$

The spectral back scattering coefficient $b_b(\lambda)$: relating to light scattered from the beam in a backward direction. It can be expressed as:

$$b_b(\lambda) = 2\pi \int_{\pi/2}^{\pi} \beta(\theta, \lambda) \sin\theta \, d\theta \tag{2.5}$$

The single scattering albedo $\omega_0(\lambda)$: defined as the ratio of the scattering coefficient to the beam attenuation coefficient $c(\lambda)$: $\omega_0(\lambda) \equiv \frac{b(\lambda)}{c(\lambda)}$ (2.6)

where $c(\lambda) = a(\lambda) + b(\lambda)$ (2.7)

2.2 Sensors useful for ocean color (past, present and future satellite missions)

The earliest of all ocean color satellite sensors was the Coastal Zone Color Scanner (CZCS), which was launched by NASA on the Nimbus-7 satellite in 1978 and operated until 1986. The next sensor launched was the Ocean Color and Temperature Sensor (OCTS). OCTS was launched by the National Space Development Agency of Japan (NASDA) on ADEOS (Advanced Earth Observation Satellite). OCTS was operational from August 1996 until June 1997. Early studies were performed using the MSS (Multispectral Scanner) and the TM (Thematic Mapper) sensors onboard the Landsat satellites although they were primarily designed for terrestrial applications. Other sensors used for oceanic research are the Chinese Fenyeng sensors. On 1988, 1990 and 1999 three polar orbiting meteorological satellites FY-1A, FY-1B and FY-1C, respectively, were successfully launched by the Chinese National Satellite Meteorological Center (NSMC). The Sea Viewing Wide Field of View Sensor (SeaWiFS) was launched by NASA in August 1997, shortly after the failure of ADEOS. Another sensor on the Indian IRS-P3 satellite is one

developed by DLR (German Space Agency), the Modular Optoelectronic Scanner (MOS). It was launched in March 1996. As a successor to OCTS, the GLI has flown on the ADEOS-2 satellite. Moderate-resolution imaging spectrometer (MODIS) is NASA's ocean color sensor. MODIS was launched on TERRA in December 1999 and on AQUA in May 2002. Medium-Resolution Imaging Spectrometer (MERIS) is the European Space Agency's first ocean color sensor. MERIS was launched on ENVISAT in March 2002. NPOES satellites will carry two new oceanographic instruments, the Conical-Scanning Microwave Imager/Sounder (CMIS) and the Visible/Infrared Imager/Radiometer Suite (VIIRS). The NPOESS satellites are scheduled to lunch in 2008 and 2009. The Hyperspectral Environmental Suite (HES) Coastal Water Imager (CW) on the new series of GOES-R satellites will have a spatial resolution of at least 300 m at nadir. The Spectral resolution will allow measurement of ocean color and chlorophyll, in-water optical properties, and atmospheric correction data. GOES-R is scheduled to launch in 2012.

2.3 Case I And Case II Waters

Case I waters are waters where the variation of the optical properties is due to the presence of phytoplankton and their by-products. Case II waters are waters where the variation of the optical properties is influenced by the presence of suspended sediments, dissolved organic matter and other particles that vary independently of phytoplankton [1]. In general, Case I waters are those of the open ocean, while Case II waters are those of the coastal zones. The estimation of water quality from Case II waters is much more complex, as the presence of the various particulates in the water,

in addition to the phytoplankton, affects the color signal measured by the satellite sensor.

2.4 Optical Properties Of Water

The optical properties of water can be divided into two categories: the first being those properties that depend on the medium, defined as inherent optical properties (IOPs). The second category is composed of those properties that depend on the medium and the directional structure of the light field. This second category is defined as the apparent optical properties (AOPs) [2].

2.4.1 Inherent Optical Properties (IOP)

Inherent Optical Properties (IOPs) depend on the type and the concentration of substance present in the water, and they do not depend on the ambient light field. There are two principal IOPs; the absorption coefficient and the volume scattering function. Other IOPs can be derived from the two principal IOPs, these include the single scattering albedo, the scattering coefficient, and the beam attenuation coefficient.

2.4.2 Apparent Optical Properties (AOP)

The apparent optical properties of water depend both on the aquatic medium (water, CDOM, phytoplankton, particulates) and on the surrounding ambient light field. Examples of the AOPs are the radiance, remote sensing reflectance and the diffuse attenuation coefficient.

2.5 Water constituents that influence the optical properties

Ocean water contains many different types of constituents and each of these interacts with the light in a different manner. In case I waters, it is mainly the phytoplankton and the pure water itself that affects the optical properties of attenuation and scattering of light. In coastal zones (case II) phytoplankton, pure water, chromophoric dissolved organic matter (CDOM) and particulate matter (TSS) interact with the light field. The total absorption coefficient $a(\lambda)$ is the sum of all the individual contributions by different water constituents:

$$a(\lambda) = a_w(\lambda) + a_{phyt}(\lambda) + a_{CDOM}(\lambda) + a_{TSS}(\lambda) \tag{2.8}$$

The total scattering coefficient is modeled as the sum of the scattering coefficients of pure sea water and particles: $b_b(\lambda) = b_w(\lambda) + b_p(\lambda)$ (2.9)

2.5.1 Properties Of Pure Sea Water

The spectral signature of pure seawater provides the baseline upon which the spectral characteristics of other types of water are built by the addition of other scatterers and absorbers. The absorption and backscattering of water are wavelength dependent as seen in figure 2.2

2.5.2 Absorption by pure water

The absorption coefficient of pure water has been measured accurately. The results of Pope and Fry [3] are shown in figure 2.2. It is this characteristic of pure water and pure sea water that makes shallow water bathymetry possible. In fact shallow bathymetry is restricted to the blue-green portion of the visible spectrum.

2.5.3 Absorption by phytoplankton

The absorption is mainly due to photosynthetic pigments, of which chlorophyll is known to be the strongest contributor. Chlorophyll is common to all photosynthetic plants, and it is a strong absorber in the blue and red regions of the spectrum and absorbs little in the green region as can be seen if figure 2.1.

The absorption of phytoplankton $a_{phyt}(\lambda)$ can be expressed as

$$a_{phyt}(\lambda) = a_{phyt}(440) \times a^{+}_{phyt}(\lambda) \qquad (2.10)$$

where $a^{+}_{phyt}(\lambda)$ is the $a_{phyt}(440)$ normalized spectral shape. For each CHL value, $a_{phyt}(440)$ is created [4],[5] with $a_{phyt}(440) = 0.05 \times [CHL]^{0.626}$ (2.11)

The parameters 0.05 and 0.626 vary from place to place.

2.5.4 Absorption by CDOM and particulates

Dissolved organic matter, often referred to as yellow matter, CDOM or gelbstoff is well understood. The absorption by CDOM follows an exponentially decreasing function with increasing wavelength.

$$a_{CDOM}(\lambda) = a_{CDOM}(\lambda_0) \exp(-S(\lambda_0 - \lambda)) \qquad (2.12)$$

where λ_0 is a reference wavelength and S is an empirically determined slope of the exponential curve. The scattering is high at short wavelengths and lower at long wavelengths (figure 2.1).

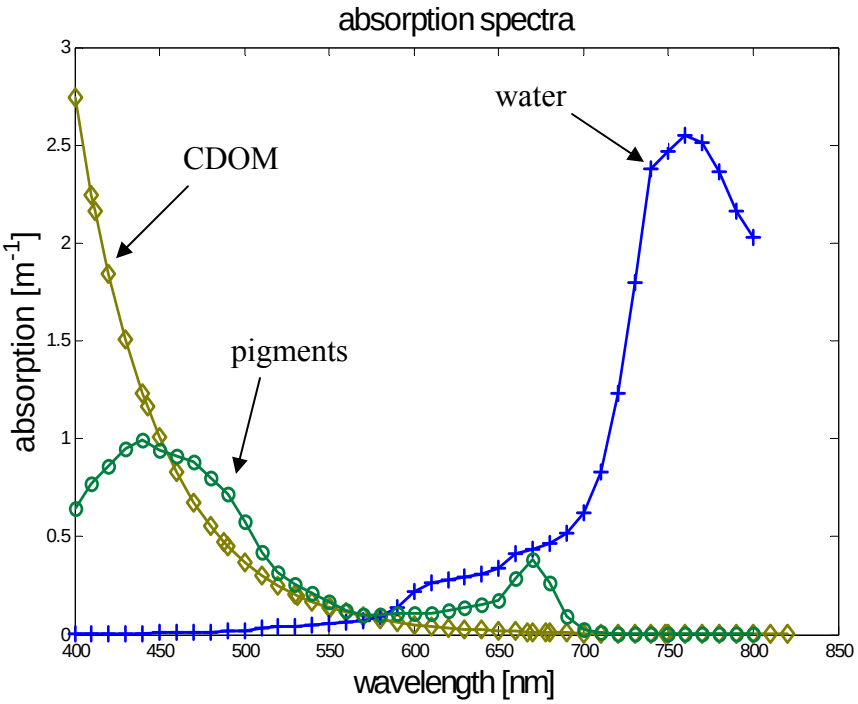

Figure 2.1. Typical absorption spectra from pure water, CDOM, and phytoplankton.

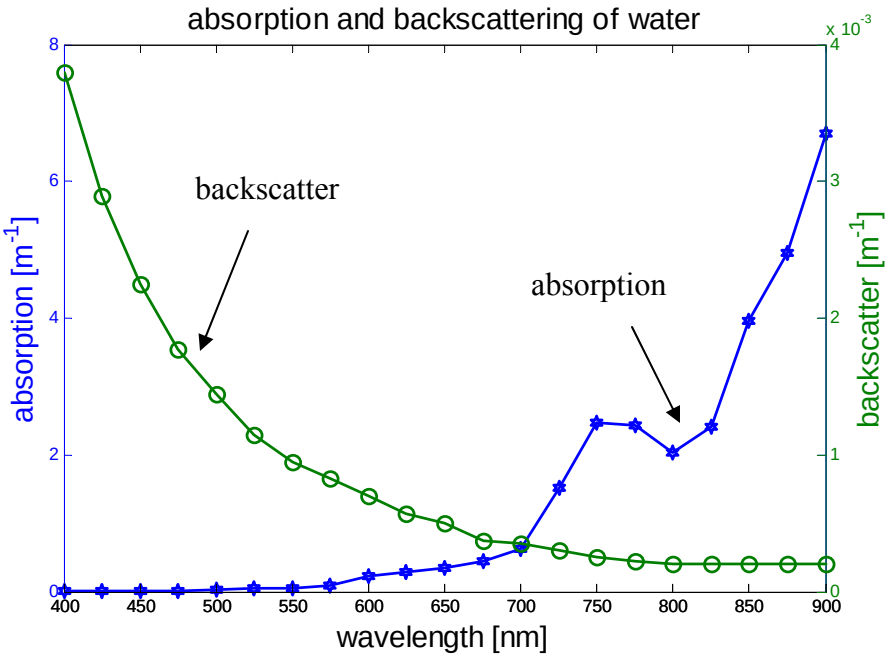

Figure 2.2 Typical absorption and backscatter of pure water

2.5.5 Scattering coefficient of pure sea water

The scattering coefficient of pure sea water is high in the blue and decreases with increasing wavelength, approximately as $\lambda^{-4.32}$ this can be seen if figure 2.2.

2.5.6 Backscattering of Water

Mobley [2] gives the volume scattering function, the phase function and the scattering coefficient of sea water as:

$$\beta(\alpha,\lambda) = 4.72\times10^{-4}\left(\frac{\lambda_0}{\lambda}\right)^{4.32}(1+0.835\cos^2\alpha) \quad m^{-1}Sr^{-1} \tag{2.13}$$

$$\widetilde{\beta}(\alpha) = 0.06225(1+0.835\cos^2\alpha) \quad Sr^{-1} \tag{2.14}$$

$$b(\lambda) = 16.06\left(\frac{\lambda_0}{\lambda}\right)^{4.32}\times4.72\times10^{-4} \quad m^{-1} \tag{2.15}$$

in the above $\lambda_0 = 400nm$

2.5.7 Backscattering of Particulates

The backscattering of particulates is often expressed in terms of chlorophyll as

$$b_{bp}(\lambda_{NIR}) = 0.416Chl^{0.766}\left(0.002+\frac{550}{\lambda_{NIR}}\right)\times\{0.02[0.5-0.25\log_{10}(Chl)]\} \tag{2.16}$$

2.6 Sources of Radiation Received by the Satellite

The radiance measured by the sensor in the visible part of the spectrum is largely dominated by the atmospheric path radiance. This radiance originates from photons scattered by air molecules and aerosols, which can also have been reflected at the sea surface, but have never penetrated the ocean. The atmospheric path radiance is

about 90% of the total radiance measured by the sensor at TOA[6]. The remaining 10% is the water leaving radiance which has to be properly extracted because from the accuracy of this extraction depends the quality of the end-product of ocean color data processing, *i.e.*, chlorophyll concentration. In Figure 2.3, we show the different pathways of light reaching the satellite sensor.

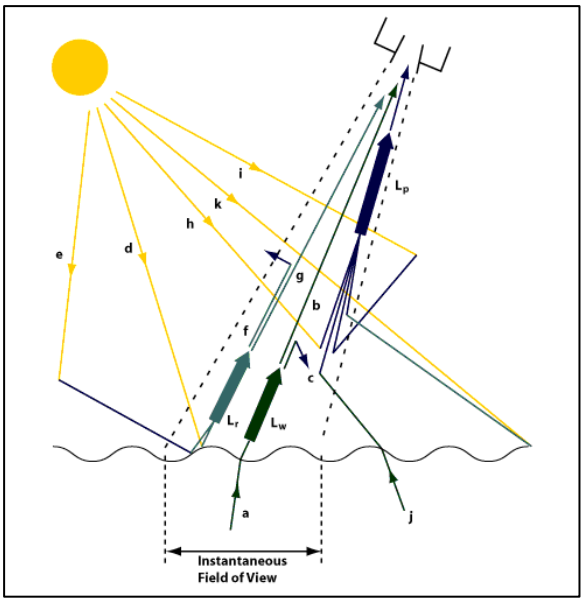

Figure 2.3. Optical pathways to sensor (from Robinson) [7]

a) Water-Leaving Radiance L_w

b) Portion of L_w reaching satellite

c) Portion of L_w scattered away

d) Sun Glint

e) Sky Glint

f) Portion of L_r scattered away

g) Portion of L_r reaching satellite

h) Single-scattered sun rays

i) Multi-scattered rays

j) Water-leaving radiance scattered into IFOV - not part of L_w

k) Surface Reflections scattered into IFOV - not part of L_r

$h + i + j + k =$ Atmospheric Path Radiance L_p

2.7 Effect of the Atmosphere

The retrieval of oceanic constituents is performed in two steps: atmospheric correction followed by a bio-optical algorithm to obtain the desired parameters. It is known that about 90% of the signal received by an ocean color sensor at the TOA originates from the atmosphere rather than the ocean. In the presence of clouds no signal from the sea surface is obtained at all. Therefore, the effect of the atmosphere has to be stripped off from the signal received by the sensor to obtain accurate measurements of the water-leaving radiance $L_w(\lambda)$.

The signal received by the satellite sensor may be written as [8]

$$L_T(\lambda) = L_R(\lambda) + L_A(\lambda) + L_{RA}(\lambda) + t(\lambda)L_G(\lambda) + t_D(\lambda)L_{wc}(\lambda) + t_D(\lambda)L_w(\lambda) \qquad (2.17)$$

where $L_R(\lambda)$ is the scattering of the photons due to air molecules (Rayleigh scattering), $L_A(\lambda)$ is the scattering due to atmospheric aerosols, $L_{RA}(\lambda)$ represents interactions between the two previous effects, $L_G(\lambda)$ is the sunglint contribution, $L_{wc}(\lambda)$ is the whitecap contribution , and $L_w(\lambda)$ is the desired water-leaving radiance. t and t_D are the direct and diffuse transmittance of the atmosphere that is

the effects of the atmosphere on the signal from the sea surface. In all of the following, we will ignore glint and foam effects.

2.8 Atmospheric Correction

The standard atmospheric correction algorithms are based on 'the black pixel assumption' [9],[10],[11]. These algorithms were primarily designed for clear deep ocean areas. The information about atmospheric aerosols is derived from channels in the red and near-infrared (above 740nm), where the water leaving radiance is close to zero. Using appropriate look up tables constructed for different atmospheric models and for different illumination geometries, it is possible using channels above 740nm to estimate the aerosol models. For example, in the MODIS algorithm, the aerosol model is determined by matching a database of aerosol properties to the TOA 748 and 869nm channels. From this model, the derived aerosol information is extrapolated towards the visible channels and the atmospheric contribution is calculated and removed. One of the chief benefits of using NIR algorithms is to minimize the extrapolation effects. Unfortunately, for the turbid coastal environment, the ocean can no longer assumed to be black in the red and near-infrared because of strong back scattering by suspended materials. Under these conditions, 'the black pixel assumption' is no longer valid [12],[13] for deriving information on atmospheric aerosols since the TOA signals can no longer be completely attributed to the aerosol component. As a result, the algorithms developed for applications to clear ocean waters cannot be easily modified to retrieve water leaving radiance from remote sensing data acquired over the coastal environments. Besides, even in the open ocean,

the commonly used algorithms for atmospheric correction fail in the presence of strongly-absorbing aerosols [14].

If the aerosol is strongly absorbing, due to soot or dust component, the visible reflectance can not be derived from the NIR reflectance [15]. The size distribution of strongly absorbing aerosols can be similar to that of the weakly absorbing aerosols typically present over ocean. Since the spectral variation of aerosol scattering depends mostly on the aerosol size distribution and only weakly on the refractive index, the spectral variation of scattering in the NIR is not sufficient to distinguish between weakly and strongly absorbing aerosols.

References Chapter 2

[1] Morel, A., & Prieur, L. (1977). Analysis of variations in ocean color. Limnol. Oceanogr.,22, 709-722.

[2] Mobley C. D., "Light and Water: Radiative Transfer in Natural Waters", Academic Press, New York, 1994

[3] Pope, R. M. and Fry, E. S. (1997). Absorption spectrum (380 - 700 nm) of pure water: II. Integrating cavity measurements. Appl. Optics 36**:** 8710-8723

[4] Bricaud, A., Babin, M., Morel, A., and Claustre, H. (1995). Variability in the chlorophyll-specific absorption coefficients of natural phytoplankton: Analysis and parameterization. J. Geophys. Res. 100: 13321-13332.

[5] Fischer, J., and Fell, F. (1999). Simulation of MERIS measurements above selected ocean waters. Int. J. Remote Sensing 20: 1787-1807.

[6] Wang, M., A sensitivity study of the SeaWiFS atmospheric correction algorithm: Effects of spectral band variations, Remote Sens. Environ., 67, 348– 359, 1999.

[7] Robinson, I. S. (1985). Satellite Oceanography. Chichester, UK: Ellis Horwood.

[8] Wang, M., 2002, The Rayleigh lookup tables for the SeaWiFS data processing: Accounting for the effects of ocean surface roughness. International Journal Remote Sensing, 23, 2693–2702.

[9] Gordon, H. R., & Clark, D. K. (1981). Clear water radiances for atmospheric correction of coastal zone color scanner imagery. Appl. Opt., 20, 4175-4180.

[10] Gordon, H. R. and M. Wang. ,"Retrieval of water-leaving radiance and aerosol optical thickness over the oceans with SeaWiFS: A preliminary algorithm". Applied Optics, 33, 443–452. (1994)

[11] Siegel, D. A., Wang, M., Maritorena, S., & Robinson, W. (2000). Atmospheric correction of satellite ocean color imagery: the black pixel assumption. Appl. Opt., 39, 3582-3591.

[12] Chomko, R. and Gordon, H. R. (1998). Atmospheric correction of ocean color imagery: use of the Junge power-law aerosol size distribution with variable refractive index to handle aerosol absorption. Appl. Optics **37:** 5560-5572.

[13] Li, L., H. Fukushima, R. Frouin, B. G. Mitchell, M.-X. He, I. Uno, T. Takamura, and S. Ohta, Influence of submicron absorptive aerosol on Sea-viewing Wide Field-of-view Sensor (SeaWiFS)-derived marine reflectance during Aerosol Characterization Experiment (ACE)-Asia, J. Geophys. Res., 108(D15), 4472, doi:10.1029/2002JD002776, 2003.

[14] Fukushima, H., and M. Toratani (1997), Asian dust aerosol: Optical effect on satellite ocean color signal and a scheme of its correction, J. Geophys. Res., 102(D14), 17,119–17,130.

[15] V. Ransibrahmanakul and R. P. Stumpf, ‘Correcting ocean colour reflectance for absorbing aerosols”, International Journal of Remote Sensing , 27, 1759 - 1774 , 2006

Chapter 3 Ocean Color Algorithms

3.1 Bio-Optical Algorithms

Bio-optical algorithms are needed to extract the pigment concentration information from ocean color measurements. Water constituents are estimated based on the water leaving radiance; these algorithms related to biological oceanographic properties are referred to as bio-optical algorithms. Algorithms for retrieval of water constituents from water reflectance can be divided into two main groups. The first group is referred to as empirical algorithms. They are based on the empirical correlation between radiance or reflectance band ratios and water constituent concentrations. These ratio algorithms for determining the phytoplankton pigment concentration have proved useful in global mapping of the ocean phytoplankton pigments[1]. These simple empirical algorithms are not reliable for Case 2 coastal waters. In such cases the second group, called semi-analytical algorithms, is used [2]. Semi-analytical algorithms use a reflectance model as well as a spectral model of the inherent optical properties (IOPs). The IOPs of water constituents are derived from inversion of the reflectance model which can be performed either by direct solution of reflectance model equations or by minimization of the spectral difference between measured and modeled reflectance spectra [3],[4].

3.2 Ratio Algorithms (empirical algorithms)

The conventional algorithms for the retrieval of the sea water constituents such as the chlorophyll concentration are usually based on the ratio of radiance or reflectance measured in the blue and green spectral bands [5]. A polynomial is

usually used to represent the relation between the logarithm of the band ratios and the logarithm of chlorophyll concentration. The coefficients of the polynomial are found by regression between the band ratios and the sea-truth value of chlorophyll concentration measured from water samples taken at various places [6]. This method based on band ratios works reasonably well in open ocean waters (case I waters), where chlorophyll and covarying substances such as detritus determine the optical properties [7]. Examples of these algorithms taken from various sources are given in the table number 3.1.

3.3 Semi-analytic algorithms

Semi-analytic algorithms use analytical, optical, remote sensing reflectance models (Rrs) that can be inverted to derive chlorophyll, absorption coefficients of other optically active components in the water, such as gelbstoff, or backscattering coefficient (b_b). Empiricism is involved in the parameterization of several terms used in these models. The mixture of theory and empiricism is the reason the term semi-analytic has been applied [1] to describe such algorithms.

3.4 Optimization algorithms

Optimization methods make use of models of the remote sensing reflectance that are applied to data from satellite or field measurements. The remote sensing reflectance is compared with the spectrum from measurements. The difference between the two spectral curves is minimized by adjusting the model values in a predictor–corrector scheme; no information in addition to the measured reflectance is

required. When the difference reaches a minimum, or the set of variables is optimized, absorption coefficients along with other properties are derived simultaneously [3],[8],[9].

Algorithm	General Form
SeaWIFS OC4-v4 [5]	$[Chl-a]=10^{(a+bR+cR^2+dR^3+eR^4)}$ R is the $\log_{10}$ of the maximum band ratio: $R=\log_{10}\{\max[R_{rs}(443)/R_{rs}(555), R_{rs}(490)/R_{rs}(555), R_{rs}(510)/R_{rs}(555)]\}$ The coefficients are determined by linear regression A=0.366; b=-3.067; c=1.930; d=0.649; e=-1.532
Terra-MODIS Chlor_MODIS (MOD-19, parameter 14) Chlorophyll-a concentration For case I waters [10]	$\log_{10}[Chl-a]=a\left[\log\left(\frac{R_{rs}(443)}{R_{rs}(551)}\right)^3\right]+b\left[\log\left(\frac{R_{rs}(443)}{R_{rs}(551)}\right)^2\right]+c\left[\log\left(\frac{R_{rs}(443)}{R_{rs}(551)}\right)\right]+d$ The coefficients are: a=-1.594; b=1.122; c=-1.396; d=-0.0922
Terra MODIS OC3 Chl_a_2 (MOD-21, parameter 26) Chlorophyll-a concentration For case II waters [11]	$\log_{10}[Chl-a]=0.283-2.753R+1.457R^2+0.659R^3-1.403R^4$ R is the $\log_{10}$ of the maximum band ratio: $R=\log_{10}\{\max[R_{rs}(443)/R_{rs}(551), R_{rs}(488)/R_{rs}(551)]\}$
Terra MODIS OC3 Chl_a_3 (MOD-21, parameter 27) Chlorophyll-a concentration For case II waters [11]	For default cases, the Chl-a concentration was calculated from Empirical algorithms: $chlor\_a\_3=10^{(0.289-3.20R+1.2R^2)}$ where $R=\log_{10}\frac{R_{rs}(488)}{R_{rs}(551)}$

Table 3.1. Description of ratio algorithms (SeaWIFS and MODIS)

3.5 Relationship Between Reflectance and Chlorophyll in Case I waters.

Figure 3.1 shows the reflectance as a function of wavelength and Chlorophyll concentration and forms the basis of the prevalent ocean color algorithms for case I waters.

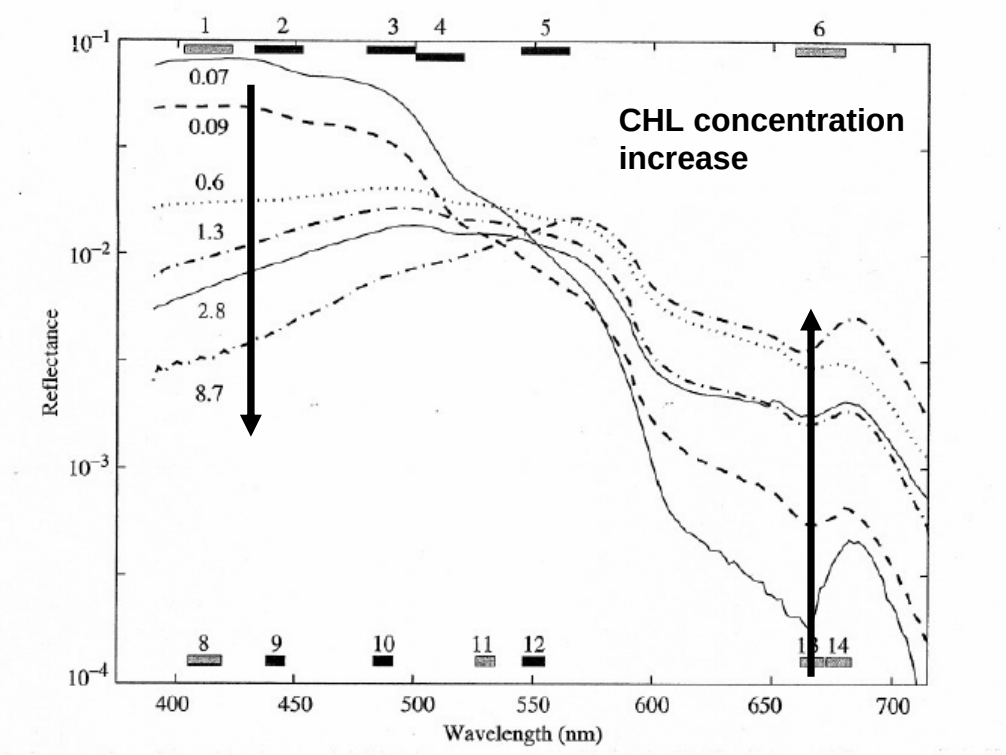

Figure 3.1 Reflectance as a function of wavelength for different chlorophyll concentrations.

We note the dependence of reflectance on wavelength since chlorophyll has a strong absorption peak in the blue and a lesser one in the red. The Reflectance of blue light (about 400 nm) decreases with concentration, also, the reflectance of yellow light (500-600 nm) increases with chlorophyll concentration, and is a more sensitive indicator of high concentrations and finally, the reflectance near 550 nm is relatively insensitive to chlorophyll concentration; this is the so-called hinge point. These observations suggest that measurements of a ratio of reflectance in one band to that in

another band near the hinge-point can be used to measure chlorophyll concentration. The reason for doing this rather than using raw radiances is that the radiance will vary with incoming solar radiation, but the reflectance ratio will be a function of only the chlorophyll concentration. Although the absolute reflectance values differ greatly with different chlorophyll species, the spectral shape and its variation with chlorophyll concentration remains similar. Therefore, a chlorophyll algorithm to interpret visible-wavelength radiance measurements from space should be based on spectral ratios, not the actual magnitude. To test the Blue-Green ratio algorithm (empirical algorithms) in Case I waters we determine the chlorophyll concentration using regression of coincident reflectance ratios and in situ measurements of chlorophyll in the Peconic Bay, NY (2002). Figure 3.2 shows the remote sensing spectra and figure 3.3 shows the regression retrieval.

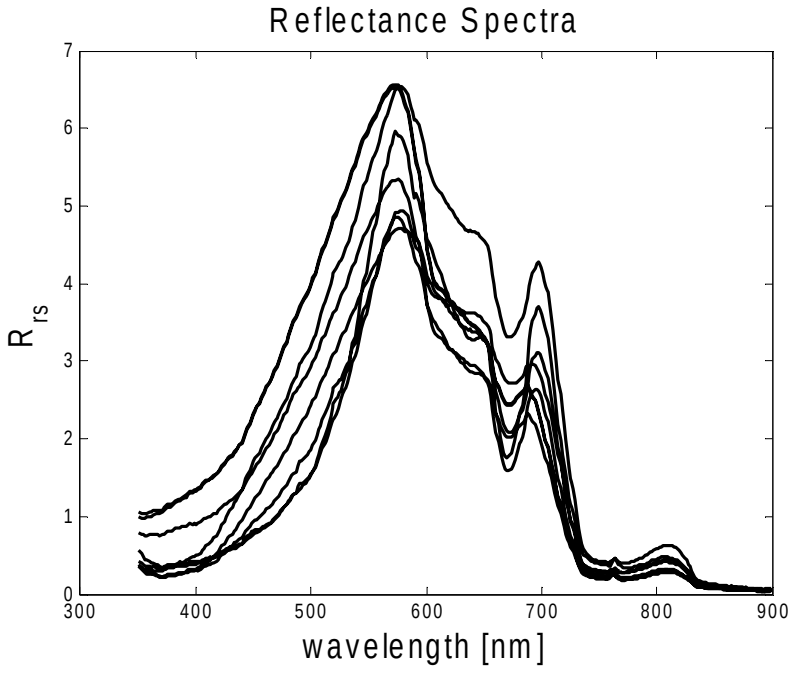

Figure 3.2 Remote sensing reflectance (Case I)

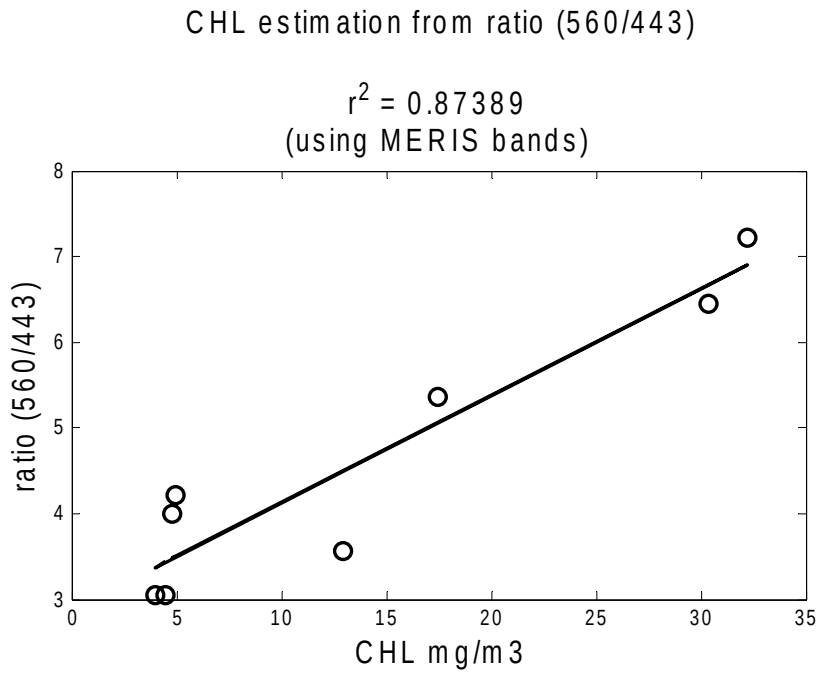

Figure 3.3 CHL retrieval using Blue-Green ratios (Case I waters)

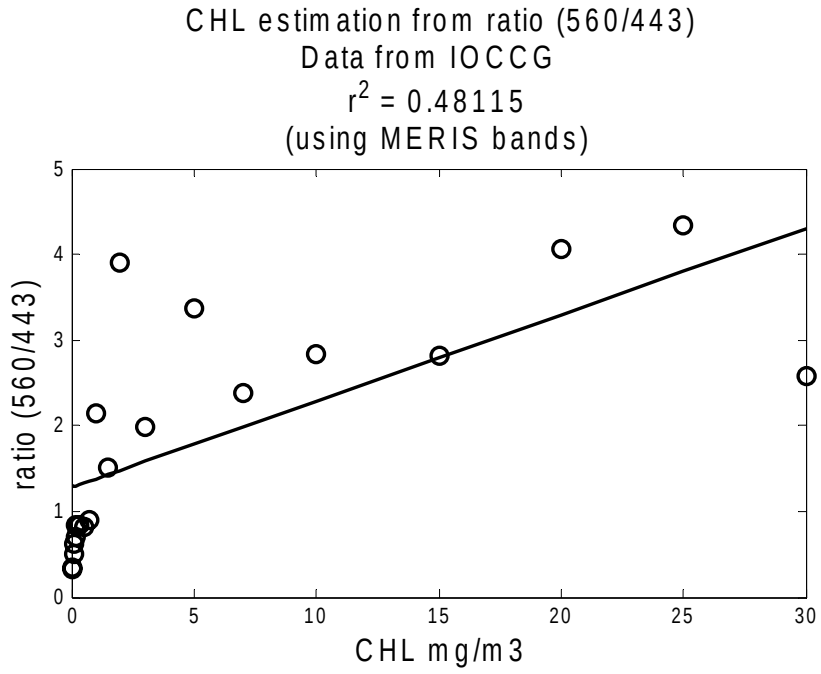

Figure 3.4 CHL retrieval using Blue-Green ratios (Case II waters from IOCCG web archive)

It is clear that over a limited sampling region, the blue green ratio performed adequately but it must be emphasized that the “slope” of the regression curves may vary significantly over different regions.

The simple band ratio algorithms do not work well for Case II waters that contain large amounts of suspended sediments and CDOM. As an example figure 3.4 shows a scatter plot of CHL predictor versus reflectance ratios over the web based archive of the IOCCG [12].

From above it is clear that unlike case I waters, case II waters are more complex and besides the organic algae signifying productive waters, case II waters also contain inorganic particulates (TSS) as well as dissolved organic matter (CDOM) making quantification of Chlorophyll (CHL) concentrations much more complex. It is therefore clear that ocean algorithms utilizing the blue-green band ratios can not be used in turbid waters. Chlorophyll in deep turbid waters can be related to band ratios in the red / NIR portion of the spectrum.

3.6 Optical properties of Case II Waters

The optical properties of turbid ocean waters (case II waters) are due to a mix of phytoplankton, total suspended sediments (TSS), and chromophoric dissolved organic matter (CDOM) which can vary independently from each other. In Case II sediment dominated waters, conventional atmospheric correction fails because the assumption of zero water leaving radiance in the near infrared is invalid [13],[14].
In turbid Case II waters, the magnitude of the reflectance in the near infrared (NIR) is controlled by the backscatter from suspended particulate material (SPM) and by the

absorption of water. CDOM absorbs strongly in the blue and UV, and follows an exponential decrease with increasing wavelength. When high concentrations of CDOM are present, two band ratio algorithms yield abnormally high chlorophyll values, because the absorption of co-existing CDOM can not be distinguished and separated from chlorophyll. However, the spectral signature of CDOM is different from that of chlorophyll. Chlorophyll absorbs strongly at 443nm and the covarying carotenoids at 490 and 510 nm, whereas CDOM displays an exponential decrease in absorption with wavelength. Thus the extent of the anomalous over-estimate diminishes for the 490nm and 510nm, two band ratio algorithms. In waters with low CDOM, estimates of chlorophyll based absorption at these three wavelengths will be broadly similar; a test which examines the discrepancy of chlorophyll estimation will indicate high CDOM concentrations. By definition the scattering in Case II waters results from chlorophyll, detritus and particles. This scattering is in proportion of the chlorophyll concentration [1], although not directly attributable to the phytoplankton. Waters that exhibit high scattering are called Case II waters.

3.7 RED-NIR Ratio Algorithms for Case II Waters

Case II waters are characterized by high concentrations of chlorophyll, CDOM, and suspended matter. The scattering and absorption characteristics are now determined not only by chlorophyll, but also by CDOM and non-chlorophyllous suspended matter [6]. Coastal sea waters are typically case II waters. The simple blue-green band ratio algorithms do not work well for this category of waters. Empirical algorithms for Case II can be improved by using NIR wavebands instead of

the blue and green bands used in Case I waters. This decreases the influence of TSS and CDOM on the algorithms. The remote-sensing reflectance $R_{RS}(\lambda)$ can be expressed in terms of the inherent optical properties, total absorption (a) and backscattering (b_b) coefficients as $R_{RS}(\lambda) \propto \frac{f}{Q} \times \frac{b_b(\lambda)}{a(\lambda)+b_b(\lambda)}$ (3.1)

where the $\frac{f}{Q}$ ratio describes the dependence of $R_{RS}(\lambda)$ on the geometry of the light field emerging from the water body. Following the approach of Dall'Olmo and Gitelson [15], we can select a set of wavelengths to remove the CDOM and TSS backscatter effects from the remote sensing reflectance. The retrieval algorithm uses a set of close wavelengths within the second absorption band of chlorophyll in the near infrared (NIR). The algorithm to extract the Chlorophyll-a absorption spectrum is

$$a_{Chla}(\lambda_1) \propto [R_{RS}^{-1}(\lambda_1) - R_{RS}^{-1}(\lambda_2)] \times R_{RS}(\lambda_3) \quad (3.2)$$

Thus by selecting three appropriate spectral regions λ_1, λ_2 and λ_3 it is possible to determine the chlorophyll-a absorption coefficient at λ_1 from R_{RS}. We can always relate the concentration of chlorophyll-a to the absorption of chlorophyll.

3.7.1 Theoretical Basis For Three Band Ratio Algorithm (NIR-RED)

To understand the three-band algorithm structure we first assume that the $\frac{f}{Q}$ ratio is spectrally invariant in the range 650-750nm, and that the total backscattering coefficient $b_b(\lambda)$ is invariant in the same spectral range. Furthermore, to avoid the overlapping absorption by CDOM, particulates and phytoplankton in the blue-green,

we use the red absorption maximum about 675nm. Under these assumptions, we can write the reciprocal reflectance of $R_{RS}(\lambda)$

$$R_{RS}^{-1}(\lambda_1) \propto \frac{Q}{f}\frac{a_{Chl}(\lambda_1)+a_{TD}(\lambda_1)+a_w(\lambda_1)+b_b}{b_b} \tag{3.3}$$

where $a_{Chl}(\lambda_1)$ is the chlorophyll absorption coefficient, $a_{TD}(\lambda_1)$ is the combined absorption of tripton (non-algal particulates) and CDOM, and $a_w(\lambda_1)$ is the absorption of water. To sum up so far, we have selected λ_1 so that $R_{RS}(\lambda_1)$ is maximally sensitive to a_{Chl} i.e., $660 \le \lambda_1 \le 690nm$.

At this stage, we want to isolate $a_{Chl}(\lambda_1)$ from equation (2) by minimizing the effects of b_b and $a_{TD}(\lambda_1)$, using $R_{RS}(\lambda)$ at two wavelengths different than λ_1. To remove b_b and $a_{TD}(\lambda_1)$ from equation (3.3) we need a second spectral region λ_2 such that $a_{TD}(\lambda_1) \approx a_{TD}(\lambda_2)$ and $a_{Chl}(\lambda_1) >> a_{Chl}(\lambda_2)$. These conditions force λ_2 to be chosen beyond 700nm. Once chosen, subtracting $R_{RS}(\lambda_2)$ from $R_{RS}(\lambda_1)$ gives

$$R_{RS}^{-1}(\lambda_1) - R_{RS}^{-1}(\lambda_2) \propto \frac{Q}{f}\frac{a_{Chl}(\lambda_1)+a_w(\lambda_1)-a_w(\lambda_2)}{b_b} \tag{3.4}$$

Finally, to remove b_b and $\frac{Q}{f}$ from (3.4) we select a third spectral region λ_3 where $a_{Chl}(\lambda_3)+a_{TD}(\lambda_3) \approx 0$ and thus $a(\lambda_3) \approx a_w(\lambda_3) \approx$ constant (under our assumptions). λ_3 can be found in the NIR (i.e., $\lambda_3 > 730nm$). In the NIR $a >> b_b$; thus the reflectance in this region can be approximated as:

$$R_{RS}^{-1}(\lambda_3) \propto \frac{Q}{f} b_b \tag{3.5}$$

multiplying equations (3.4) and (3.5) we obtain the desired form for CHL absorption as:

$$a_{Chl}(\lambda_1) \propto [R_{RS}{}^{-1}(\lambda_1) - R_{RS}{}^{-1}(\lambda_2)] \times R_{RS}(\lambda_3) \quad (3.6)$$

Thus by selecting three appropriate spectral regions λ_1, λ_2 and λ_3 it is possible to determine the chlorophyll-a absorption coefficient at λ_1 from R_{RS}. We can then use Beer's law to relate chlorophyll-a with the function $[R_{RS}^{-1}(\lambda_1) - R_{RS}^{-1}(\lambda_2)] \times R_{RS}(\lambda_3)$.

3.7.2 Synthetic And Field Tests For Three Band Ratio Algorithm (NIR-RED)

To see the usefulness of NIR algorithms, we determine the chlorophyll-a concentration using regression between equation (3.2) and synthetically generated remote sensing reflectance spectra determined from a representative coastal bio-optical model [16]. Figure 3.5 shows the remote sensing spectra and figures 3.6, 3.7 and 3.8 show the retrievals.

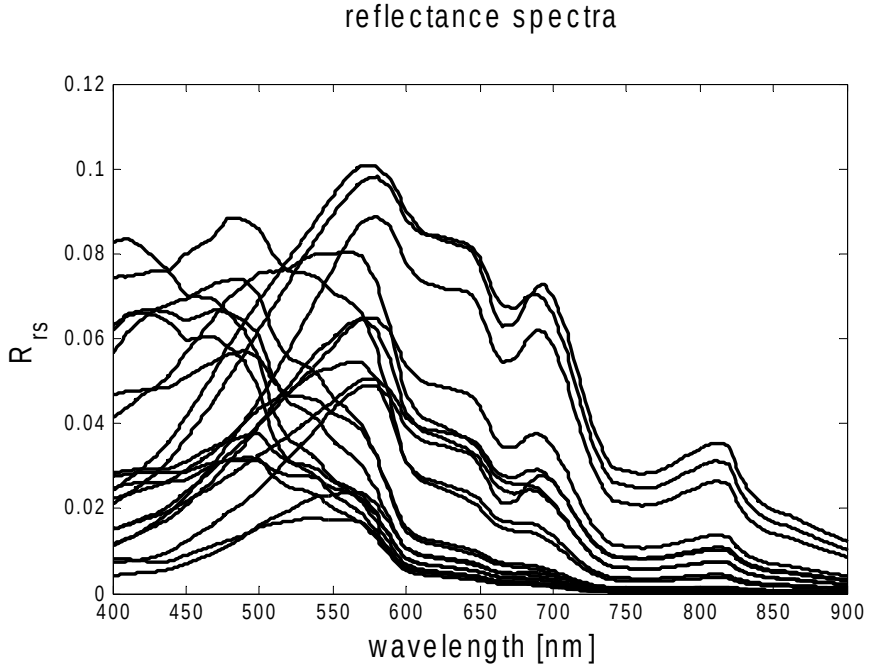

Figure 3.5 Reflectance Case II

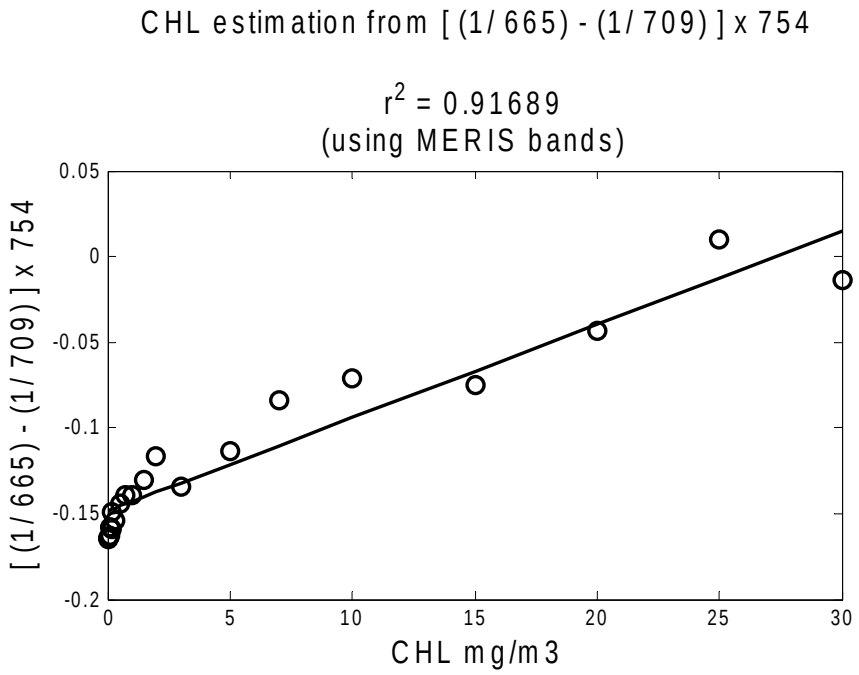

Figure 3.6 CHL retrieval 3 band NIR ratios

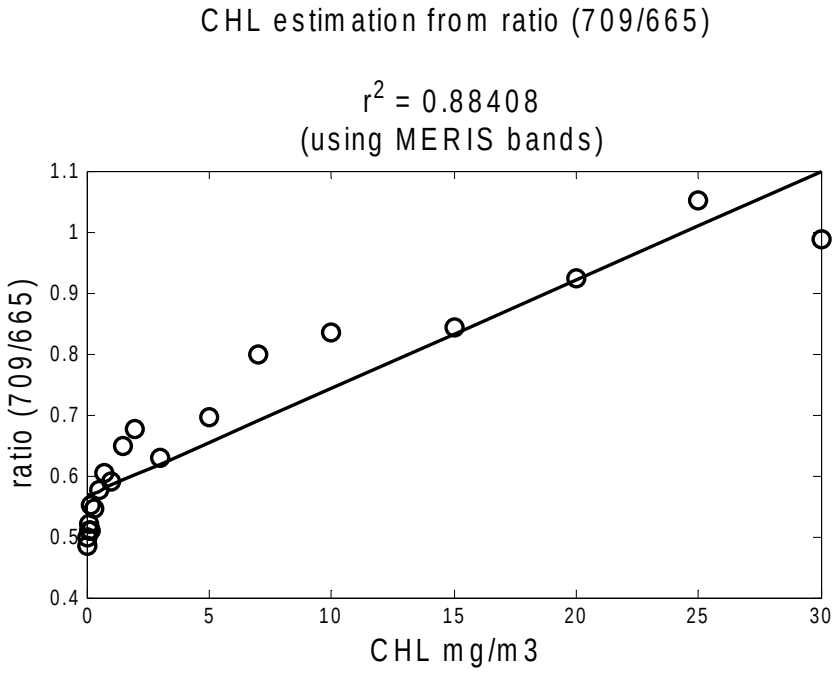

Figure 3.7 CHL retrieval 2 band NIR ratios

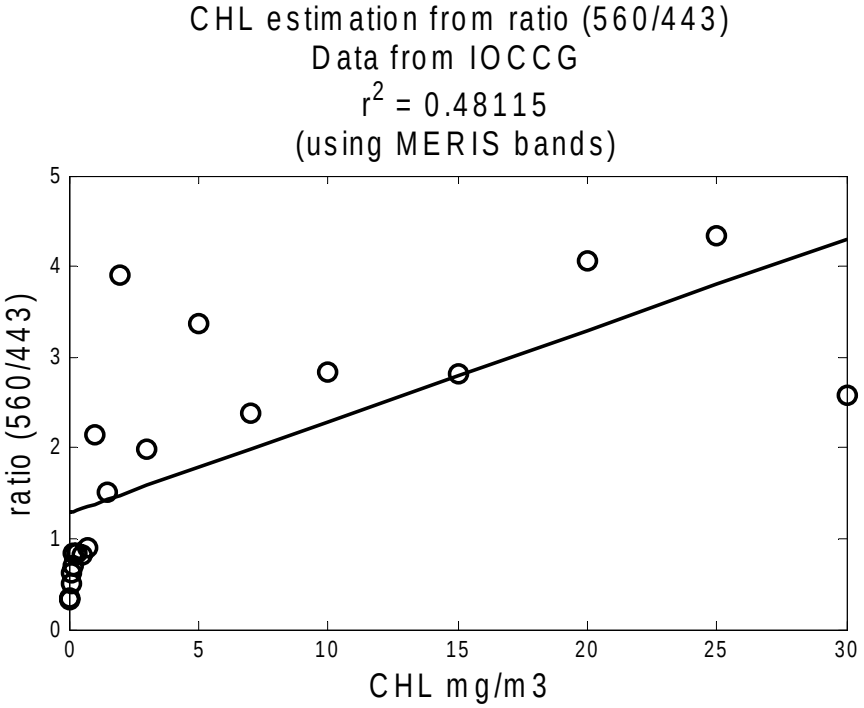

Figure 3.8 CHL retrieval 2 band ratios (Blue-Green)

From these graphs we can see that the NIR algorithms are superior to the traditional blue-green algorithms so there is the possibility of using appropriate multiband algorithms to isolate CHL with minimized uncertainties due to CDOM and suspended solids. However, it was not clear from these figures whether there is any benefit from using three band algorithms instead of a simple 2-band ratio. To compare these algorithms, we need to study the uncertainties in the retrieval due to uncertainties in the water leaving reflectances. Since the two algorithms are in the NIR portion of the spectrum, we can assume the errors in the reflectances are the same for the different algorithms

3.8 Chesapeake Bay Experiment

During the summer of 2005 the CCNY NOAA-CREST experimental group participated in a field campaign in the Chesapeake Bay in collaboration with the partners from other universities (Florida A&M University, Creighton University, University of Nebraska, Morgan State University, Kent University) and obtained comprehensive sets of data. These included bio-optical parameters of the waters in the bay, adjacent rivers and harbor. They represent a wide variety of water constituents: phytoplankton, CDOM, and suspended solids. These parameters were measured simultaneously using a variety of instruments and techniques at each location.

3.8.1 Measurement of Inherent Optical Properties

More extensive in-situ measurements were carried out at 44 stations shown in Fig. 3.9 across the whole Chesapeake Bay area from July 11th to 20th 2005 using a ship-deployed profiling package [17] assembled by WET Labs (Philomath, Oregon). This package consists of three instruments: an AC-S, an ECO-scattering meter and a CTD. The AC-S has dual 25cm flow cells in which spectral absorption and attenuation are measured every 250 ms at 82 wavelengths from 400nm to 800nm. To obtain accurate absorption measurements, the inner side of the tube is coated with quartz which can reflect the scattered light back into the chamber and finally collected by the detector. In order to increase the field of view, the tube has a larger inner radius with large effective detection area. The inside of the attenuation tube is thin with a small detector area and is made of black plastic so that it absorbs most of the light hitting the wall and only allows the signal along the light path to reach the

detector. The water sample is pumped into the chambers through one of the intakes and a filter is installed at another intake to prevent large objects such as stones from entering the tubes and damaging the meters. At the same time, the upwelling and downwelling radiance from the water were collected and delivered by fiber bundles to the spectroradiometers (Ocean optics). The fiber probe for upwelling measurements was placed just beneath the surface so that reflectance from the ocean surface can be obtained from normalizing the upwelling radiance to the downwelling radiance. The water leaving signals below the surface were then adjusted to account for the surface fresnel effects (figure 3.10).

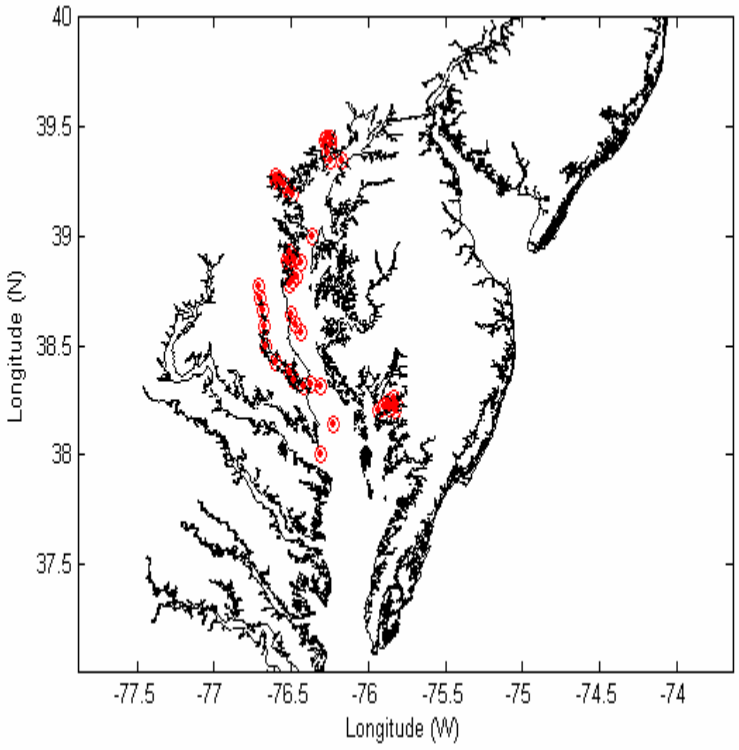

Figure 3.9 Field Measurement Campaign locations

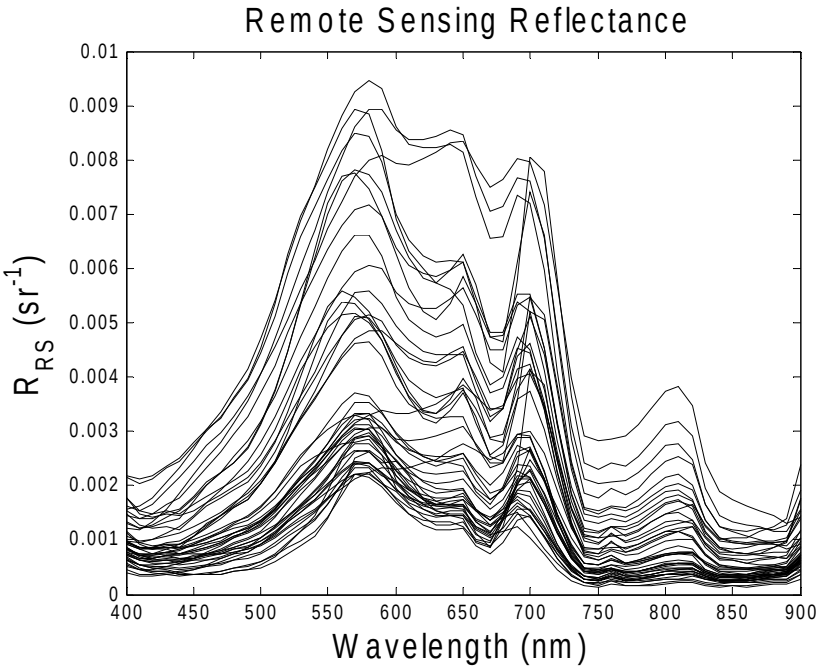

Figure 3.10 Measured remote sensing reflectance

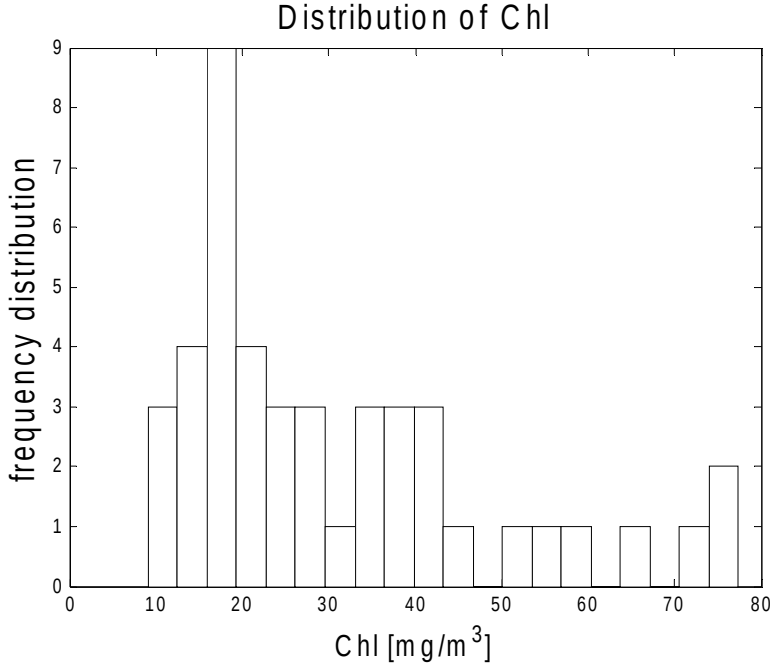

Figure 3.11 Frequency distribution of CHL measured.

The analysis of the data illustrates the diversity and complexity of these coastal waters. Figure 3.10 shows the remote sensing reflectance measured at Chesapeake Bay which has two distinct features, the first is the very low reflectance in the blue due to the high absorption by CDOM in these coastal waters and the second the non-negligible reflectance in the NIR (765,865) due to the high total backscattering coefficient. The concentration of chlorophyll was measured in the range 9.1 to 77.4 mg/m3. Figure 3.11 shows the frequency distribution of the concentration of chlorophyll measured. The strong degradation in the water leaving radiance in the blue band is clearly due to the strong CDOM absorption feature.

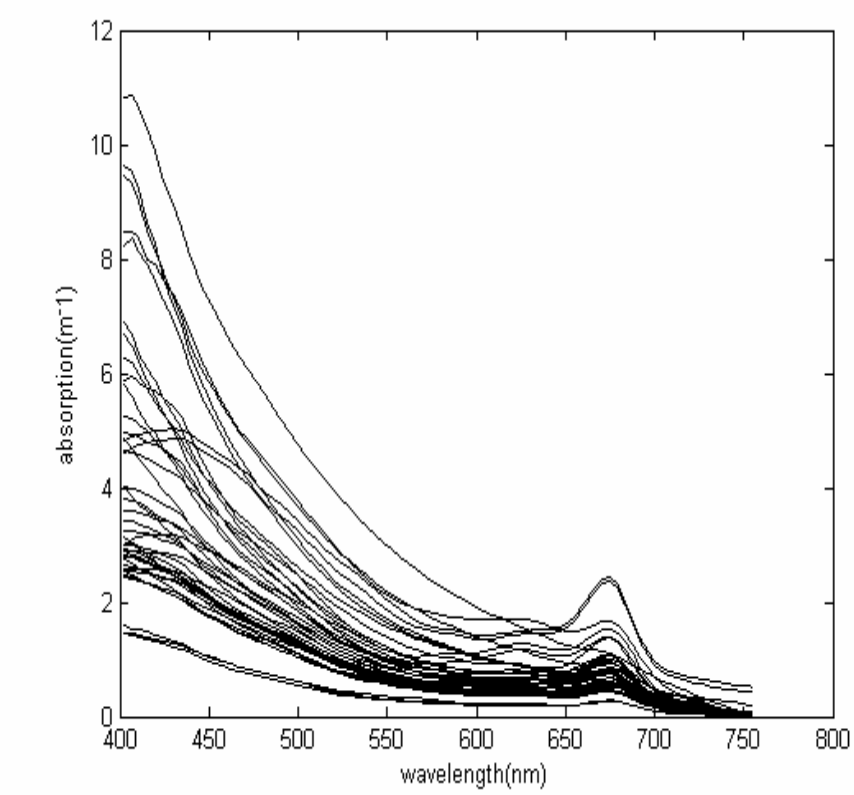

Figure 3.12 Measured absorption coefficients versus wavelength near water surface

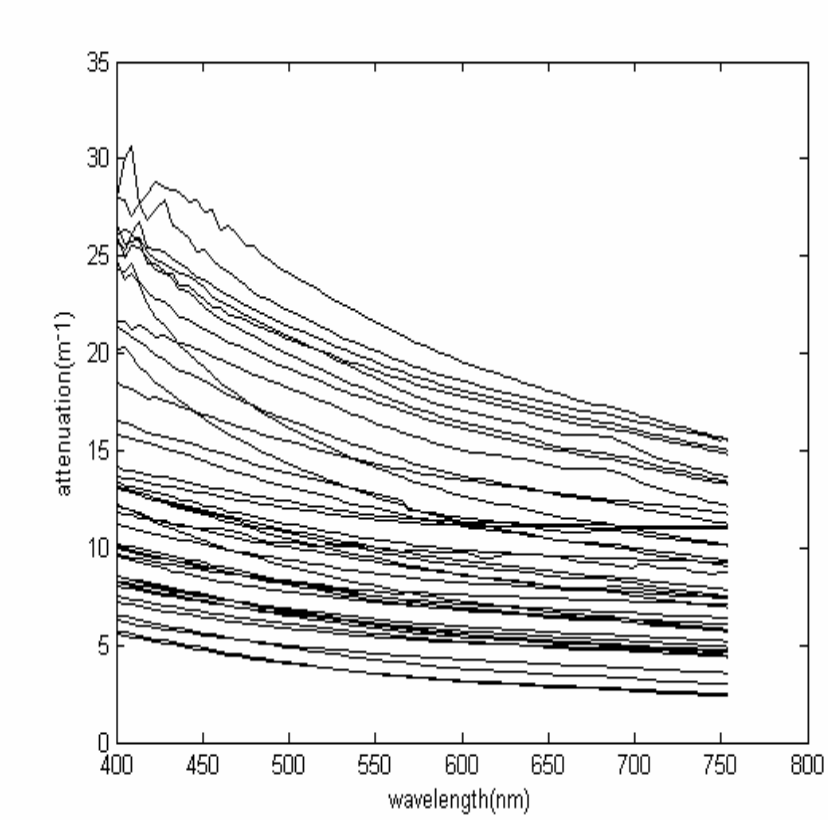

Figure 3.13 Measured attenuation coefficients versus wavelength near water surface

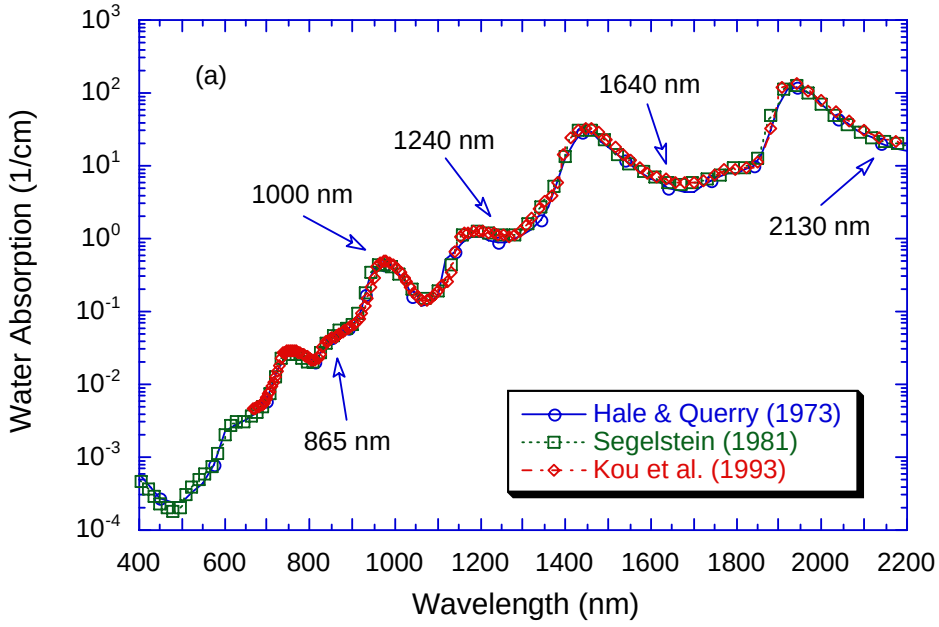

Figure 3.14 water absorption (from Menghua Wang NOAA/NESDIS/ORA)

The absorption and extinction are shown in figures 3.12 and 3.13 respectively for all the stations. Clearly, the absorption coefficients obtained from these measurements in the blue are comparable to the water absorption at 865 (see figure 3.14) and therefore, will result in "dark pixel" behavior which may be exploited.

3.9 Band Ratio Algorithm development

In the complex soup found in the Chesapeake Bay waters, it is quite clear that traditional blue-green algorithms will not be useful [15], [18]. More recently, the use of CHL algorithms in the second absorption band near 680nm has been revisited. While historically, these bands were not used due to fluorescence contamination and poor SNR, the development of improved SNR for next generation sensors makes these algorithms quite useful options for space platforms. To assess these possible algorithms, we simulate the remote sensing reflectance signals $R_{rs}(\lambda_i)$ seen by the satellite (i.e. SeaWIFS, MODIS) centered at wavelength λ_i by convolving the data with the respective sensor response function using the formula

$$R_{rs}(\lambda_i) = \frac{\int R_{rs}(\lambda) S_i(\lambda) d\lambda}{\int S_i(\lambda) d\lambda} \qquad (3.7)$$

where $S_i(\lambda)$ is the spectral response function of the i^{th} spectral band. Figures 3.15 and 3.16 show the MODIS spectral response functions and the remote sensing reflectance seen by the MODIS satellite respectively.

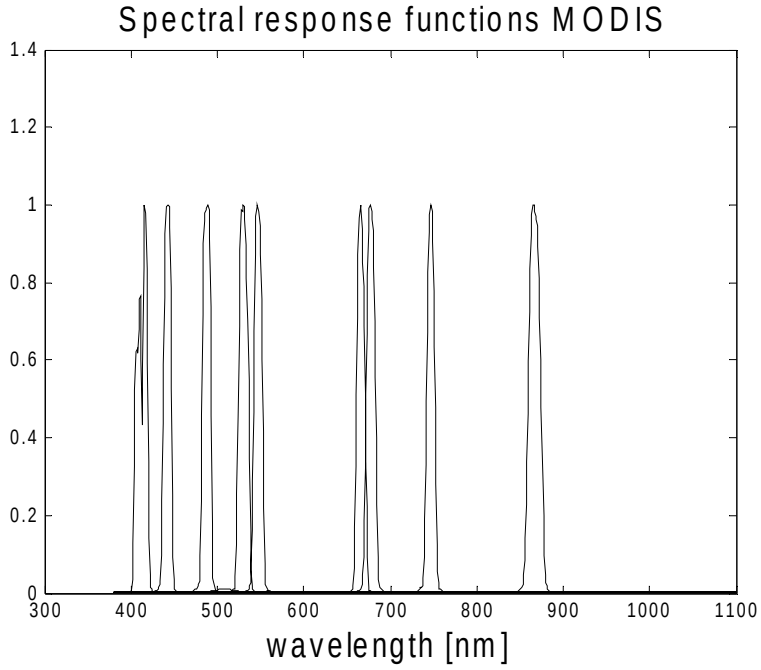

Figure 3.15 Spectral response functions (MODIS)

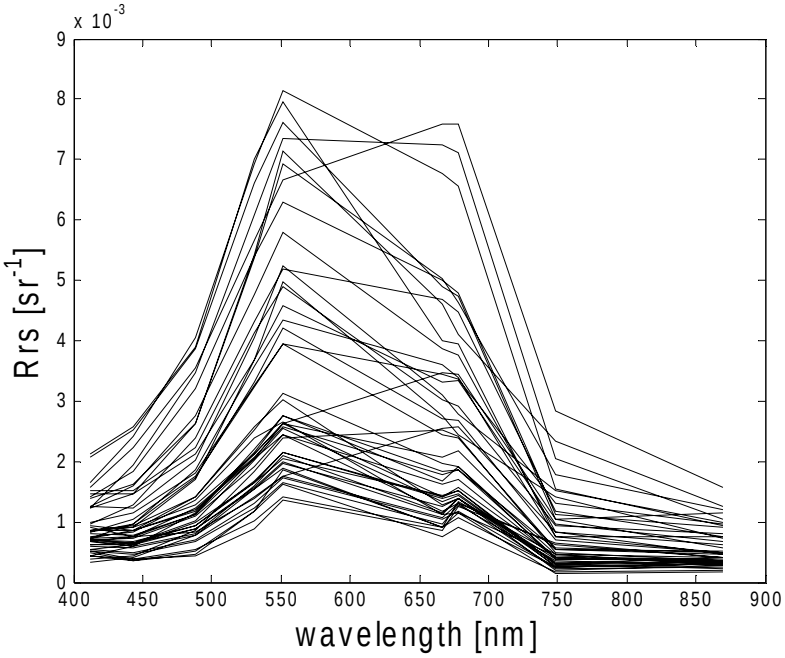

Figure 3.16 Remote sensing reflectance seen by the satellite (MODIS)

From these spectrally averaged measurements, the testing of different band ratios can be simulated including a MODIS band ratio $R_{rs}(748)/R_{rs}(678)$ as well as the ratios that might be available in GOES-R $R_{rs}(710)/R_{rs}(670)$. In both cases, the measurement datasets were fitted to models of the form $CHL = C_o \times 10^{\left(m\left(\frac{R_j}{R_i}\right)\right)}$ in a least squares way. Given these least square estimators, we can assess the uncertainty in the CHL estimator as a function of the CHL loading in the limit of perfect reflectance measurements. The results are shown in figures 3.17 and 3.18 for the MODIS and GOES-R measurements respectively. In particular, we see significant improvement in the GOES-R for lower CHL concentrations illustrating the possible improvement in ocean color monitoring for the 710 channel under debate. However, we also observe residuals as high as 50% implying that even in the absence of atmospheric correction, much work is needed to improve on simple band ratio algorithms.

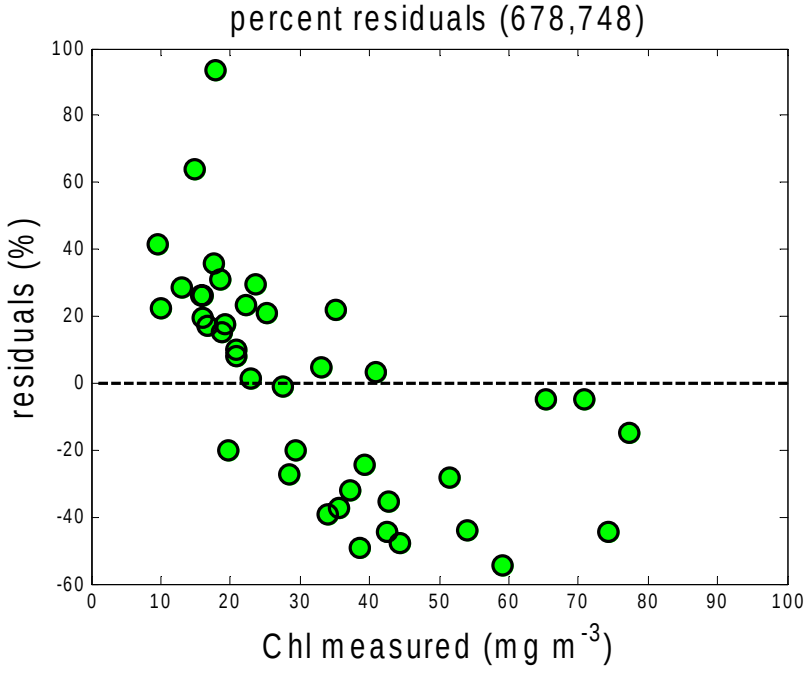

Figure 3.17 CHL ratio algorithm retrieval residuals from ratio 678-748

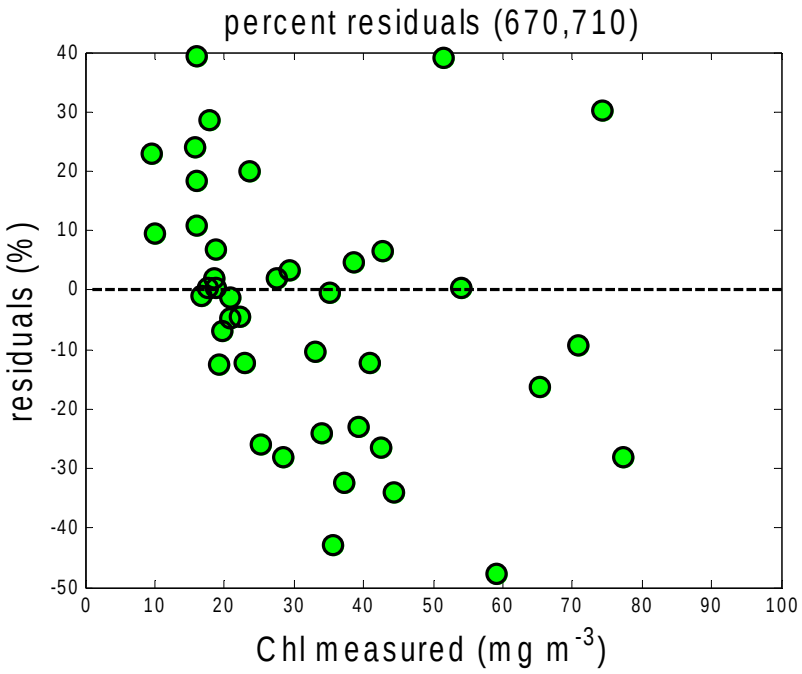

Figure 3.18 CHL ratio algorithm retrieval residuals from ratio 670-710

References Chapter 3

[1] Gordon, H. R. and Morel, A. (1983). Remote Assessment of Ocean Color for Interpretation of Satellite Visible Imagery. A Review, Lecture Notes on Coastal and Estuarine Studies, R. T. Barber, N. K. Mooers, M. J. Bowman and B. Zeitzschel (eds.), Springer-Verlag, New York, 114 p.

[2] Acker J G, Vasilkov A, Nadeau D, Kuring N (2004) Use of SeaWiFS ocean color data to estimate neritic sediment mass transport from carbonate platforms for two hurricane-forced events, CORAL REEFS 23: (1) 39-47

[3] Lee Zhongping, Kendall L. Carder, Curtis D. Mobley, Robert G. Steward, and Jennifer S. Patch. Hyperspectral remote sensing for shallow waters: 2. Deriving bottom depths and water properties by optimization. Applied Optics 38, 3831-3843 (1999)

[4] Garver, S. A., and D. A. Siegel (1997), Inherent optical property inversion of ocean color spectra and its biogeochemical interpretation 1. Time series from the Sargasso Sea, J. Geophys. Res., 102(C8), 18,607–18,626.

[5] O'Reilly, J. E., S. Maritorena, B. G. Mitchell, D. A. Siegel, K. L. Carder, S. A. Garver, M. Kahru, and C. R. McClain (1998), Ocean color chlorophyll algorithms for SeaWiFS, J. Geophys. Res., 103, 24,937–24,953.

[6] Liew S. C., Aik Song Chia, Kim Hwa Lim and Leong Keong Kwoh. Modeling the reflectance spectra of tropical coastal waters. SPIE Proc. 4488B – Ocean Color Remote Sensing and Applications Part of SPIE's International Symposium on Optical Science and Technology, 29 July to 3 August 2001, San Diego, California, USA.

[7] Morel A, "Optical properties of oceanic Case I waters, revisited," Ocean Optics XIII, SPIE Proc. 2963, pp. 108-114, 1996.

[8] Roesler, C. S., and M. J. Perry (1995), In situ phytoplankton absorption, fluorescence emission, and particulate backscattering spectra determined from reflectance, J. Geophys. Res., 100(C7), 13,279–13,294.

[9] Burenkov VI, Vasilkov AP, Stephantsev LA (1995) Retrieval of spectral inherent optical properties of seawater from the spectral reflectance. Oceanology 25:49–54

[10] D.K. Clarke, MODIS Algorithm Theroretical Basis Document, Bio-Optical Algorithms – Case 1 Waters, version 1.2, http://modis.gsfc.nasa.gov/data/atbd/atbd_mod18.pdf, 1997.

[11] K.L. Carder, F.R. Chen, Z.P. Lee and S.K. Hawes, “Semi-analytic moderate-resolution imaging spectrometer algorithms for chlorophyll a and absorption with bio-optical domains based on nitrate depletion temperatures,” Journal of Geophysical Research, vol. 104, pp. 5403-5421, 1999.

[12] IOCCG. Ocean-Colour Algorithms. http://www.ioccg.org/groups/OCAG_data.html

[13] Darecki M and Stramski D 2004 An evaluation of MODIS and SeaWiFS bio-optical algorithms in the Baltic Sea Remote Sens. Environ. 89 326–50

[14] Siegel D. A., M. Wang, S. Maritorena, and W. Robinson, "Atmospheric Correction of Satellite Ocean Color Imagery: The Black Pixel Assumption ," Appl. Opt. 39, 3582-3591 (2000)

[15] Dall’Olmo G. and Gitelson A., Effect of the variability of bio-optical parameters on the remote estimation of chlorophyll-a concentration in turbid productive waters: experimental results. Applied Optics 44, 422-6338 (2005)

[16] IOCCG Ocean Color Algorithm Working Group. June 2003 Models, parameters, and approaches that used to generate wide range of absorption and backscattering spectra http://www.ioccg.org/groups/lee_data.pdf

[17] Wetlabs instrument manual

[18] Ruddick, K. G., H. J. Gons, M. Rijkeboer, and G. Tilstone, "Optical Remote Sensing of Chlorophyll a in Case 2 Waters by Use of an Adaptive Two-Band Algorithm with Optimal Error Properties ," Appl. Opt. 40, 3575-3585 (2001)

Chapter 4 Hyperspectral Remote Sensing for Shallow Water Imaging

4.1 Introduction

In most cases of interest, the water bottom does not affect the retrieval of optical properties since the light field is attenuated before reaching the bottom. However, for near coastal waters, lakes and tributaries with depths < 20meters, the light field can interact with the water bottom.

The shallow water inversion problem in its most general form is the radiative transfer equation [1]. The application of the radiative transfer equation to the shallow water inversion problem requires one to simultaneously solve for bathymetry, bottom reflectance, and vertically-structured IOPs when attempting to retrieve an optical reflectance signal [2].

Remote sensing is used for surveying large bodies of optically shallow waters, but the limitations of multispectral sensors have not provided sufficient spectral resolution necessary for accurate bottom type characterization or resource assessment in coastal waters. The retrieval of bathymetry, bottom albedo and IOPs requires hyperspectral imagery in contrast to the open ocean where the water column properties alone are of interest and for which multispectral imagery is sufficient.

Multispectral data analyses with one-dimensional radiative transfer models has proven to be effective in estimating coral densities, deriving water optical properties, and mapping [3-6] but these analyses can be further enhanced by the introduction of hyperspectral sensors. HyperSpectral Imaging (HSI) increases the number of spectral bands by which to invert the radiative transfer equation in shallow waters [7-9].

The usefulness of Hyperspectral Imaging capabilities fueled NOAA's interest in the development of a Geostationary GOES-R HES Imager and during the design aspects of this sensor, sensitivity analyses were needed to determine the additional improvement in IOPs and surface bottom retrieval when the full Hyperspectral channel specification was used. Therefore, we undertook to compare the different channel configurations which were being debated for the GOES-R HES-CW Imager and assess the retrieval capacity.

The approach we have undertaken is to develop a modeled set of multispectral and hyperspectral synthetic spectra for both deep and shallow waters using a bio-optical model existing in the literature based on extensive Hydrolight Radiative Transfer calculations. These synthetic spectra are then perturbed by noise whose level and specifications are determined from the sensor specifications as well as variable noise levels to test SNR requirements. LSQ retrievals were then undertaken on the noisy data to provide optimal simultaneous retrieval of depth, surface albedo intensity, and inherent optical properties. The work undertaken can be broken into 2 phases:

Step #1 (assuming perfect atmospheric correction), determine level of improvement for retrieval of bio-optical parameters between threshold (multispectral) and optimal (hyperspectral)

Step #2 Second, (assuming perfect atmospheric correction), determine level of improvement for retrieval of bio-optical parameters in shallow waters using the semi-empirical model.

It should be noted however that after this work, the HES CW Imager was unfortunately eliminated from the GOES-R platform at the time of printing but with good sense, may be developed in the future.

4.2 GOES-R Capabilities

The full capabilities of the HES hyper- or multi- spectral imaging task (CW) at the time of this study were under investigation. In particular, the choice was between a base configuration comprising the minimal spectral coverage with 14 bands as seen in table 4.1

Channel Center (microns)	Resolution (microns)
0.412	±0.01
0.443	±0.01
0.477	±0.01
0.490	±0.01
0.510	±0.01
0.530	±0.01
0.550	±0.01
0.645	±0.01
0.667	±0.01
0.678	±0.01
0.750	±0.01
0.763	±0.01
0.865	±0.01
0.905	±0.01

Table 4.1 CW Sensor threshold Spectral Resolution.

whereas the GOAL specifications would result in full hyperspectral coverage from 400nm to 2285nm (20nm resolution). The point of this investigation was to intercompare the BASE and GOAL configurations

4.3 Remote sensing in shallow coastal waters

In shallow waters, it is not sufficient to use simple ratio algorithms since the bottom albedo and the column height play a role. In particular, the chlorophyll absorption is now modulated by the height of the water column and contaminated by the albedo. Therefore, more spectral information is needed and as a preliminary test bed, we used the shallow water bio-optical model [10],[11] to investigate the possibility of simultaneous retrieval.

Step #1

The above water emote sensing reflectance is converted to subsurface as

$$R_{RS}(\lambda) = \frac{0.5 r_{rs}}{1 - 1.5 r_{rs}} \tag{4.1}$$

R_{RS} = Above water r_{rs} = Below water

Step #2

The remote sensing reflectance is decomposed into a contribution from the finite water column and the surface using appropriate parameterized beam attenuation parameters, also, the water column is corrected for finite depth.

$$r_{rs} = r_{rs}^{c} + r_{rs}^{B} \tag{4.2}$$

$$r_{rs}^{c} = r_{rs}^{dp}\left(1 - \exp\left\{-\left[\frac{1}{\cos(\theta_w)} + D_u^c\right]\kappa H\right\}\right) \tag{4.3}$$

$$r_{rs}^{B} = \frac{1}{\pi}\rho_B \exp\left\{-\left[\frac{1}{\cos(\theta_w)} + D_u^B\right]\kappa H\right\} \tag{4.4}$$

where r_{rs}^{dp} defines the unperturbed remote sensing for deep waters, ρ_B is the reflection of the ocean bottom H represents the column depth and θ_w is the subsurface zenith angle of the direct solar beam. The parameterization of the beam

attenuation coefficients and the deep water remote sensing reflectance in terms of the absorption (a) and backscatter (b_b) takes the form

$$r_{rs}^{dp} = (0.084 + .170u)u \tag{4.5}$$

$$D_u^c = 1.03(1 + 2.4u)^{0.5} \tag{4.6}$$

$$D_u^B = 1.04(1 + 5.4u)^{0.5} \tag{4.7}$$

$$where \quad u \equiv \frac{b_b}{a + b_b} \quad \kappa \equiv a + b_b$$

The IOP's are then decomposed in the conventional way as

$$a_{total}(\lambda) = a_w(\lambda) + a_\varphi(\lambda) + a_g(\lambda) \tag{4.8}$$

$a_w(\lambda)$ is the absorption coefficient due to water

$a_\varphi(\lambda)$ is the absorption coefficient due to phytoplankton

$a_g(\lambda)$ is the absorption coefficient due to gelbstoff

$$b_{tot}(\lambda) = b_{bw}(\lambda) + b_{bp}(\lambda) \tag{4.9}$$

$b_{bw}(\lambda)$ is the backscattering of water

$b_{bp}(\lambda)$ is the backscattering by particulate matter

The spectral backscatter and absorption optical properties are themselves parameterized to reduce the degrees of freedom while maintaining the core variability of the bio-optical parameters. The resulting parameters to be retrieved are: **P, G, X, Y, H, B**. where P and G are phytoplankton and gelbstoff absorption at 440, X and Y determine the backscatter magnitude and power law exponent, H is the column height and B is the ocean bottom albedo. For open ocean waters (case I) the model reduces to a four parameter model, and the parameters retrieved are: ***P, G, X,***

Y. The inversion of the reflectance model is performed by least squares optimization between measured and modeled reflectance spectra. The spectral bands used in the multispectral simulation are:

412, 443, 477, 490, 510, 530, 550, 645, 667, and 678 nm. corresponding to the combination MERIS-MODIS, while 31 hyperspectral bands are used corresponding to GOES-R from 410 to 680nm.

Figures 4.1 to 4.6 show the error in the retrieval of the parameters Y,P,H,B, G and X as a function noise. Noise sensitivities were varied from 1% to 20% which are reasonable values to account for uncertainties in atmospheric retrieval. However, since the errors due to atmospheric retrieval are well correlated, the errors in all channels were taken to be proportional to a single fractional error.

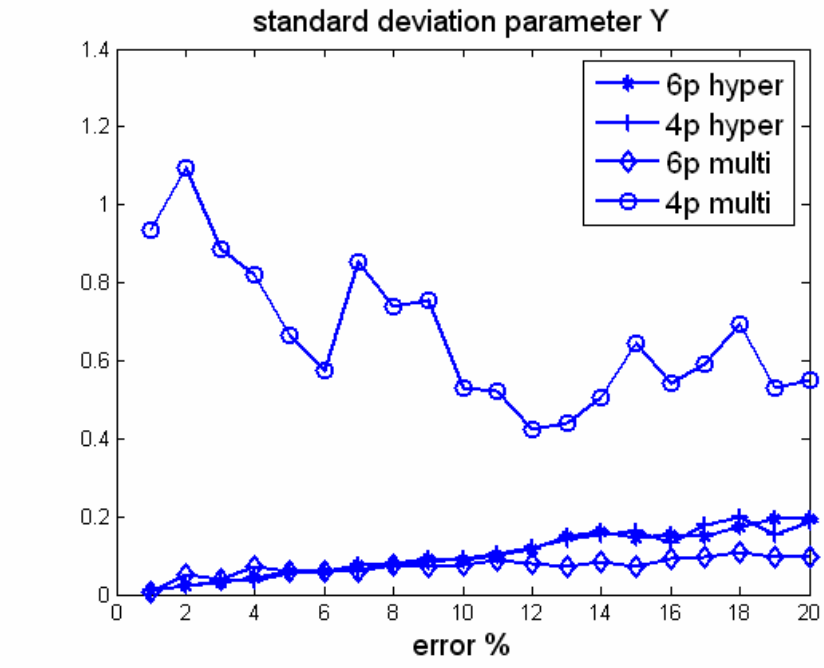

Figure 4.1 Parameter Y

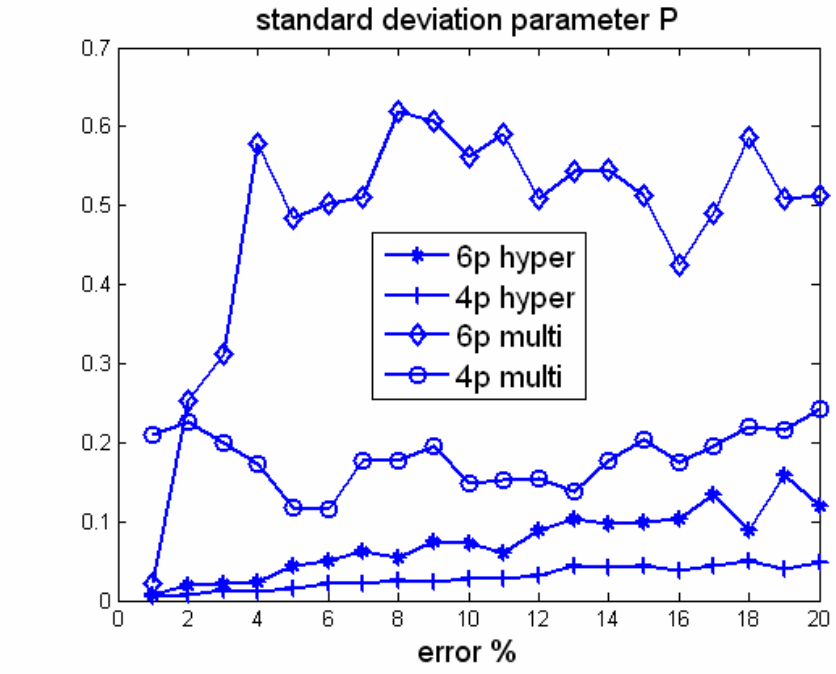

Figure 4.2 Parameter P

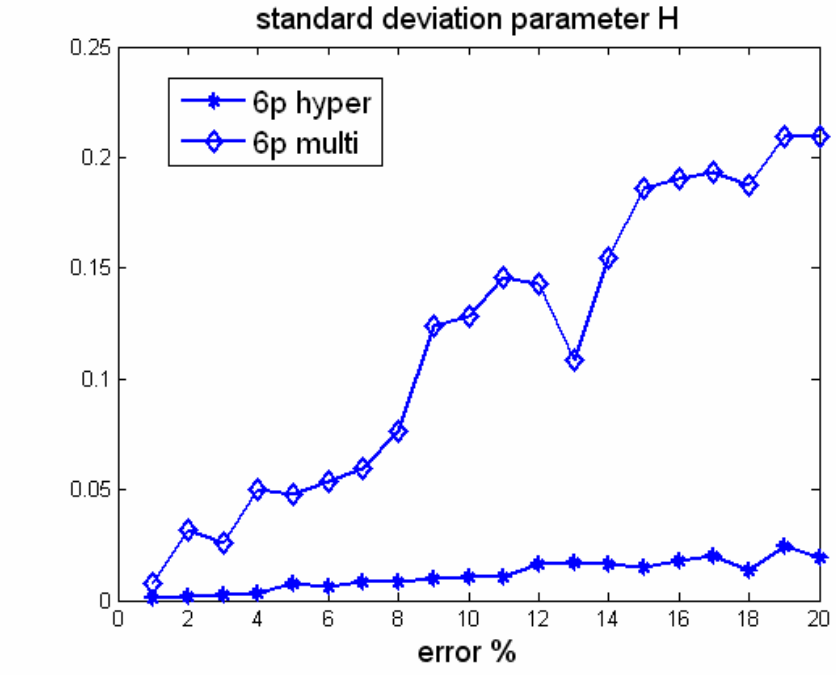

Figure 4.3 Parameter H

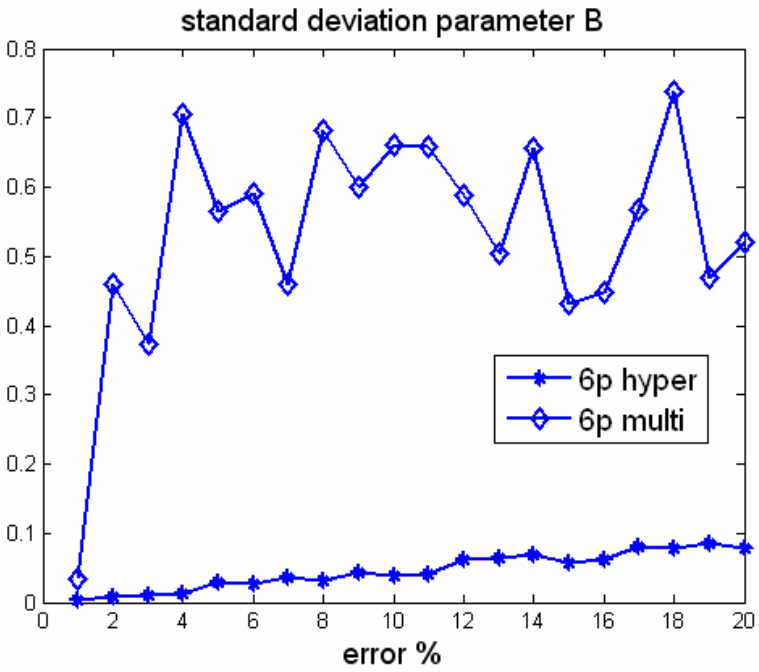

Figure 4.4 Parameter B

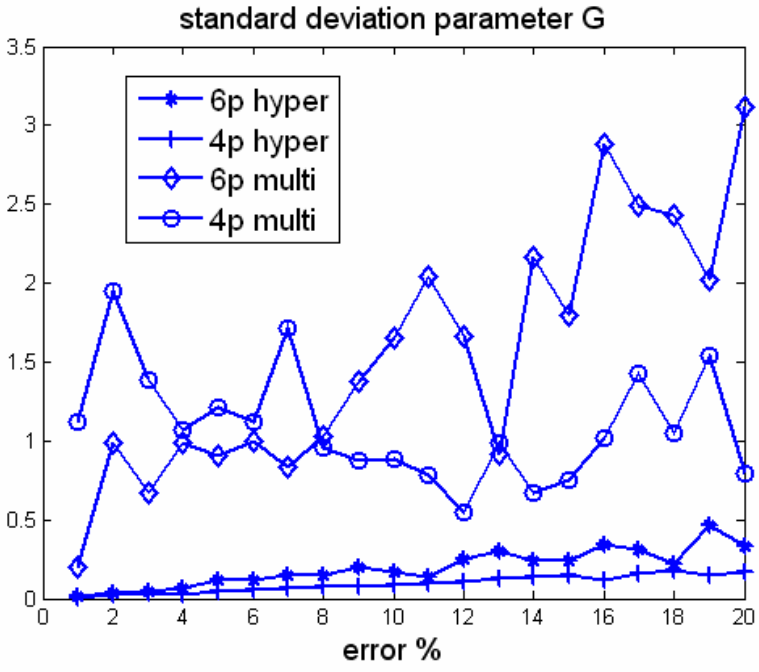

Figure 4.5 Parameter G

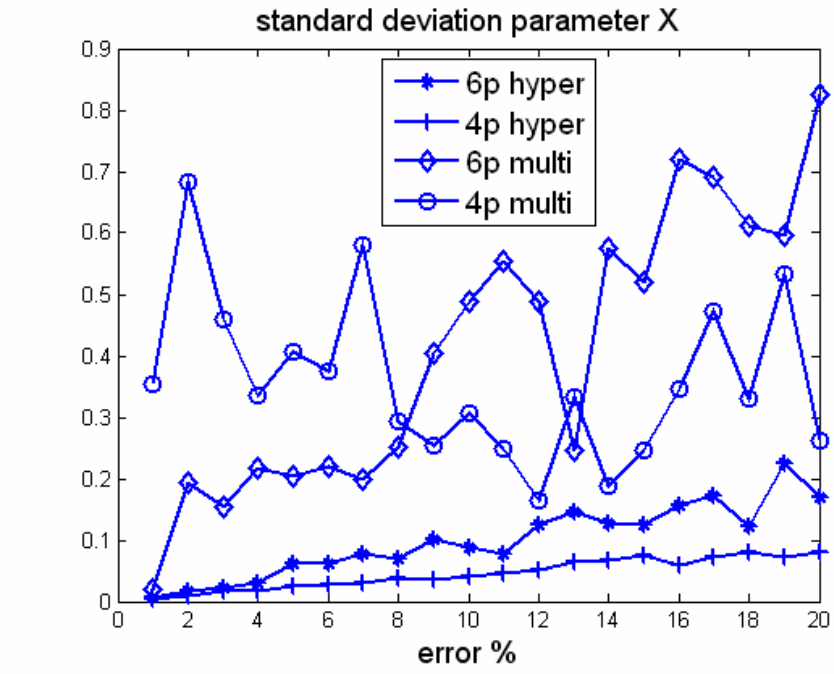

Figure 4.6 Parameter X

Analysis of these figures show clearly that hyperspectral channels significantly improved the retrievals for all parameters with the most dramatic improvements being observed for surface albedo and height although ocean column parameters are also much better retrieved using the hyperspectral configuration.

4.4 Least Square Fitting of Data to IOCCG Model of Remote Sensing Reflectance

While the numerical results are impressive, we also explored the feasibility of fitting the multicomponent bio-optical models to our experimental data. In this case, shallow water issues were not relevant so instead of the Lee and Carder bio-optical

model, we used a similar model based on the IOCCG committee which was specifically developed to connect to CHL. This was necessary since our field campaigns were not able to isolate the component absorption and backscattering.

4.5 The IOCCG Bio-optical Algorithm

The IOCCG Bio-optical Algorithm is as follows:

A four component model is used to generate the IOPs of the bulk water. Specifically, absorption (a) and backscattering (bb) coefficients are described as:

$$\begin{aligned} a(\lambda) &= a_w(\lambda) + a_{ph}(\lambda) + a_{dm}(\lambda) + a_g(\lambda) \\ bb(\lambda) &= bb_w(\lambda) + bb_{ph}(\lambda) + bb_{dm}(\lambda) \end{aligned} \tag{4.10}$$

$a_w(\lambda)$ from Pope and Fry [12] and $bb_w(\lambda)$ from Morel [13] at defined temperature and salinity are used. Phytoplankton concentration [C], will be used as a free parameter to define different waters. [C] is in the range 0.03-30 μg/l

4.6 Absorption terms

4.6.1 Phytoplankton Pigment Absorption, $a_{ph}(\lambda)$

$a_{ph}(\lambda)$ is expressed as $a_{ph}(\lambda) = a_{ph}(440) \times a^{+}{}_{ph}(\lambda)$ (4.11)

with $a^{+}{}_{ph}(\lambda)$ the $a_{ph}(440)$ - normalized spectral shape For each [C] value, $a_{ph}(440)$ is created as $a_{ph}(440) = 0.05[C]^{0.626}$ (4.12)

It should be pointed out that the parameters 0.05 and 0.626 can significantly from place to place.

4.6.2 Detritus Mineral, $a(\lambda)_{dm}$

The Mineral absorption $a_{dm}(\lambda)$ spectrum is modeled as Roesler et al. [14] and Bricaud et al. [15] as $a_{dm}(\lambda) = a_{dm}(440) \times \exp(-S_{dm}(\lambda - 440))$ (4.13)

with S_{dm} randomly valued between 0.007 and 0.015 nm^{-1} for each [C]. The strength of the absorption $a_{dm}(440)$, is randomly determined for each [C]. This randomness however, is constrained based on observations. In particular, if we define p1 as the ratio of $a_{dm}(440)/a_{ph}(440)$, then $a_{dm}(440) = p_1 \times a_{ph}(440)$, (4.14)

with p_1 generated from $p_1 = 0.1 + \frac{0.5 \times \Re_1 a_{ph}(440)}{0.5 + a_{ph}(440)}$ (4.15)

Here $\Re_1$ is a random number between 0 and 1 (makes p_1 in a range 0.1-0.6).

4.6.3 Gelbstoff (Colored dissolved organic matter) absorption, $a_g(\lambda)$

The Gelbstoff absorption spectrum $a_g(\lambda)$ is modeled as Bricaud et al. [15]

$a_g(\lambda) = a_g(440) \times \exp(-S_g(\lambda - 440))$ (4.16)

with S_g randomly valued between 0.01-0.02 for each [C] value. The strength of the absorption $a_g(440)$ the gelbstoff absorption at the reference wavelength, is also randomly as before. If we define p_2 as the ratio $a_g(440)/a_{ph}(440)$, then

$a_g(440) = p_2 \times a_{ph}(440)$ (4.17)

with p_2 generated from $p_2 = 0.3 + \frac{5.7 \times \Re_2 \times a_{ph}(440)}{0.02 + a_{ph}(440)}$ (4.18)

Again, $\Re_2$ is a random value between 0 and 1 (making p_2 fall in a range of 0.3-6.0).

4.7 Backscattering Terms

4.7.1 Backscattering of Phytoplankton, $bb_{ph}(\lambda)$

Following Bukata et al. [16] Stramski et al. [17] and Roesler and Boss [18], the phytoplankton backscatter $bb_{ph}(\lambda)$ is modeled as a fraction of the total scatter which itself is modeled as the difference of CHL extinction and absorption.

$$\begin{aligned} bb_{ph}(\lambda) &= \tilde{b}_{ph} \times b_{ph}(\lambda) \\ b_{ph}(\lambda) &= c_{ph}(\lambda) - a_{ph}(\lambda) \\ c_{ph}(\lambda) &= c_{ph}(550)\left(\frac{550}{\lambda}\right)^{n1} \end{aligned} \tag{4.19}$$

where the values of $\tilde{b}_{ph}$ depend on the phase function of phytoplankton. In most cases, $\tilde{b}_{ph} \approx .01$. The total extinction $c_{ph}(550) = p_3 \times [C]^{0.57}$ (4.20)

with p_3 randomly valued between 0.06 and 0.6 for a given [C] value.

Here, n1 is generated as $n_1 = -0.4 + \dfrac{1.6 + 1.2\Re_3}{1 + [C]^{0.5}}$ (4.21)

so that n_1 falls is in a range -0.1 to 2.0, but varies for each [C].

Finally, $P_3 = 0.06 + 5.94 \times \Re_a$ (4.22)

$\Re_a$ is a random value between 0 and 1.

4.7.2 Backscattering of detritus, mineral and others, $bb_{dm}(\lambda)$

The mineral backscatter is given as

$$\begin{aligned} bb_{dm}(\lambda) &= \tilde{b}_{dm} \times b_{dm}(\lambda) \\ b_{dm}(\lambda) &= b_{dm}(550) \times \left(\frac{550}{\lambda}\right)^{n2} \end{aligned} \tag{4.23}$$

Here, the value of $\tilde{b}_{dm}$ depends on the selected phase function, and is 0.0183 when Petzold average particle phase function is used. As above, $b_{dm}(550)$ and n_2 are created as follows: $b_{dm}(550) = p_4 \times [C]^{0.766}$ (4.24)

with p_4 randomly valued between 0.06 and 0.6 for any [C] value; n_2 is generated with

$$n_2 = -0.5 + \frac{2.0 + 1.2\Re_4}{1 + [C]^{0.5}} \quad (4.25)$$

so n_2 falls in the range of -0.2 to 2.2 and $P_4 = 0.06 + 5.94 \times \Re_b$ (4.26)

$\Re_b$ is a random value between 0 and 1.

To assess whether this model could be used as a good predictor, we fit (LSQ) the Chesapeake spectra to the IOCCG reflectance model. To reduce the uncertainty due to too many degrees of freedom, we use a minimization with constrained bounds The values for the lower bound, upper bound and guess are given in table 4.2

Component	Lower Bound	Upper Bound	Guess
CHL	0.0	400	30
Sdm	0.007	0.015	0.01
Sg	0.01	0.02	0.015
K	0.0	0.1	0.01
R1	0.0	1.0	0.5
R2	0.0	1.0	0.5
R3	0.0	1.0	0.5
R4	0.0	1.0	0.5
Ra	0.0	1.0	0.5
Rb	0.0	1.0	0.5

Table 4.2 Initializations and parameter bounds for LSQ realization

The maximum number of function evaluations allowed was 2×10^3, the termination tolerance on the function value was 1×10^{-16} and the termination tolerance on x was

1×10^{-16}. Figures 4.7 to 4.18 show the results for stations 1 to 12 respectively. Figure 4.19 shows the residuals of LSQ fitting of Chesapeake Bay data to IOCCG model of remote sensing reflectance. Figure 4.20 shows CHL retrievals (CHL measured versus CHL retrieved by LSQ fitting), and Figure 4.21 shows the CHL residuals. Unfortunately, we found that the residual errors are extremely large meaning that more work is needed to build large parameter bio-optical models with more variety in the specific absorption as well as lower the degrees of freedom.

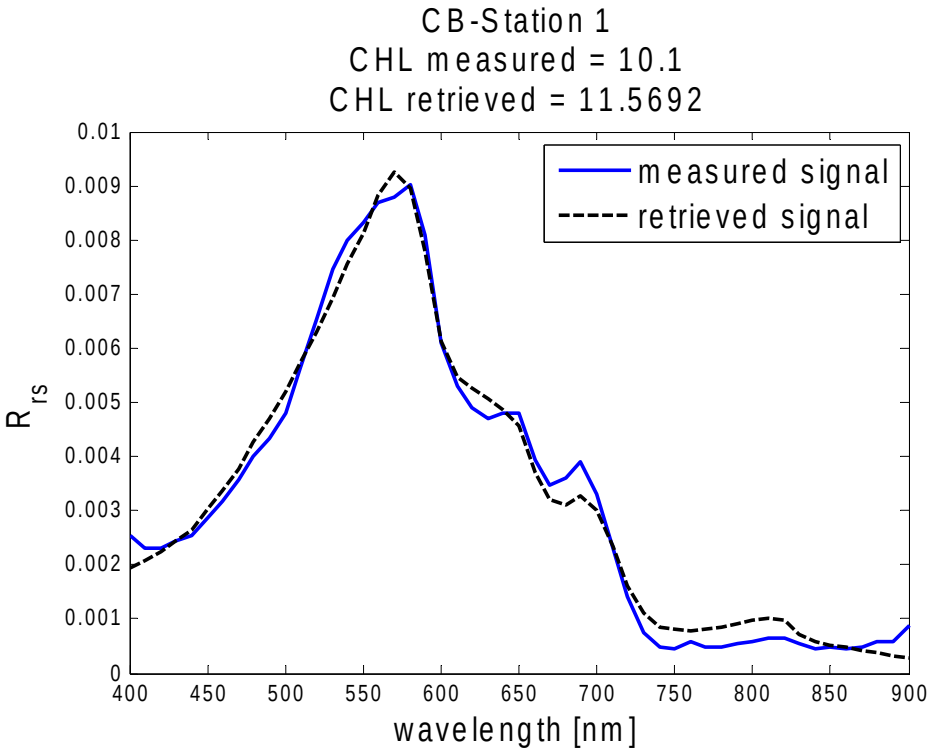

Figure 4.7 LSQ fitting result station 1

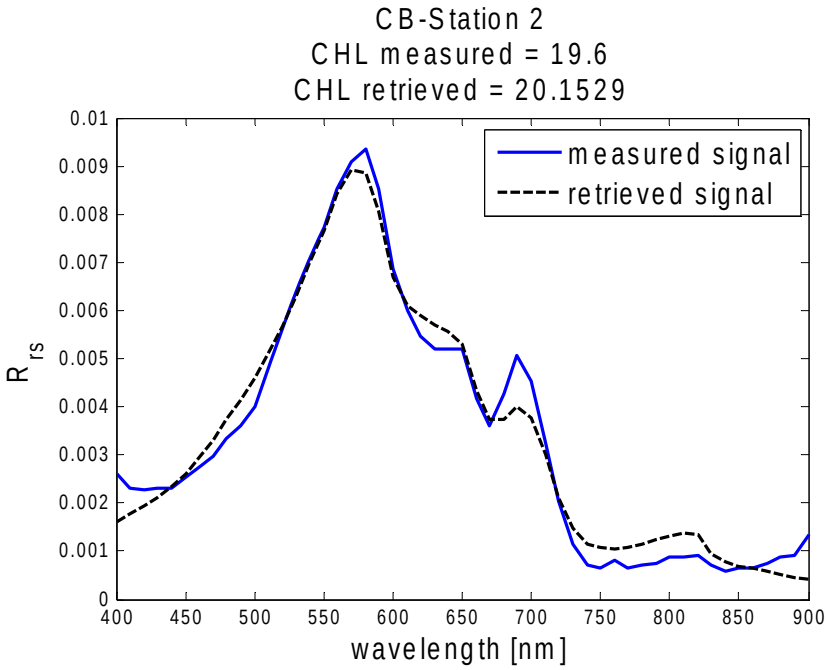

Figure 4.8 LSQ fitting result station 2

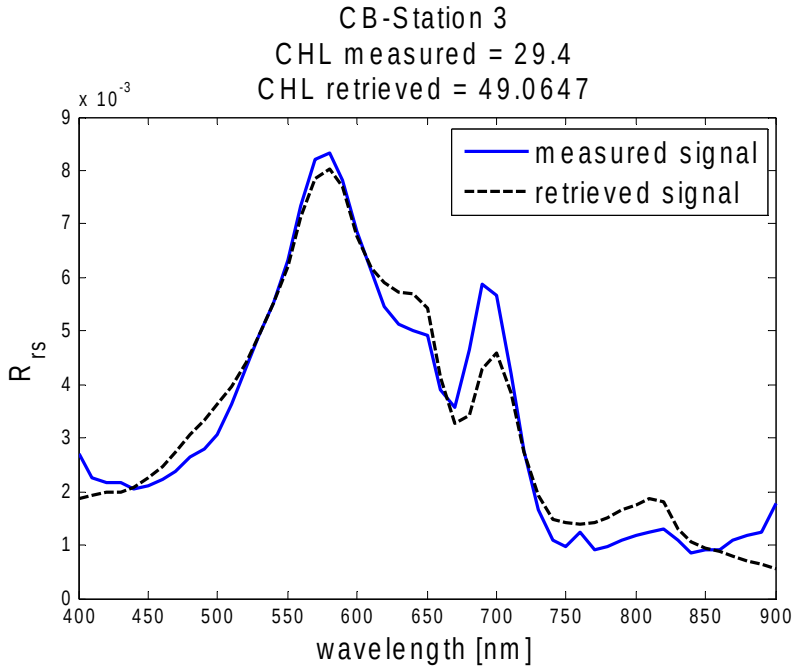

Figure 4.9 LSQ fitting result station 3

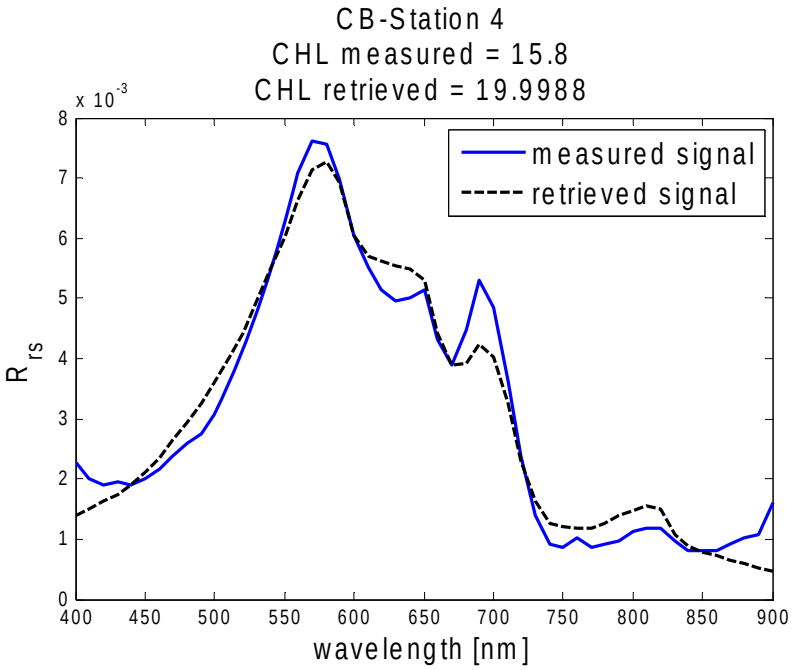

Figure 4.10 LSQ fitting result station 4

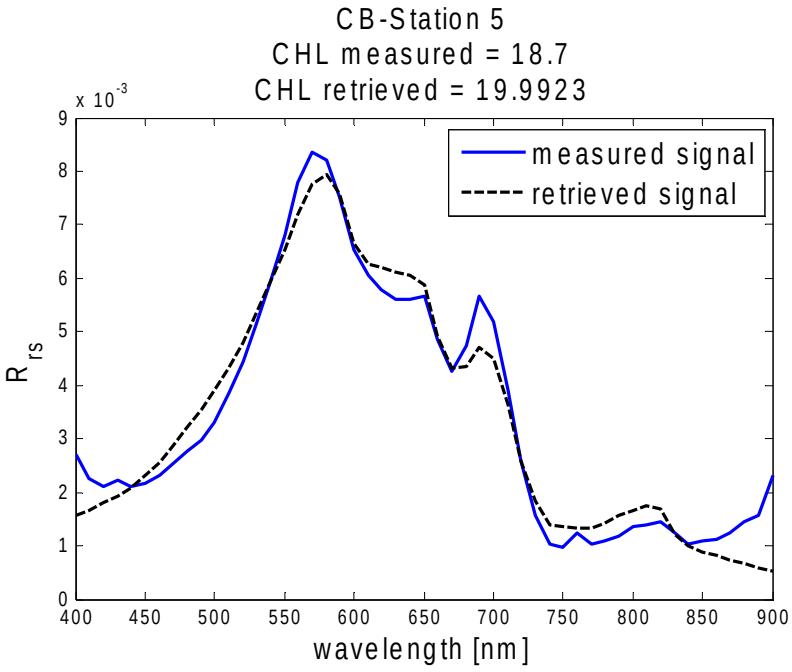

Figure 4.11 LSQ fitting result station 5

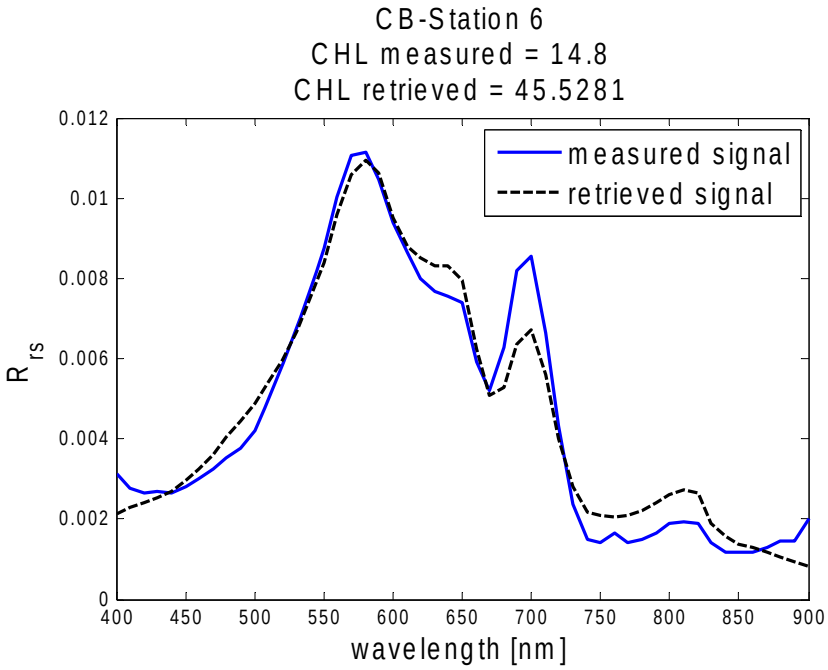

Figure 4.12 LSQ fitting result station 6

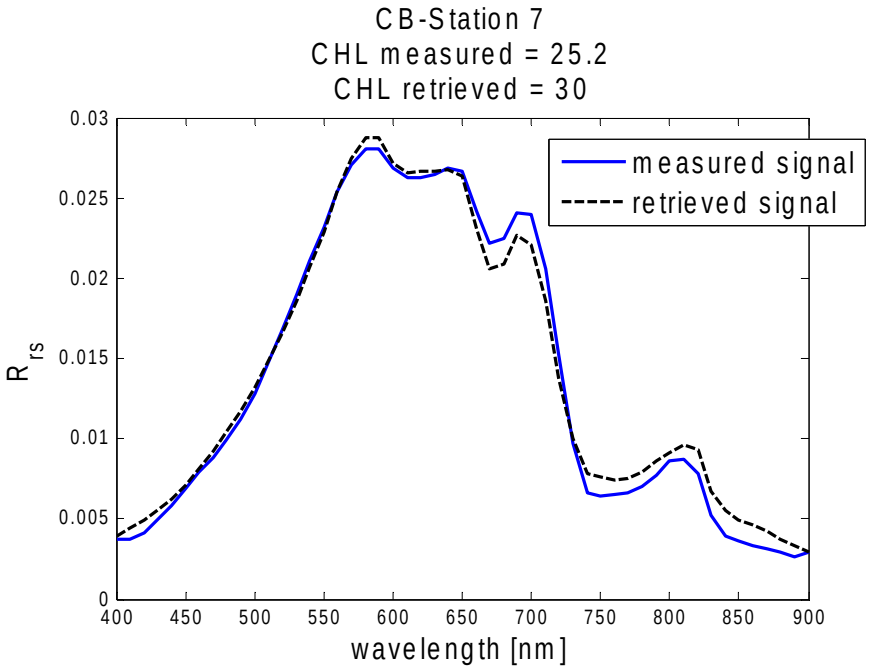

Figure 4.13 LSQ fitting result station 7

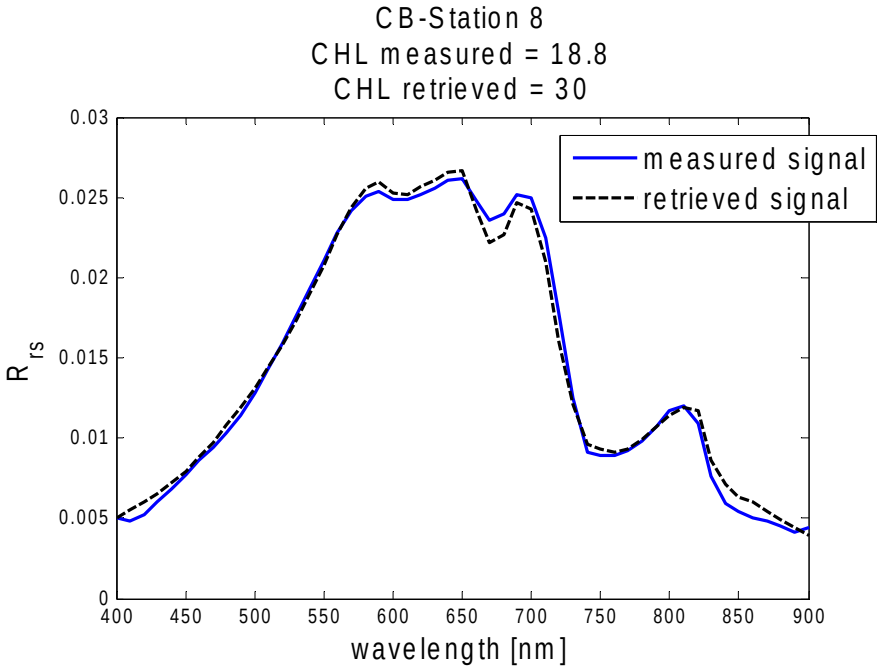

Figure 4.14 LSQ fitting result station 8

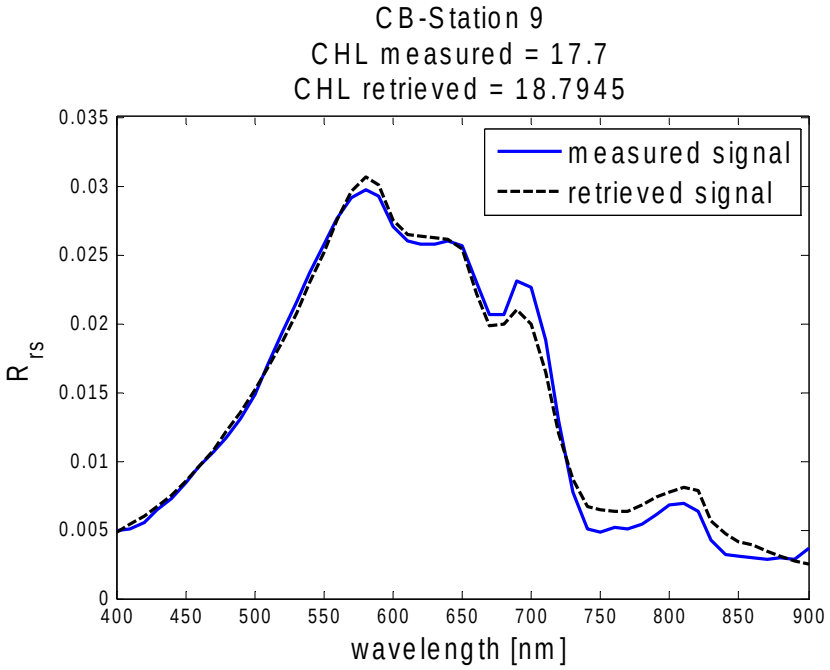

Figure 4.15 LSQ fitting result station 9

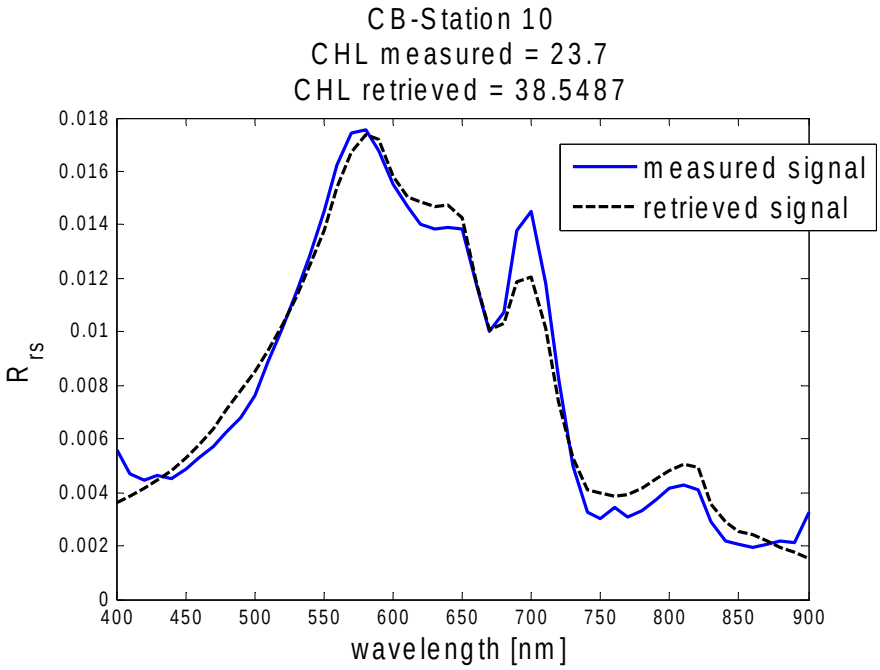

Figure 4.16 LSQ fitting result station 10

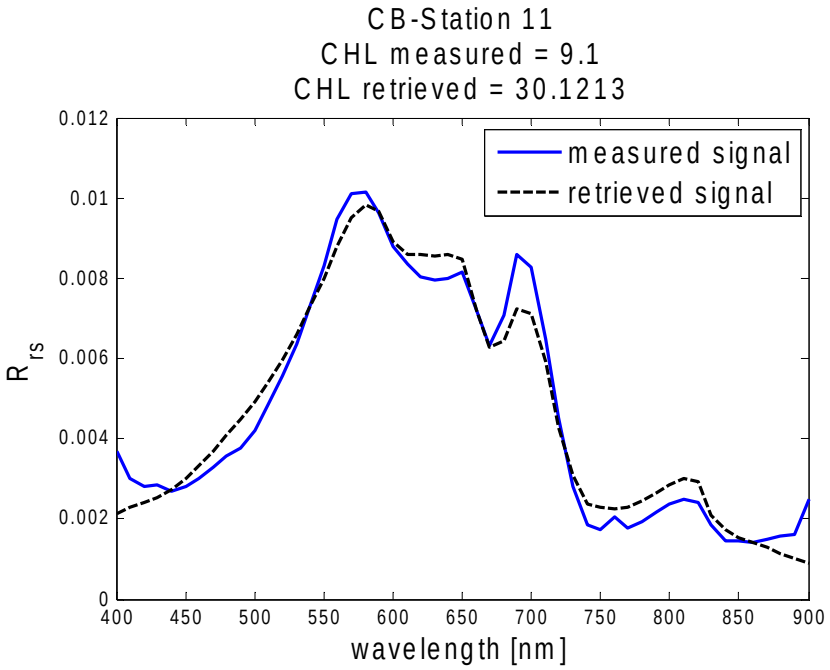

Figure 4.17 LSQ fitting result station 11

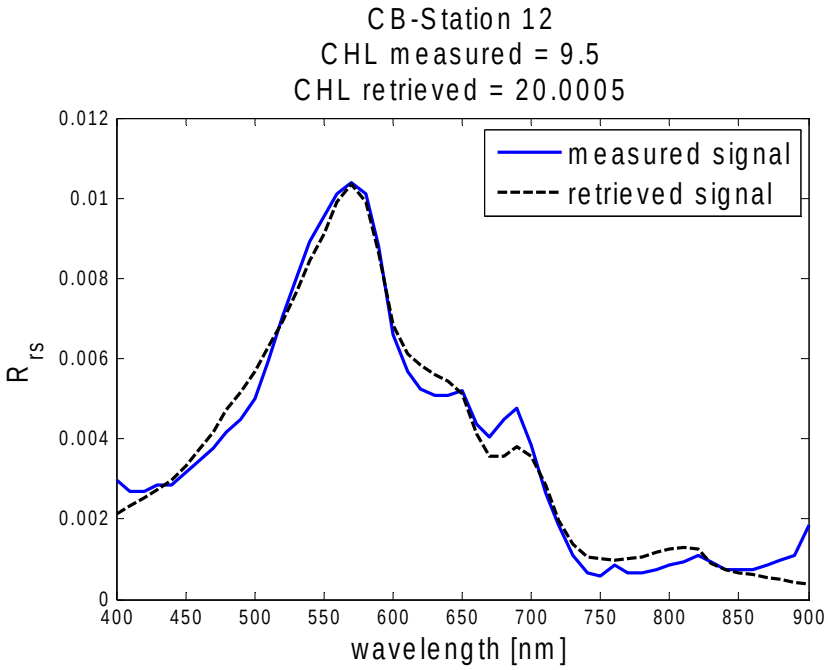

Figure 4.18 LSQ fitting result station 12

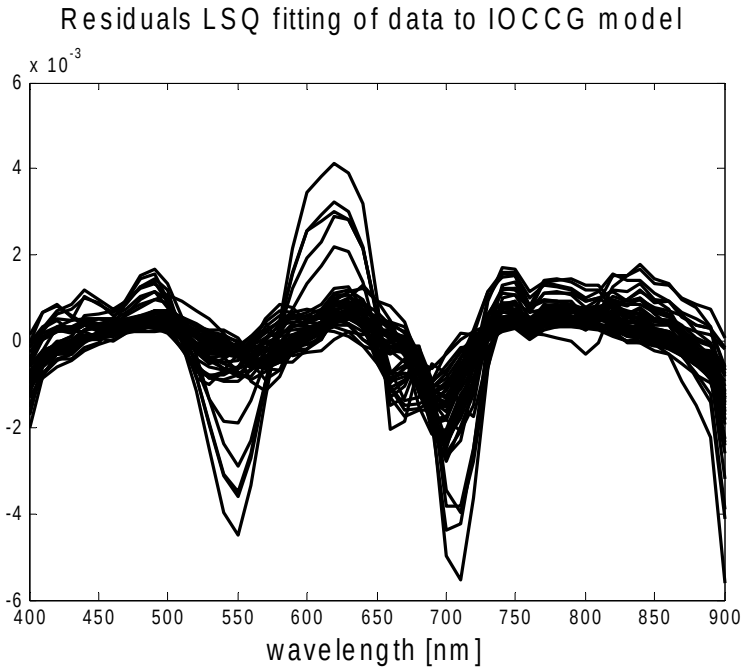

Figure 4.19 residuals of LSQ fitting of Chesapeake bay data to IOCCG model of remote sensing reflectance

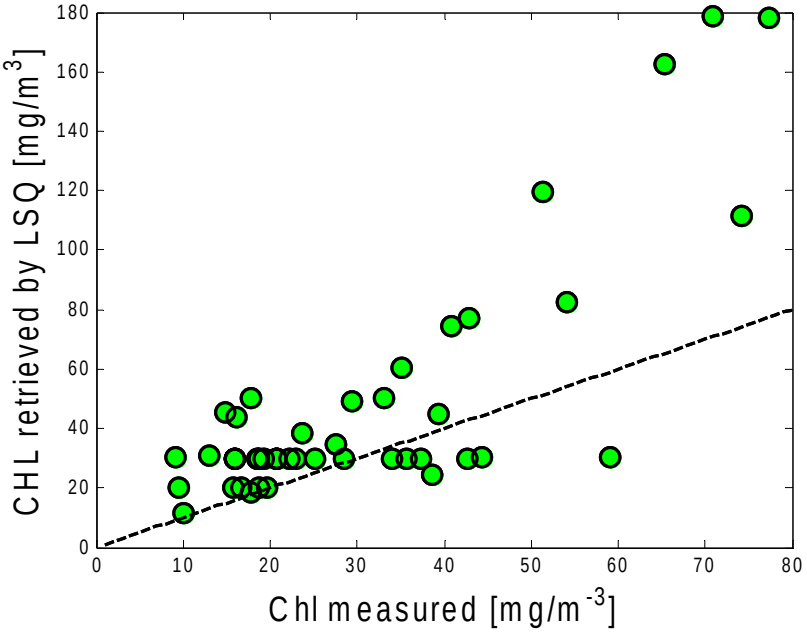

Figure 4.20 CHL measured versus CHL retrieved by LSQ fitting

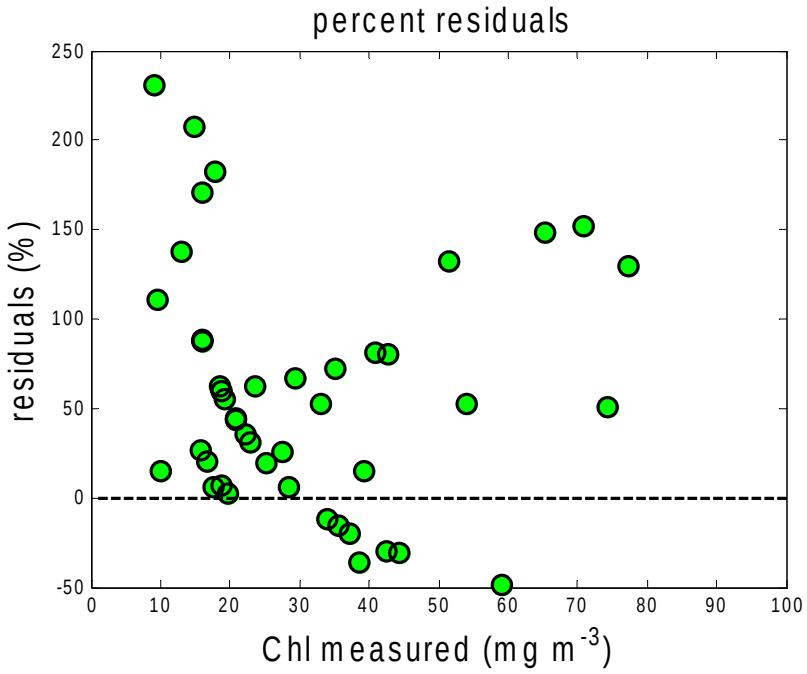

Figure 4.21 CHL residuals

References Chapter 4

[1] Mobley, C. D., Light and Water, 592, Academic Press, San Diego, CA, 1994.

[2] Bissett W. P,, Sharon DeBra, Mubin Kadiwala, David D. R. Kohler, Curtis Mobley, Robert G. Steward, Alan Weidemann, Curtiss O. Davis, Jeff Lillycrop, Robert Pope. Development, Validation, and Fusion of High Resolution Active and Passive Optical Imagery. Signal Processing, Sensor Fusion, and Target Recognition XIV, edited by Ivan Kadar, Proc. of SPIE Vol. 5809 (SPIE, Bellingham, WA, 2005)

[3] Lyzenga, D. R. 1981. Remote sensing of bottom reflectance and water attenuation parameter in shallow water using aircraft and Landsat data. Int. J. Remote Sens. 2: 71.

[4] Philpot, W. D. 1988. Bathymetric mapping with passive multispectral imagery. Appl. Opt. 28: 1569–1578.

[5] Lee, Z., K. L. Carder, R. G. Steward, T. G. Peacock, C. O. Davis, And J. L. Mueller. 1997. Remote sensing reflectance and inherent optical properties of oceanic waters derived from above-water measurements. In S. G. Ackleson [ed.], Ocean opticsXIII. Proc. SPIE 2963: 160–166.

[6] Holden, H., And E. Ledrew. 1998. Monitoring the health of coral reefs. Backscatter: Aquat. Inf. Technol. 9(3): 28–31.

[7] Lee, Z.P. and Carder, K.L., 2002. Effects of spectral band numbers on the retrieval of water column and bottom properties from ocean color data. Applied Optics, 41(12): 2191-2201.

[8] Louchard, E., Reid, R., Stephens, F., Davis, C., Leathers, R. and Downes, T., 2003. Optical remote sensing of benthic habitats and bathymetry in coastal environments at Lee Stocking Island, Bahamas: A comparative spectral classification approach. Limnol. Oceanogr., 48(1, part 2): 511-521.

[9] Stumpf, R., Holderied, K. and Sinclair, M., Mapping Coral Reef Bathymetry With High-Resolution, Multispectral Satellite Imagery, Seventh International Conference on Remote Sensing for Marine and Coastal Environments, Miami, (2002)

[10] Lee, Z., Carder, K.L., Mobley, C.D., Steward, R.G. and Patch, J.S., 1998. Hyperspectral remote sensing for shallow waters. 1. A semianalytical model. Applied Optics, vol. 37(no. 27): 6329-6338.

[11] Lee, Z., Carder, K.L., Mobley, C.D., Steward, R.G. and Patch, J.S., 1999. Hyperspectral remote sensing for shallow waters: 2. Deriving bottom depths and water properties by optimization. Applied Optics, 38(18): 3831-3843.

[12] Pope, R., and E. Fry, Absorption spectrum (380 - 700 nm) of pure waters: II. Integrating cavity measurements, Applied Optics, 36, 8710-8723, 1997.

[13] Morel, A., Optical properties of pure water and pure sea water, in Optical aspects of oceanography, edited by N.G. Jerlov, and Nielsen, E. S., pp. 1-24, Academic, New York, 1974.

[14] Roesler, C.S., M.J. Perry, and K.L. Carder, Modeling in situ phytoplankton absorption from total absorption spectra in productive inland marine waters, Limnol. Oceanogr., 34, 1510-1523, 1989.

[15] Bricaud, A., M. Babin, A. Morel, and H. Claustre, Variability in the chlorophyll-specific absorption coefficients of naturnal phytoplankton: Analysis and parameterization, J. Geophy. Res., 100, 13321-13332, 1995.

[16] Bukata, R.P., J.H. Jerome, K.Y. Kondratyev, and D.V. Pozdnyakov, Optical Properties and Remote Sensing of Inland and Coastal Waters, CRC Press, Boca Raton, FL, 1995.

[17] Stramski, D., A. Bricaud, and A. Morel, Modeling the inherent optical properties of the ocean based on the detailed composition of the planktonic community, Applied Optics, 40, 2929-2945, 2001.

[18] Roesler, C.S., and E. Boss, Spectral beam attenuation coefficient retrieved from ocean color inversion, Geophys. Res. Lett., 30 (9), 1468, 2003.

Chapter 5 Efforts to Compensate for Bright Pixel Contamination

5.1 Introduction

In coastal waters or highly turbid waters there is significant water leaving reflectance in the NIR bands due to the backscattering of particulates and even the bottom can contribute to the reflectance. Therefore, there is a need to go beyond the black pixel approximation. Efforts in this direction include the use of regression formulae connecting chlorophyll directly to NIR water leaving reflectances [1].

In this scheme, several empirical formulae based on radiative transfer calculations connecting CHL (or water leaving radiances in the visible) to the NIR water leaving radiances were developed and tested against the SeaBAM database. While the estimator in general tracks the measured water leaving signal, we found that these earlier estimators have a great deal of dispersion.

5.1.1 SeaWIFS Model

Values of $[\rho_W(\lambda)]_N$ can be modeled as a function of the spectral absorption $[a(\lambda)]$ and backscattering $[b(\lambda)]$ coefficients,

$$[\rho_W(\lambda)]_N \cong \pi\left(\frac{t}{n}\right)^2 \times \sum_{i=1}^{2} g_i \left[\frac{b_{bp}(\lambda_{NIR}) + b_{bw}(\lambda_{NIR})}{b_{bp}(\lambda_{NIR}) + b_{bw}(\lambda_{NIR}) + a_w(\lambda_{NIR})}\right]^i \qquad (5.1)$$

where the necessary parameters are presented in table 5.1

Parameters used to determine $[\rho_w(\lambda_{NIR})]_N$			
Parameter	$\lambda = 670\ nm$	$\lambda = 760\ nm$	$\lambda = 865\ nm$
$a_w(\lambda)\ (m^{-1})$	0.4346	2.550	4.286
$a_{bw}(\lambda)\ (m^{-1})$	0.00041	0.00024	0.00014
$F_0(\lambda)\ (\mu W\ cm^{-2}\ nm^{-1})$	153.41	122.24	98.82

Table 5.1 Parameters used to determine SeaWIFS $[\rho_w(\lambda_{NIR})]_N$

Here $(t/n)^2$ accounts for the transmission of upwelling radiance and downwelling irradiance across the sea surface and the constants g_1 and g_2 are 0.0949 and 0.0794 sr^{-1} respectively obtained through Hydrolight Radiative transfer algorithms. The bio-optical modeling of $b_{bp}(\lambda_{NIR})$ can take different forms.

In Case I waters where the backscatter is algal in nature, the variability in the NIR backscatter is driven by the chlorophyll content of the water

$$b_{bp}(\lambda_{NIR}) = 0.416 Chl^{0.766}\left(0.002 + \frac{550}{\lambda_{NIR}}\right) \times \{0.02[0.5 - 0.25\log_{10}(Chl)]\} \tag{5.2}$$

However, for case II waters, $b_{bp}(\lambda_{NIR})$ is derived from reflectance based estimates of $b_{bp}(\lambda)$. This parameterization assumes that the magnitude of spectral backscatter is a linear function of the water leaving reflectance at 551 nm, $[\rho_w(551)]_N$, whereas the spectral slope of particulate backscatter is a function of the ratio $[\rho_w(443)]_N$ to $[\rho_w(488)]_N$ so

$$b_{bpOC}(\lambda_{NIR}) = \{X_0 + X_1[\rho_w(551)]_N\} \times \left(\frac{551}{\lambda_{NIR}}\right)^{Y_0 + Y_1 \times \frac{[\rho_w(443)]_N}{[\rho_w(488)]_N}} \tag{5.3}$$

where the regression parameters based measurements

$X_0 = -0.00182, \quad X_1 = 0.655, \quad Y_0 = -1.13, \textit{and } Y_1 = 2.57$

If these relationships had little spread, they could be used as an estimate of the NIR radiances which can then be fed into subsequent iterations. However, as seen below, using the newest IOCCG datasets, we found that there is significant dispersion between the NIR reflectance estimators and the actual NIR values.

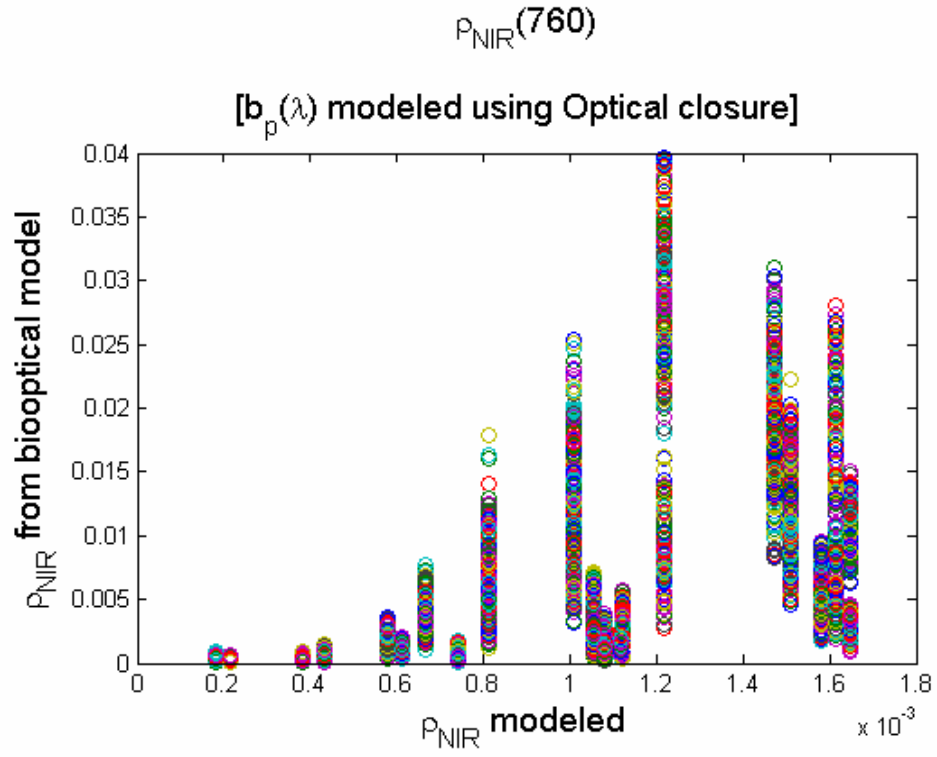

Figure 5.1 Scatter plot reflectance NIR (760)

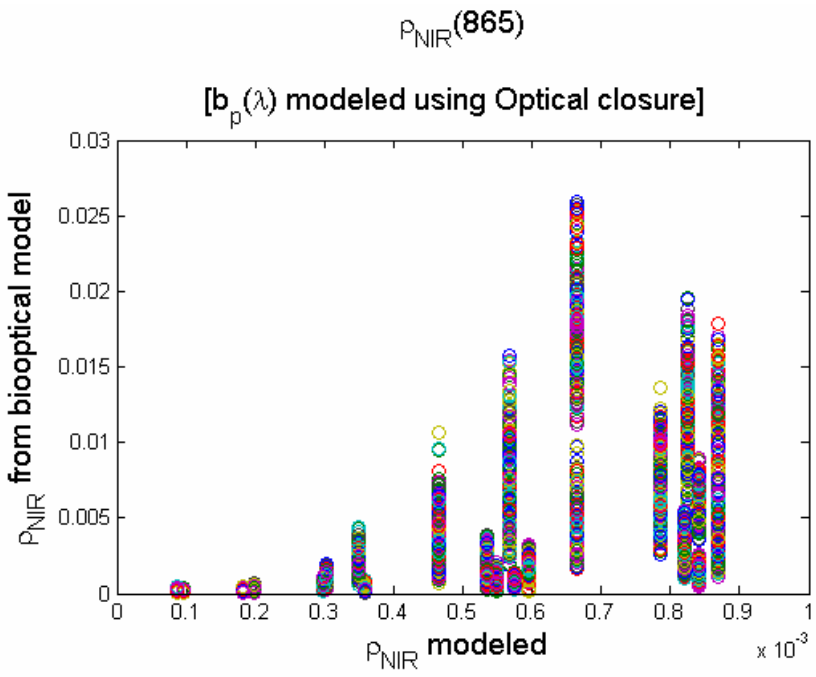

Figure 5.2 Scatter plot reflectance NIR (865)

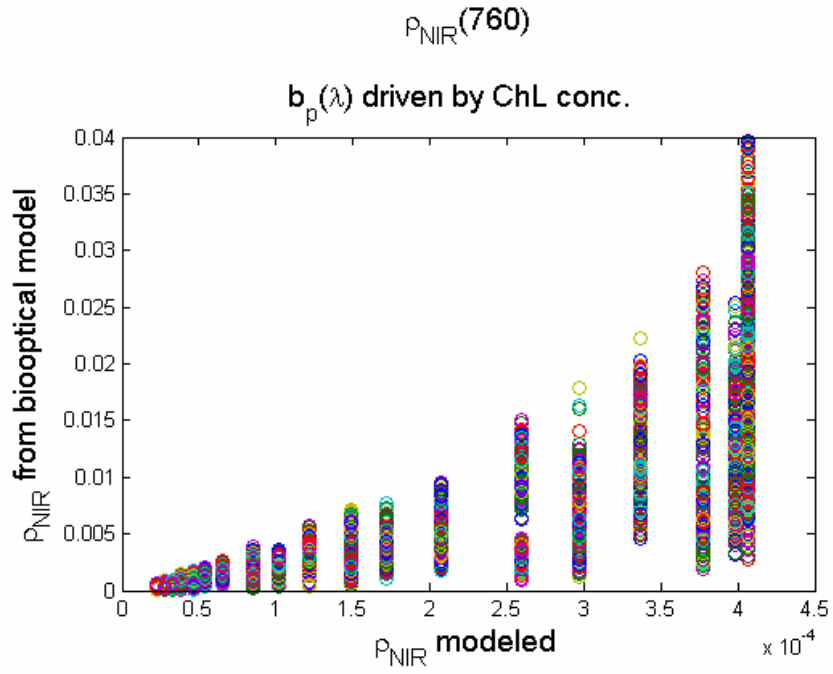

Figure 5.3 Scatter plot reflectance NIR (760)

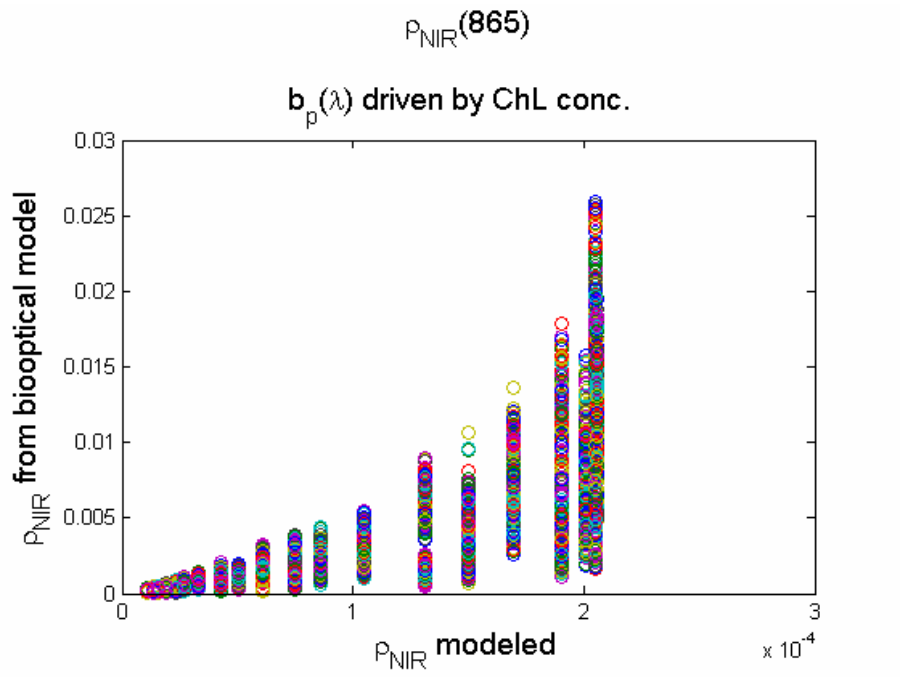

Figure 5.4 Scatter plot reflectance NIR (865)

SeaDAS uses an iterative algorithm [2] to predict the NIR reflectances based on CHL and VIS bands, the approach uses empirical relationships.

The inputs to the algorithm are CHL, $R_{rs}(551)$ and $R_{rs}(667)$.

The equations presented here were taken from SeaDAS 5 source code. The necessary parameters are presented in table 5.2.

The procedure to calculate the reflectances in the NIR is as follows:

First, compute particulate absorption at 667 (algal and non-algal)

$$a_p(667) = 0.019890 Chl^{0.817742} \tag{5.4}$$

next, compute absorption by gelbstoff and detritus at 667

$$a_{dg}(667) = 0.15 - 0.19 \times \left[\frac{R_{rs}(551) - R_{rs}(667)}{R_{rs}(551)} \right] \tag{5.5}$$

the total absorption at 667nm becomes

$$a_{tot}(667) = a_w(667) + 0.8 \times a_p(667) + a_{dg}(667) \tag{5.6}$$

then, compute normalized water-leaving reflectance at each NIR wavelength

$$bb(\lambda) = \left[\frac{-0.00113\lambda + 1.62517}{0.86807}\right] \times \frac{R_{rs}(667) \times a(667)}{0.051} \tag{5.7}$$

$$salbedo(\lambda) = \frac{bb(\lambda)}{a_w(\lambda) + bb(\lambda)} \tag{5.8}$$

$$R_{rs}(\lambda) = g_1 \times salbedo(\lambda) + g_2 \times [salbedo(\lambda)]^2 \tag{5.9}$$

$$[\rho_w(\lambda)]_N = 0.544 \times \pi \times R_{rs}(\lambda) \quad \lambda = 667, 748, 869 \tag{5.10}$$

Parameters used to determine $[\rho_w(\lambda_{NIR})]_N$			
Parameter	$\lambda = 667\ nm$	$\lambda = 748\ nm$	$\lambda = 869\ nm$
$a_w(\lambda)\ (m^{-1})$	0.5655	2.8134	4.7038
$a_{bw}(\lambda)\ (m^{-1})$	8.48E-4	5.33E-4	2.82E-4

Table 5.2 Parameters used to determine MODIS $[\rho_w(\lambda)]_N \quad \lambda = 667, 748, 869$

Using both the IOCCG synthetic data and the Chesapeake data, the SeaDAS VIS-NIR prediction algorithm provides a good linear prediction but the slope seems to need adjustment, as seen in figure number 5.5

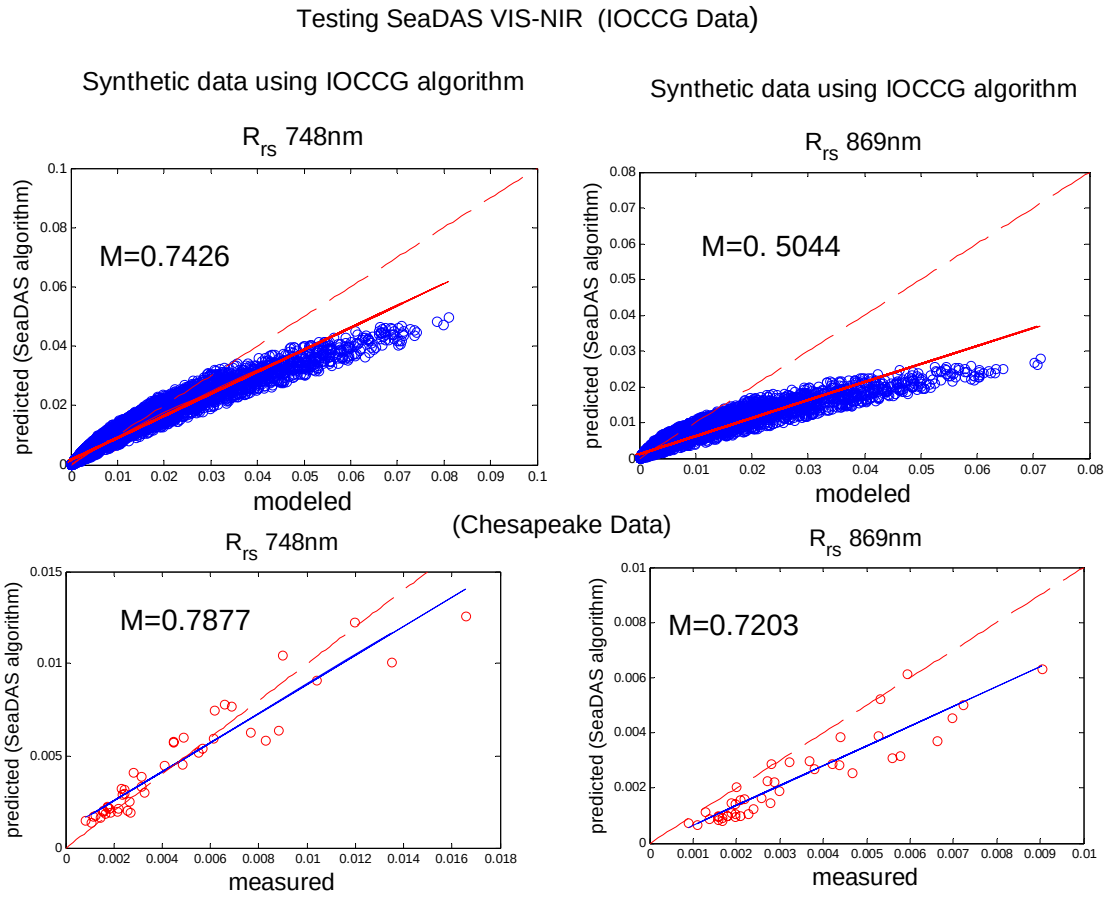

Figure 5.5 Scatter plot reflectance NIR 748 and 869 (IOCCG and Chesapeake data)

Since our intent is to study the iterative algorithm, any bias in slope will lead to biases in the retrieval. Therefore, we wanted to construct relations which were "tuned" to the Chesapeake measurements. Therefore, instead of using the SeaDAS relations, we built our own regression relations connecting the in-situ water leaving reflectances in the visible to the NIR reflectances bypassing the CHL result. The visible bands used are 550, 620 and 670nm

$$\rho_w(765,865) = a_0 + a_1\rho_w(550) + a_2\rho_w(620) + a_3\rho_w(670) \qquad (5.11)$$

The results using the dataset from the IOCCG are shown in figure 5.6a and 5.6b.

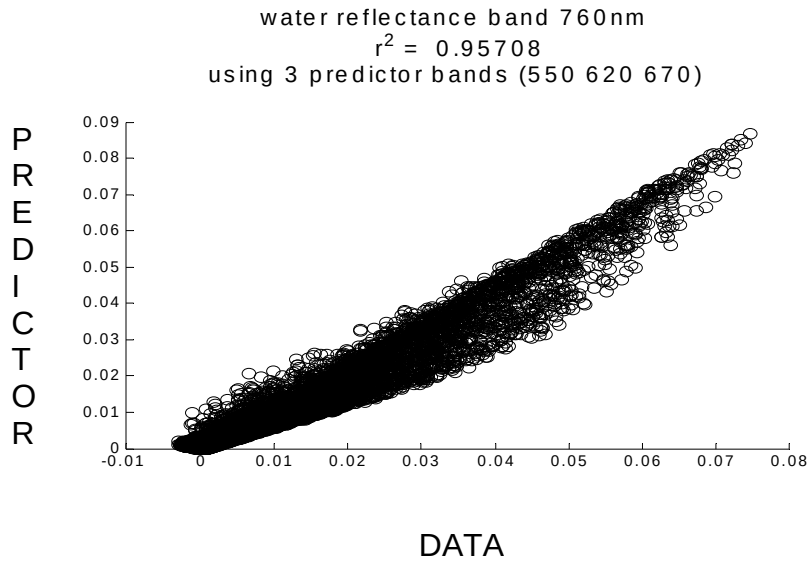

Figure 5.6a Scatter plot reflectance NIR 760nm

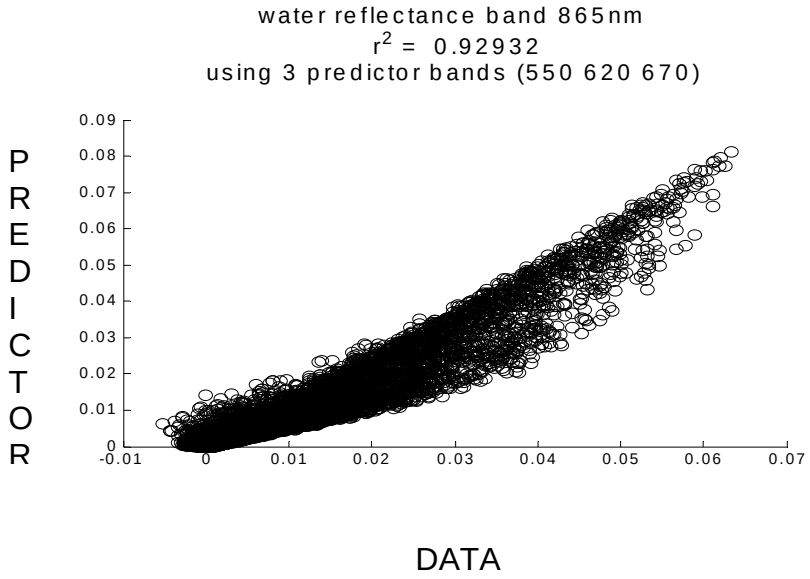

Figure 5.6b Scatter plot reflectance NIR 865nm

The results above show that the NIR estimators have significant errors which may give rise to retrieval problems. To investigate the retrieval problem, we now examine the retrieval problem using synthetic data obtained using a suitable Radiative transfer calculation.

5.2 Radiative Transfer Calculation for Synthetic Data

The signal received at TOA by an ocean color satellite sensor (i.e., SeaWIFS, MODIS) may be written as [3]

$$L_t(\lambda) = L_r(\lambda) + L_A(\lambda) + t_u(\lambda)L_{wc}(\lambda) + T_u(\lambda)L_g(\lambda) + t_u(\lambda)L_w(\lambda) \tag{5.12}$$

where $L_r(\lambda), L_A(\lambda), L_{wc}(\lambda), L_g(\lambda)$ and $L_w(\lambda)$, are the contributions to the total radiance due to molecular scattering (Rayleigh), aerosol and Rayleigh-aerosol scattering (i.e. $L_A(\lambda) = L_a(\lambda) + L_{ra}(\lambda)$), whitecaps, sunglint, and ocean water respectively. Here, $T_u(\lambda)$ and $t_u(\lambda)$ are the direct and diffuse upwelling transmittances of the atmosphere. The radiance L can be converted to reflectance ρ using the formula:

$$\rho = \frac{\pi L}{F_0 \cos\theta_0} \tag{5.13}$$

where F_0 is the extraterrestrial solar irradiance and θ_0 is the solar zenith angle. Assuming that the contributions from sunglint and whitecaps have been removed, equation (5.12) can be written as

$$\rho_A(\lambda) = \rho_t(\lambda) - \rho_r(\lambda) - t_u(\lambda)t_d(\lambda)\rho_{wn}(\lambda) \tag{5.14}$$

where the conventional normalized water reflectance which is used to separate the atmospheric illumination affects from the reflection process $\rho_{wn} = \rho_w/t_d$ has been adopted.

For conventional atmospheric correction as discussed in the introduction both SeaWIFS and MODIS have bands in the NIR (i.e., 765/865 nm and 748/869 nm respectively) for which $\rho_{wn}(\lambda)$ is assumed zero. While this is normally valid in case

I waters (Dark Pixel Approximation), coastal waters with large sediment concentrations will often have significant water leaving signals at both NIR bands. This observation has led to an approach in coastal waters of using the SWIR bands available for the MODIS sensor at 1240nm and 2130nm in which the dark pixel assumption is valid under all reasonable conditions [4],[5]. This approach is further investigated in section 6.

In either case, although the wavelengths are different, the approach is the same. Defining λ_s and λ_l to represent the shorter and longer IR bands, the multiple scattering epsilon function $\varepsilon^{MS}(\lambda_s,\lambda_l) = \rho_A(\lambda_s)/\rho_A(\lambda_l)$ may be obtained directly from the aerosol models generated within a pre-calculated look up table (LUT) and equated to the top of atmosphere (TOA) result within the dark pixel approximation. Since the aerosol spectral slope is not very sensitive to optical depth, the resultant epsilon value can be then used to select the most appropriate aerosol model from the suite of aerosol models. Once the aerosol model is determined, the optical depth for that aerosol model can then be determined by equating the aerosol reflectance $\rho_{A,Mod}(\lambda_s,\tau)$ to the TOA reflectance. Once the aerosol model and optical depth at λ_S is determined, the atmospheric contribution can be obtained from the LUTs for all relevant wavelengths and the ocean reflectance $\rho_{wn}(\lambda)$ calculated from equation (5.14) for the visible bands.

5.3 Iterative retrieval algorithm

The numerical approach utilizing the NIR estimators in an iterative scheme is as follows.

Step #1. Apply the Black Pixel approximation to get estimates of Rrs in the visible channels.

Step #2. Obtain first estimate of NIR water signal based on the NIR estimators employed by the SeaDAS Algorithm.

Step #3 Reestimate atmosphere signal in the IR channels and go back to step 1.

The algorithm is applied to two cases. In the first case, the atmosphere over the bright pixel is taken to be one of the representative atmospheres in the SeaDAS database (figure 5.7a) while in the second case, the atmosphere was chosen to have spectral variability outside the SeaDAS database (figure 5.7b) which was indicative of urban fine particulate matter.

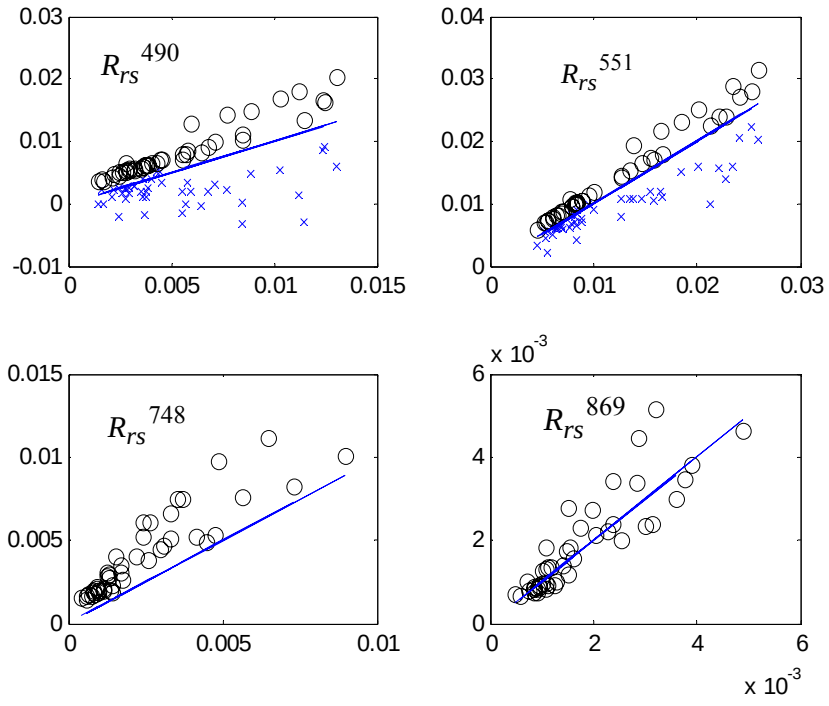

Fig 5.7a Iterative retrieval of water leaving reflectance for Chesapeake waters using SeaDAS Atmosphere (x=Iteration 1 (BP), o=Iteration 10)

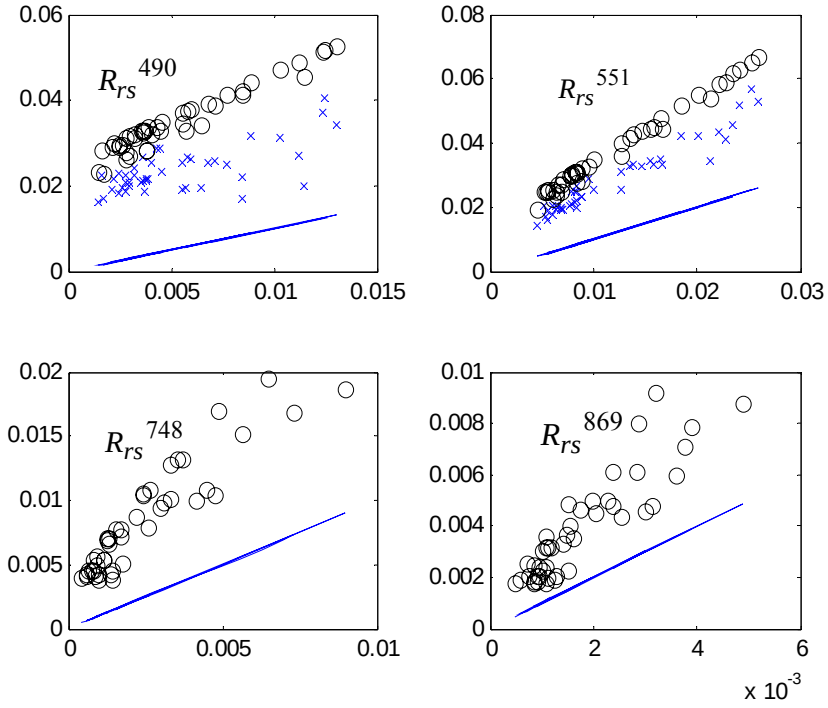

Fig 5.7b Iterative retrieval of water leaving reflectance for Chesapeake waters using High Angstrom Coefficient Atmosphere outside SeaDAS database (x=Iteration 1 (BP), o=Iteration 10)

We find in general that if the atmosphere is within the SeaDAS database, an improvement on the Dark Pixel estimates is obtained. However, for atmospheres outside the SeaDAS database, we find that the result is worse due to an unevenness in the water leaving reflectance estimator performance between the two NIR atmosphere channels.

These experiences with the iterative "closure" algorithms show the importance of extending the atmospheric database to be more representative of the aerosol spectral variability. This theme is taken up in chapter 6 where again it is demonstrated in more detail the necessity for more representative aerosols while highlighting the problems associated with extending the database.

References Chapter 5

[1] Siegel D. A., M. Wang, S. Maritorena, and W. Robinson, "Atmospheric Correction of Satellite Ocean Color Imagery: The Black Pixel Assumption," Appl. Opt. 39, 3582-3591 (2000)

[2] Stumpf, R. P., R. A. Arnone, R. W. Gould, P. M. Martinolich, and V. Ransibrahmanakul (2003), A Partially Coupled Ocean-Atmosphere Model for Retrieval of Water-Leaving Radiance From SeaWiFS in Coastal Waters, SeaWiFS Postlaunch Tech. Rep. Ser., vol. 22, NASA Tech. Memo. 2003-206892, edited by S. B. Hooker and E. R. Firestone, pp. 51– 59, NASA Goddard Space Flight Cent., Greenbelt, Md.

[3] Wang, M., 2002, The Rayleigh lookup tables for the SeaWiFS data processing: Accounting for the effects of ocean surface roughness. International Journal Remote Sensing, 23, 2693–2702.

[4] Wang M. and W. Shi "Estimation of ocean contribution at the MODIS near-infrared wavelengths along the east coast of the U.S.: Two case studies" Geophys. Res. Lett, 32, L13606, doi:10.1029/2005GL022917, (2005)

[5] Franz, B.A., P.J. Werdell, G. Meister, E.J. Kwiatkowska, S.W. Bailey, Z. Ahmad, and C.R. McClain (2006). MODIS Land Bands for Ocean Remote Sensing Applications, Proc. Ocean Optics XVIII, Montreal, Canada, 9-13 October 2006.

Chapter 6 Improving The SWIR Retrieval Algorithm Using Water Leaving Reflectance Constraints at 412nm

6.1 Introduction

The traditional atmospheric correction algorithm [1] used by SeaWIFS and MODIS make use of the NIR bands to estimate the aerosol type. The method requires a priori knowledge of the water-leaving radiance in these longer wavelengths to separate the aerosol and water contributions to the total radiance. To compensate for bright pixel contamination, SeaDAS employs an iteration scheme [2] to estimate the water-leaving radiances in the NIR from retrieved water-leaving radiances in the visible, but the modeling approach is based on empirical relationships that may not be valid in all waters and will result in significant sources of error. In contrast, as seen in figure 6.1, since water is so strongly absorbing in the SWIR spectral regime, even highly reflective turbid waters appear black and no compensation should be needed.

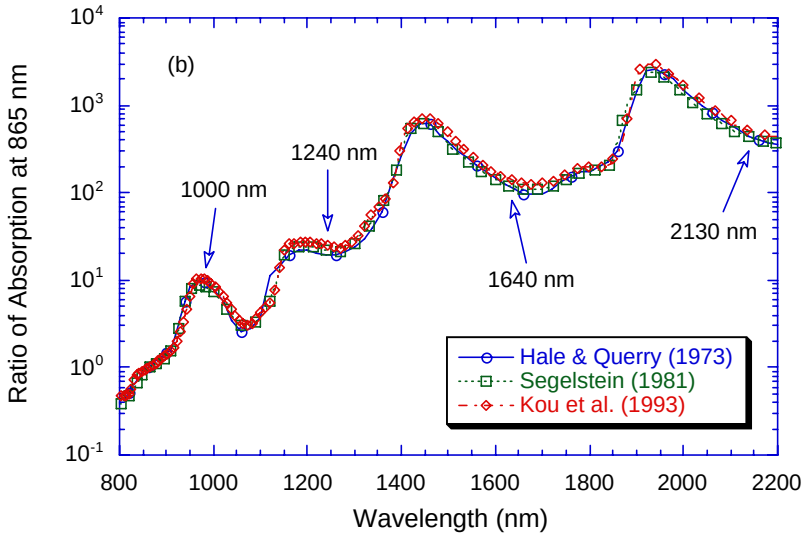

Figure 6.1 water absorption normalized to 865 (from Menghua Wang NOAA/NESDIS/ORA)

From this observation [3], the SWIR bands at 1240 and 1640 were used to determine aerosol model and optical depth. Similarly to the NIR scheme, this information can then be extrapolated to the visible wavelengths via aerosol models, but since the SWIR bands are quite noisy and the aerosol signal in the SWIR is quite low, and the extrapolation error to the VIS channels is large, it is expected [4] that without additional constraints on atmospheric retrieval, retrieval errors can be quite severe.

In order to explore the accuracy of the newly developed SWIR correction scheme which was designed to remove the bright pixel contamination, we run extensive computer simulations and show that significant retrieval errors in the blue wavelengths will occur if a more diverse atmospheric model set combining oceanic and local aerosol models are used. However, we find that the use of the 412nm sounding channel can significantly reduce retrieval errors for biologically productive waters such as the Chesapeake Bay in which the 412nm water leaving signal is significantly reduced through a combination of CDOM and CHL absorption providing a strong constraint on the aerosol models at 412nm. From our calculations, the tight constraints imposed make it possible for a more diverse and representative set of aerosol models based on global and local climatology to be incorporated.

6.2 Measurements of Reflectance Spectra

To obtain an estimate on the magnitude and statistics of the 412 nm water leaving reflectance $\rho_{wn}(412)$, in-situ measurements were carried out at 44 stations (shown in figure 3.13) across the whole Chesapeake Bay area from July 11th to 20th 2005. The upwelling radiance and downwelling irradiance in the water were

collected and measured by a GER spectroradiometer. The fiber probe for upwelling measurements was placed just beneath the surface so it was necessary to take into account the surface fresnel effect to obtain the above water radiance. The downwelling irradiance (measured above the water) was obtained using a diffuse spectralon reflector.

The normalized water leaving reflectance spectra are plotted in figure 6.2. The resultant spectra clearly show two distinct features. First, we note the very low reflectance in the blue due to the high absorption by CDOM in these coastal waters. Second, we see the non-negligible reflectance in the NIR (765,865) due to the high total backscattering coefficient. Simultaneous fluorometer measurements were also taken with the chlorophyll concentration measured in the range 9.1 to 77.4 mg/m^3. From this limited set, a first estimate of the normalized reflectance could be set to $\rho_{wn}(412) \approx .003 \pm .0015$. It is this uncertainty in the water leaving signal that results in the largest uncertainty of the aerosol reflectance $\rho_a(412)$ which can be simply expressed as $\sigma(\rho_a(412)) \sim \bar{t}_d(412)\bar{t}_u(412)\sigma(\rho_{wn}(412)) < \sigma(\rho_{wn}(412))$ where $\bar{t}_{d,u}$ represent the mean diffuse downwelling and upwelling transmission factors. Other perturbations to the TOA signal such as those due to ozone and NO_2 can be corrected with concentration information obtained using UV profilers such as the OMI sensor on Aura [5].

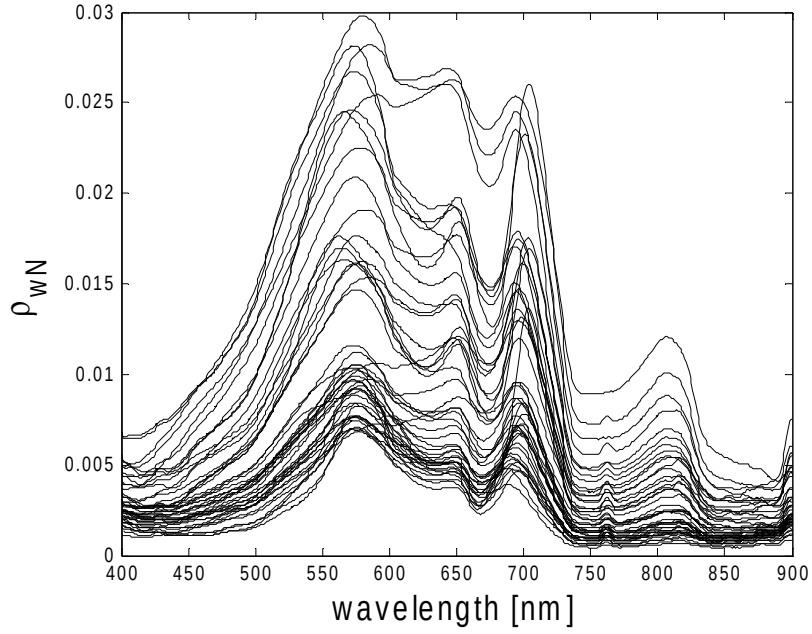

Figure 6.2 Field Measurement Normalized Water Leaving Reflectance Spectra

This dataset is clearly not as extensive as we would like so we have also extracted all the $\rho_{wn}(412)$ in situ data stored in the NOMAD database [6],[7]. The combined datasets within the Chesapeake Bay confines totaled 276. In figure 6.3, the geographical distribution of $\rho_{wn}(412)$ is displayed with the color coding providing the $\rho_{wn}(412)$ measurement values. This clearly shows the general trend that the reflectance increases at the lower part of the bay in comparison to the middle and upper bay measurements. The location of the Aeronet site at the MD Science Center is also illustrated since we will make use of the aerosol models obtained there.

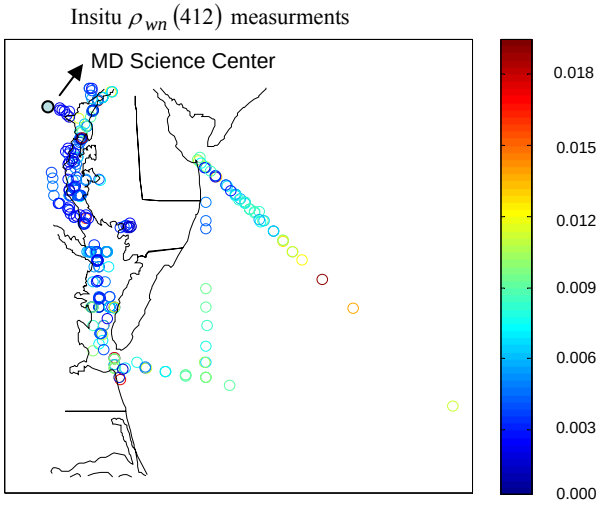

Figure 6.3 Field Measurement Normalized Water Leaving Spectra at 412nm

With this larger dataset, we can refine our best statistical estimates of $\rho_{wn}(412)$ and determine the level of confidence we have for a particular estimator. In particular, we plot in figure 6.4, the cumulative probability that a measurement will lie within the following measurement bounds:

$$.005 - \Delta\rho_{wn} \le \rho_{wn}(412) \le .005 + \Delta\rho_{wn} \qquad (6.1)$$

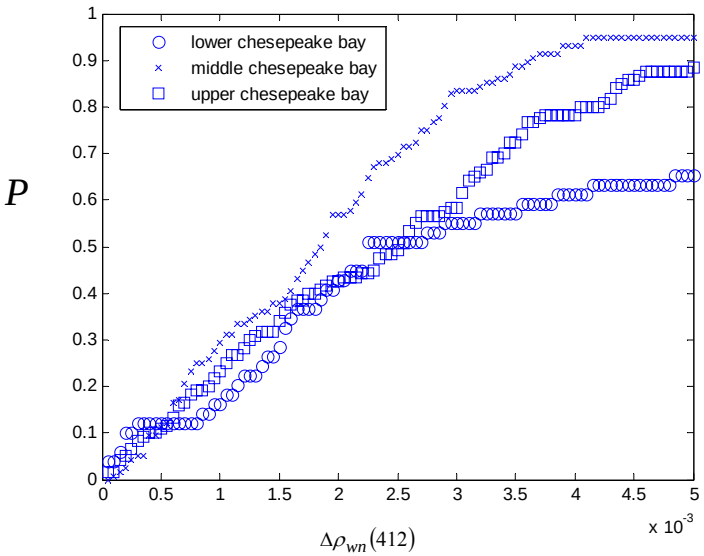

Figure 6.4 Cumulative probability distribution of measurements within a restricted range

The results show that for both the middle and upper Chesapeake regions, the cumulative probability (P) reaches the 2σ (95%) confidence value when $\Delta\rho_{wn}(412) = .005$

Recalling the fact that this upper bound should be multiplied by the two-way diffuse transmission, the confidence levels we used are conservative and a more refined analysis taking into account the diffuse transmission is performed in section 3.

6.3 Aerosol Model Selection

In order to assess the uncertainty in the normalized water leaving reflectance inherent in the SWIR approach as well as to assess the utility of the statistical estimates of $\rho_{wn}(412)$ in reducing the retrieval uncertainty, we need to calculate the appropriate LUTs based on a more representative set of atmospheric models. At present, SeaDAS uses 12 aerosol models [8] in the standard processing; these are the oceanic, maritime and tropospheric models which are based on the models developed by Shettle and Fenn [9]. Gordon and Wang [1] introduced the coastal aerosol model to represent the aerosol over the oceans near the coast. These aerosol models are the oceanic model with relative humidity of (RH= 99%) (denoted as O99), the maritime model with RH= 50%, 70%, 90% and 99% (denoted as M50, M70, M90, and M99), the coastal model with RH= 50%, 70%, 90% and 99% (denoted as C50, C70, C90, and C99), and the tropospheric model with RH= 50%, 90% and 99% (denoted as T50, T90, and T99). This suite of aerosol models is used to generate the aerosol LUTs and represents mostly non-absorbing and weakly absorbing aerosols [8].

To illustrate the variability of the SeaDAS aerosol models, figures 6.5 and 6.6 show the spectral variation of the epsilon function relevant for the NIR correction and SWIR correction $\varepsilon(\lambda,869) \equiv \rho_{aer}(\lambda)/\rho_{aer}(869)$; $\varepsilon(\lambda,2130) \equiv \rho_{aer}(\lambda)/\rho_{aer}(2130)$ which illustrates the spectral behavior of the aerosol path reflectance for both the NIR and SWIR correction schemes. The solar and view angles were chosen to maximize the atmospheric perturbations and to avoid sun-glint as follows: solar zenith angle of 60^o, sensor zenith angle of 45^o, and relative azimuth angle of 90^o.

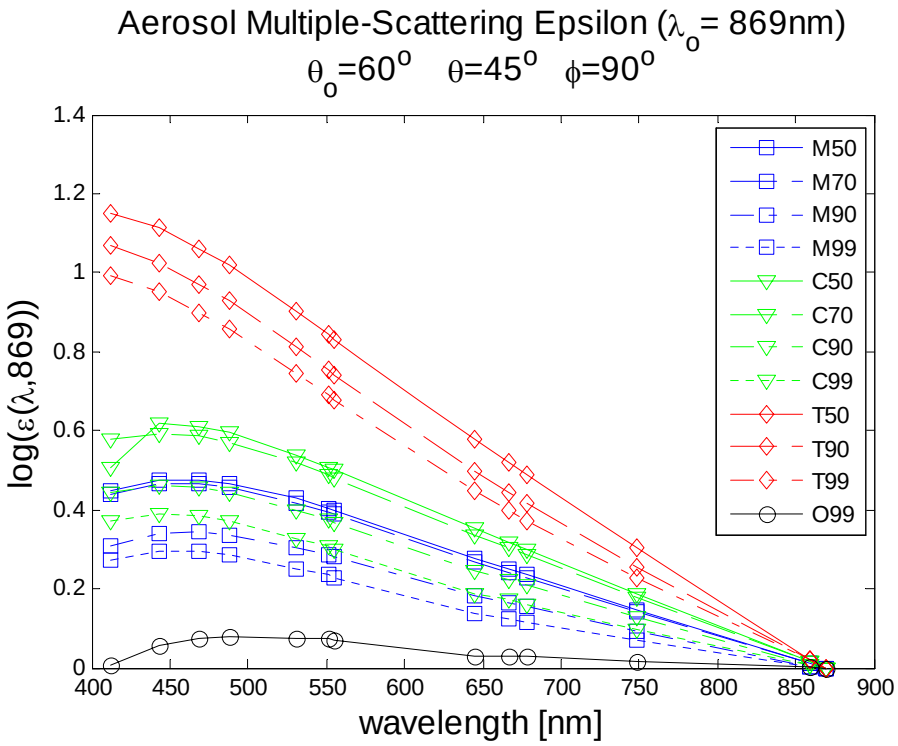

Figure 6.5 Aerosol multiple-scattering epsilon ($\lambda_0 = 869$ SeaDAS models)

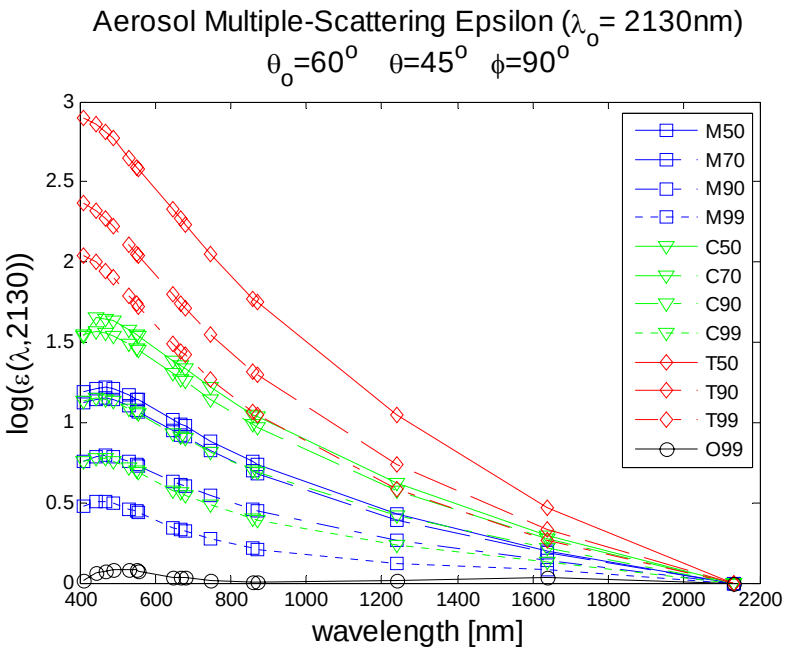

Figure 6.6 Aerosol multiple-scattering epsilon ($\lambda_0 = 2130$ SeaDAS models)

Unlike the SeaDAS approach for estimating atmospheres over water using climatological models, the MODIS retrieval of aerosol properties is governed by Aeronet based models. In the conventional scheme, a set of fine and coarse models are obtained through a cluster based analysis [10] and the retrieval is based on linear mixing of the finer and coarse modes. One approach to develop a reasonable LUT based on this scheme would be to use a linear mixture of all possible modes with a wide variety of mixing ratios to build up the database. However, it is much more representative to build up the LUT based on existing atmospheric Aeronet retrievals over a specific geographic region. In particular, since we are looking specifically at the Chesapeake Bay, we use the MD Science Center (see fig 6.3) retrievals over a period from 2000-2005. For these aerosol models, the aerosol optical depth (AOD) at 550 nm is taken to be variable ranging from 0.05-0.5 in .05 increments which covers the range of realistic AOD.

Table 6.1 Parameters and ranges used in Radiative Transfer LUT

Variable name	Symbol	Range
Wavelength	λ	(400:10:900,1240,1650,2130)
Sensor viewing angle	θ_V	(0,15,30,45,60)
Solar angle	θ_S	(0,15,30,45,60)
Azimuth	φ	(0,45,90,180)
Aerosol optical thickness	τ	(0.05:0.05:0.5)

While the SeaDAS LUTs were obtained directly from the SeaDAS 5.0 database, the atmospheric aerosol LUTs were generated with the SHARM radiative transfer code [11]. To obtain aerosol reflectance and diffuse transmission values in the SWIR bands is problematic since the aerosol models were themselves derived primarily from optical measurements $\lambda \le 1um$. Where anomalous non-monotonic spectral behavior (in the aerosol between the NIR and SWIR bands) was observed, the models were filtered out of the database. After filtering, the total number of aerosol models was 159. Furthermore, since we are primarily interested in intercomparisons of the retrieval error using different LUT, we ignore the whitecap and glint contributions in this study.

In building the LUT, the traditional approach is to use one dimension for the aerosol model and another dimension for the optical depth. This is convenient when the aerosol model is determined from the aerosol reflectance ratio epsilon (ε) parameter and afterwards the optical depth (τ) is obtained from the aerosol reflectance so the retrieval is decoupled. In our approach, we choose to merge both the aerosol model and optical depth variability together so that an atmosphere is defined by the combination of the phase function and AOD (i.e., 1590 atmospheres)

and use the TOA measurements to constrain aerosol phase function and optical depth simultaneously. This allows us to get a more accurate description of the ensemble of atmospheric models that fall within the measurement constraints which allows for a more suitable retrieval error analysis.

To see how the aerosol models compare, we plot in figures 6.7 and 6.8 the epsilon factors $\log[\varepsilon(\lambda,2130)]$ for both SeaDAS and AERONET based atmospheres.

In particular, a large number of high angstrom coefficient aerosol models $1 \le \log[\varepsilon_{aeronet}(412,2130)] \le 4$ are observed in AERONET which are not included in the SeaDAS LUTs $0 \le \log[\varepsilon_{SeaDAS}(412,2130)] \le 2.5$.

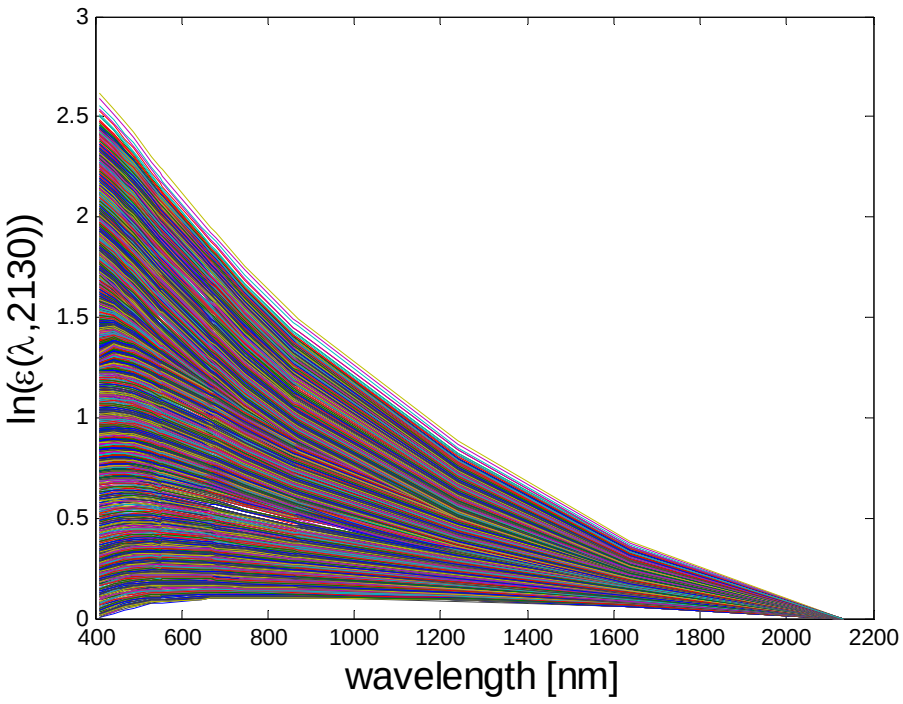

Figure 6.7 SeaDAS LUT ε factors

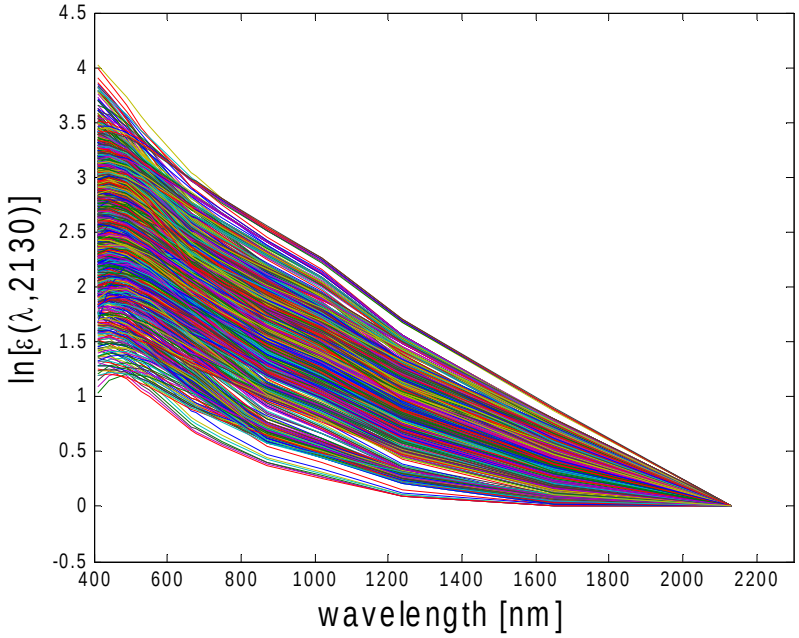

Figure 6.8 Aeronet LUT ε factors

To account for the natural variability of aerosols, it would be advantageous to combine the complementary databases using a-priori statistics to weight the likelihood of each individual elements. However, the data needed to obtain such a true weighting is limited by the restrictions placed on the AERONET retrieval which result in retrievals biased to high angstrom coefficient, making it impractical to assign relative weights to elements in the LUT. Instead, we will focus on the worst case scenario where the weights of the databases are taken to be equal. It is our purpose to show that even in this extreme case, where the uncertainties in the retrieval are expected to be very large, the constraint imposed at 412nm on the upwelling water reflectance for the Chesapeake is sufficient to reduce the retrieval errors compared to those based on the restricted SeaDAS database.

6.4 Water Leaving Reflectance Error budget

Once the appropriate LUT's are constructed, we can assess the retrieval errors for the normalized water reflectance which occur due to the uncertainties in the atmospheric model determination. As discussed earlier, the main contributor to the uncertainty seen on the VIS channels can be ascribed to the atmospheric retrieval since auxiliary measurements of total path ozone and NO_2 [3],[12] reduce gaseous transmittance and gas-aerosol uncertainties.

Based on the radiative transfer model formulation given in equation (5.14), the retrieval error is due to uncertainties in the atmospheric reflectance ρ_a retrieval, the error in the diffuse two-way transmission $\left(t^2 = t_d \times t_u \right)$ retrieval as well as the mean value of the normalized water leaving reflectance and mean value of the diffuse two-way transmission itself. The retrieval error is easily calculated based on the standard formalism for the propagation of errors as:

$$\sigma(\rho_{wn})_{k,j} = \sqrt{\left(\frac{\sigma(\rho_a)_{k,j}}{\overline{\rho}_{wn,j} \left\langle t^2 \right\rangle_{k,j}} \right)^2 + \left(\frac{\sigma(t^2)_{k,j}}{\left\langle t^2 \right\rangle_{k,j}} \right)^2} \qquad (6.2)$$

where the index (k) labels the atmosphere model and index (j) is the wavelength.

To obtain the atmospheric retrieval error parameters $\sigma(\rho_a)_{k,j}, \left\langle t^2 \right\rangle_{k,j}, and\ \sigma(t^2)_{k,j}$ we need to calculate for a given atmospheric reference (*k*), the set of possible atmospheres (*i*) with reflectance indistinguishable

from the reference within the sensor noise which is usefully expressed as the Noise Equivalent Reflectance parameter ($NE\Delta\rho_j$) for each of the atmospheric sensing channels (l) used in the atmospheric retrieval. In mathematical terms,

$$i \in S_k \quad iff \ \left\| \rho_i^{LUT}(\lambda_l) - \rho_k^{LUT}(\lambda_l) \right\| \le NE\Delta\rho_l \quad l = all\ atmospheric\ spectral\ bands \tag{6.3}$$

Once the appropriate atmospheric model set S_k is determined, the aerosol reflectances and diffuse transmission at given visible wavelength channel *(j)* can be calculated and the mean and standard deviations obtained over the set of atmospheres. For instance the mean diffuse two-way transmission for atmosphere reference (k) and spectral channel (j) can be written as:

$$\overline{\left(t^2\right)}_{k,j} = \frac{1}{N_k} \sum_{i \in S_k} \left(t^2\right)_{i,k} \tag{6.4}$$

where N_k is the number of elements in S_k

6.5 Algorithm Sensitivity Studies

To begin our analysis, the radiometric sensitivities of the MODIS channels must be specified. The MODIS noise equivalent radiances ($NE\Delta L$) were taken from IOCCG report 1 [13]. These radiances were converted to noise equivalent reflectances using $NE\Delta\rho = \frac{\pi \times NE\Delta L}{F_0 Cos(\theta_0)}$, where F_0 is the solar extraterrestrial irradiance.

The noise equivalent reflectances are given in Table 6.2

Band	Wavelength [nm]	NEΔρ
8	412	1.818×10^{-4}
9	443	1.019×10^{-4}
10	488	8.10×10^{-5}
11	531	6.01×10^{-5}
12	551	6.38×10^{-5}
13	667	3.39×10^{-5}
14	678	2.93×10^{-5}
15	748	4.63×10^{-5}
16	869	4.08×10^{-5}
5	1240	5.069×10^{-4}
6	1650	3.618×10^{-4}
7	2130	2.967×10^{-4}

Table 6.2 MODIS Noise Equivalent Delta Reflectances NEΔρ for a solar angle of 60 degrees

These noise levels are calculated for the individual pixel but in accordance to the aerosol retrieval algorithms for MODIS [14] the SWIR channels are first aggregated into 10km x 10km boxes which pass through a series of filters for clouds, glint etc. The final retrieval requires that number of quality pixels $N_p > 30$ which we set as our standard. Therefore, all per pixel $NE\Delta\rho$ values are reduced by the square root of the pixel number $NE\Delta\rho / \sqrt{N_p}$

6.6 NIR algorithm with water leaving estimator.

Before beginning sensitivity studies using the SWIR, we first revisit the traditional NIR atmospheric correction scheme. In the standard operating procedure for coastal waters, the black pixel approximation is no longer used and an NIR estimator based on normalized water leaving reflectances in the VIS (and CHL estimates) is used to predict the NIR normalized water leaving reflectance [2].

In figure 6.9, we plot the % error in the estimator relative to the measurement for $\rho_{wn}(760)$ and observe that the error in the estimator (at the 1σ level) is about 10%. with slightly poorer results for the 865nm channel. With this assessment of the errors in the compensation possible in the NIR channels, we define channel errors on the NIR bands to be $NE\Delta\rho(\lambda_{NIR}) = f\,\overline{\rho_{wn}(\lambda_{NIR})}$

where mean normalized water leaving reflectances obtained from our measurement database are used and f is the bright pixel compensation error. For example, $f = 1$ corresponds to no attempt at correcting for bright pixels, $f = 0.1$ corresponds to an estimate of the bright pixel to 10% and $f = 0.01$ corresponds to a level of bright pixel compensation to the 1% level.

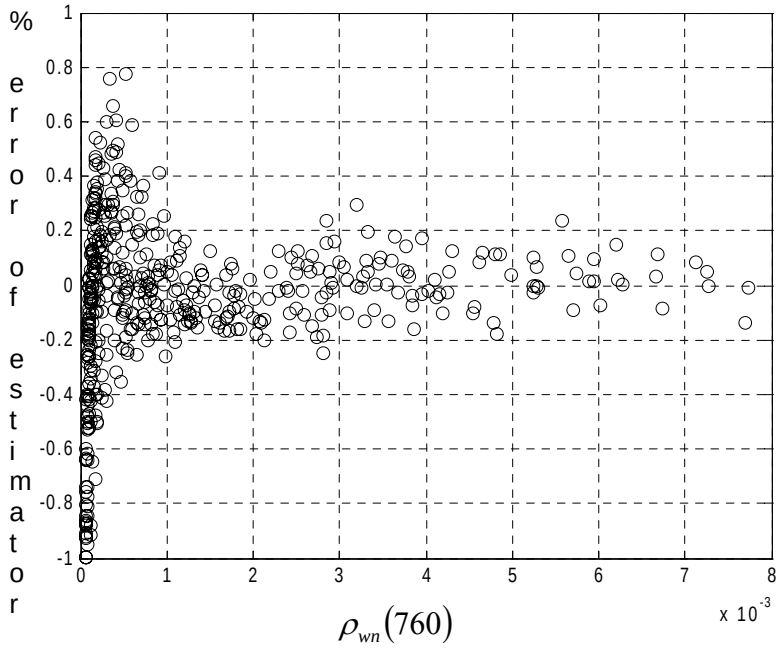

Figure 6.9 % error in the NIR estimator relative to the measurement at 760nm

The results are presented in figure 6.10 as a statistical cumulative distribution function of fractional normalized water leaving reflectance uncertainties in the visible wavelengths relevant to CHL retrieval over the set of all possible atmospheres

in the atmospheric LUT. The results of figure 6.10 illustrate that for the limited SeaDAS atmospheric database, at the 1σ level, $\rho_{wn}(443) \approx 25\%, \rho_{wn}(488) \approx 13\%,$ and $\rho_{wn}(551) \approx 4\%$. However, the same calculation based on the cumulative (SeaDAS + Aeronet) Database results in extremely high errors of $\rho_{wn}(443) \approx 120\%, \rho_{wn}(488) \approx 50\%, \rho_{wn}(551) \approx 10\%$. In particular, we note the large error in the 443 channel which dominates the error in all CHL algorithms currently employed [22].

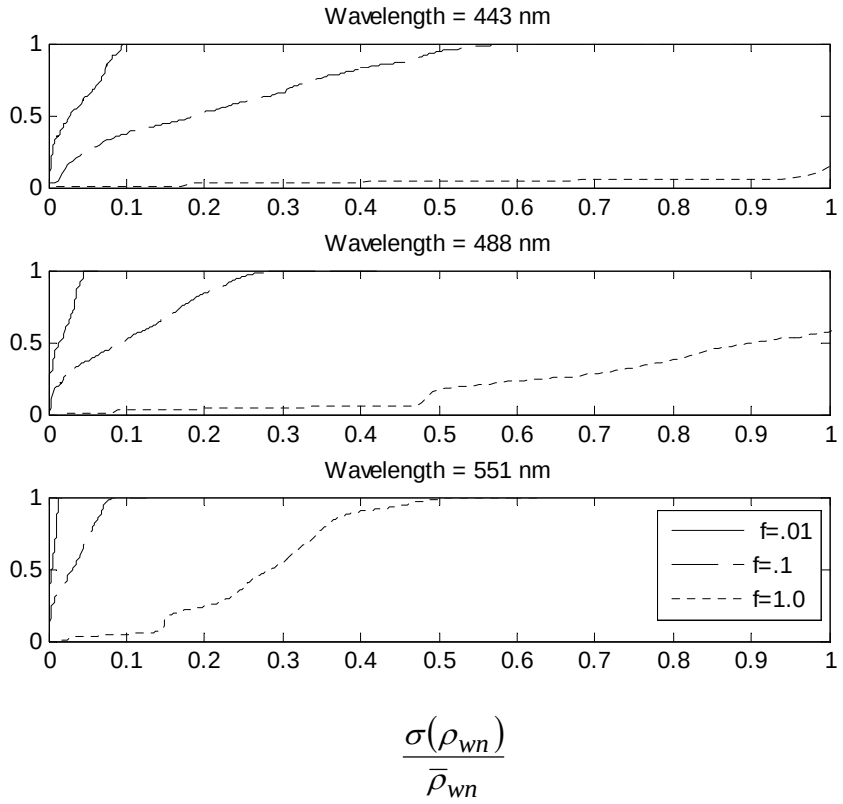

Figure 6.10 Statistical cumulative distribution function of fractional normalized water leaving reflectance uncertainties using the NIR retrieval algorithm on the SeaDAS with different bright pixel compensation levels a) 443nm b) 488nm c) 551nm

6.7 SWIR algorithm with water leaving constraints

For the SWIR correction scheme (using bands 1240,2130nm), we first examine the retrieval uncertainty using the SeaDAS LUT. The results are shown in figure 6.11 for a) no constraint at 412nm, b) for 1σ constraint $\rho_{wn}(412) = .005 \pm .003$ and c) 2σ constraint $\rho_{wn}(412) = .005 \pm .005$. The results show that for the limited SeaDAS LUT, the effect of the 412nm constraint is minimal. However, it is interesting to note that the errors using the SWIR are approximately $\rho_{wn}(443) \approx 20\%$, $\rho_{wn}(488) \approx 10\%$, and $\rho_{wn}(551) \approx 3\%$ which is ~ 25% improvement which shows the usefulness of the SWIR approach in general.

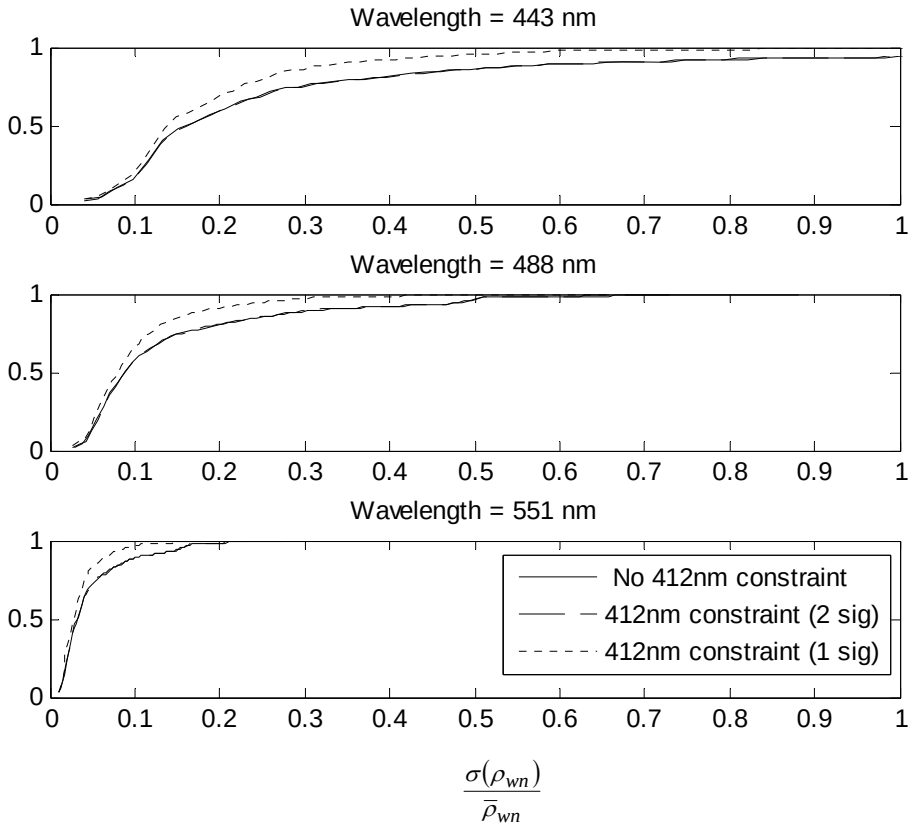

Figure 6.11 Statistical cumulative distribution function of fractional normalized water leaving reflectance uncertainties using the SWIR retrieval algorithm on the SeaDAS with different 412nm water leaving reflectance constraint levels a) 443nm b) 488nm c) 551nm

However, when the combined SeaDAS + Aeronet tables are used, the 412nm constraint is much more important as seen in figure 6.12. Without the 412 constraint, the errors at 443nm become very large. The conservative 2σ constraint helps reduce the errors to some extent but with the more stringent 1σ constraint, the errors in the water leaving retrievals are commensurate with the results using the SeaDAS database alone.

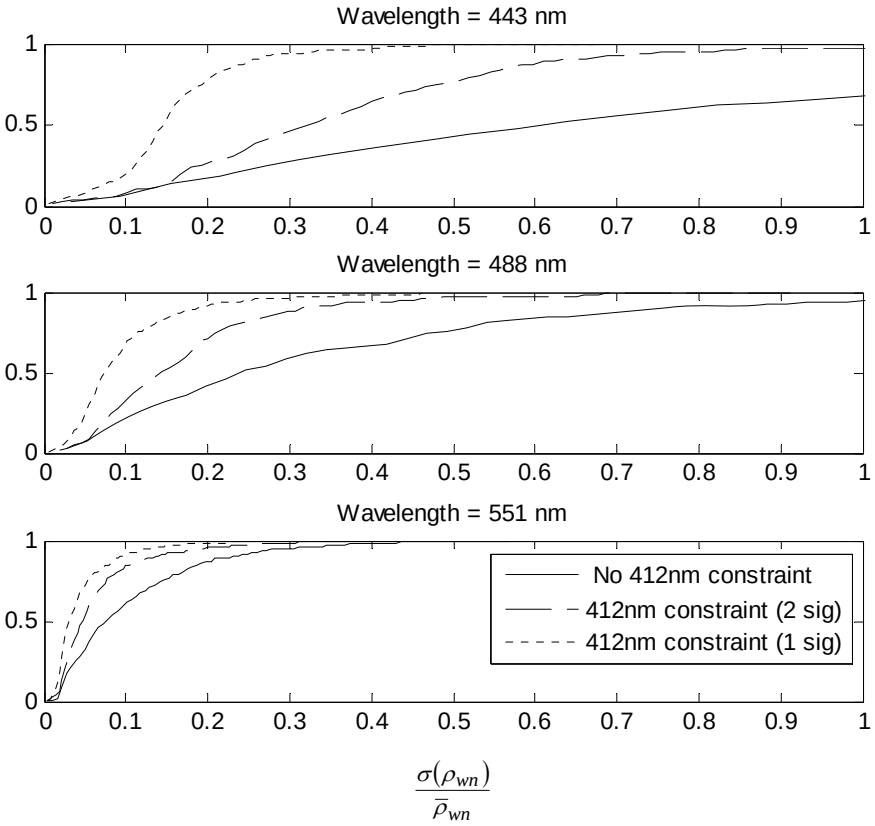

Figure 6.12 Statistical cumulative distribution function of fractional normalized water leaving reflectance uncertainties using the SWIR retrieval algorithm on the SeaDAS plus Aeronet with different 412nm water leaving reflectance constraint levels a) 443nm b) 488nm c) 551nm

6.8 Conclusions

To avoid the bright pixel contamination in the traditional NIR bands of MODIS, a SWIR algorithm was introduced within the SeaDAS development environment. However, the current operational algorithm uses a limited set of 12 ocean based aerosol models which does not address the complete variability of aerosol optical properties and will lead to poor retrieval results when confronted with aerosols models which have significantly different spectral features. Such cases include highly absorbing aerosols whose effective TOA reflectance in the blue is significantly smaller as well as urban non-absorbing aerosols with significantly higher reflectances in the blue and cannot be easily distinguished with IR estimates alone. Clearly, if the increased diversity of aerosol spectral responses in the coastal zone is included within the atmospheric LUTs used in the atmospheric correction procedure, a significantly larger retrieval error will occur unless additional constraints are used to restrict the set of aerosols for a given TOA signal.

To explore this possibility, we have performed statistical analysis of normalized water leaving reflectances at 412nm using both in situ measurements carried out by our group as well as data contained from the NOMAD [15] data archive. We found that these reflectances were contained within the limits $.005 - \Delta\rho_{wn} \le \rho_{wn}(412) \le .005 + \Delta\rho_{wn}$ where $\Delta\rho_{wn} = .003$ at the 1σ confidence level and $\Delta\rho_{wn} = .005$ at the 2σ confidence level. Once the statistical model for the water leaving signal is established, they were used as additional constraints on the SWIR algorithm. The results of the numerical experiments where the SWIR

algorithm is applied to both the SeaDAS and combined Aeronet-SeaDAS database and contrasted to the NIR scheme with bright pixel compensation are listed in Table 6.3.

For our comparisons, we first performed a baseline retrieval error experiment, using the traditional NIR algorithm with the aerosol models obtained solely from the operational SeaDAS set. If no attempt at eliminating the bright pixel contamination is made, the retrieval errors are so high as to be useless. To solve this problem, the operational scheme also provides an estimator model for the NIR water leaving reflectances based on first estimates of reflectances in the VIS channels. When we took the NIR reflectance estimator to be accurate within 10% the uncertainties in the normalized reflectances were found to be $\rho_{wn}(443) \approx 25\%, \rho_{wn}(488) \approx 13\%,$ and $\rho_{wn}(551) \approx 4\%$. However, the same calculation based on the cumulative (SeaDAS + Aeronet) Database resulted in much higher errors of $\rho_{wn}(443) \approx 120\%, \quad \rho_{wn}(488) \approx 50\%, \quad \rho_{wn}(551) \approx 10\%$ which clearly shows that an imperfect bright pixel compensation will lead to unacceptable retrieval errors.

The same procedure using the SWIR correction scheme was then performed. In this case, the additional constraint of the aerosol reflectance at both the 1σ and 2σ confidence levels were considered in turn and contrasted with the case when no 412nm constraint is used. We found that when the conventional SeaDAS database was used, the constraint at 412nm provided no additional improvement. This is quite reasonable when considering the fairly limited spectral diversity in the SeaDAS models. However, we found that the retrieval errors were $\rho_{wn}(443) \approx 20\%, \rho_{wn}(488) \approx 10\%,$ and $\rho_{wn}(551) \approx 3\%$ which is a 25% improvement

over the conventional NIR algorithm with a bright pixel compensation error of 10%, and further improvement are observed when the bright pixel estimator does not perform at 90% accuracy.

When the combined SeaDAS + AERONET tables are used, the 412nm was found to be of crucial importance. Without the 412 constraint, the errors were found to be $\rho_{wn}(443) \approx 90\%, \rho_{wn}(488) \approx 35\%,$ and $\rho_{wn}(551) \approx 10\%$. When the conservative 2σ constraint was used, the errors were reduced $\rho_{wn}(443) \approx 40\%,\ \rho_{wn}(488) \approx 15\%,$ and $\rho_{wn}(551) \approx 5\%$ and for the 1σ constraint $\rho_{wn}(443) \approx 15\%,\ \rho_{wn}(488) \approx 10\%,$ and $\rho_{wn}(551) \approx 3\%$ which compare favorably to the uncertainties obtained using the limited SeaDAS aerosol model set.

From these observations, we find that it is possible to apply stringent constraints on aerosol models at 412nm based on a statistical estimation of the water leaving reflectance measurements obtained from in situ field measurements valid for the highly productive Chesapeake coastal waters. In our numerical experiments, we purposely weighted the AERONET and SeaDAS LUTs with equal probability and used observation and solar angles which are not optimal in an effort to artificially increase the spectral diversity in the aerosol models. Even in this extreme case, we find that the inclusion of the 412nm constraint allows us to increase the extent of the atmospheric LUT to better model diverse conditions found over urban coastal waters.

Table 6.3 Fractional Normalized water leaving reflectance uncertainties

Atmospheric Correction		Constraint used	Uncertainty %		
Atmospheric Correction Method	Atmospheric Database		Band 443nm	Band 488nm	Band 551nm
Traditional NIR	SeaDAS	10% Bright pixel compensation	25%	13%	4%
Traditional NIR	SeaDAS plus Aeronet	10% Bright pixel compensation	120%	50%	10%
SWIR	SeaDAS	No constraint at 412nm	20%	10%	3%
SWIR	SeaDAS	$2\sigma\ \rho_{wn}(412)$ $\rho_{wn}(412) = .005 \pm .005$	20%	10%	3%
SWIR	SeaDAS	$1\sigma\ \rho_{wn}(412)$ $\rho_{wn}(412) = .005 \pm .003$	18%	8%	3%
SWIR	SeaDAS plus Aeronet	No constraint at 412nm	90%	35%	10%
SWIR	SeaDAS plus Aeronet	$2\sigma\ \rho_{wn}(412)$ $\rho_{wn}(412) = .005 \pm .005$	40%	15%	5%
SWIR	SeaDAS plus Aeronet	$1\sigma\ \rho_{wn}(412)$ $\rho_{wn}(412) = .005 \pm .003$	15%	8%	3%

To put this in perspective, we plot the retrieval of color ratios as a function of CHL for the Chesapeake measurements based on simulation of TOA reflectances by adding a synthetic atmosphere on top of our in situ measurements. Column 1 represents the blue-green algorithms while column 2 represents the NIR algorithms; the rows indicate either the NIR retrieval (with iteration) or the SWIR retrieval. We

see clearly the importance of the NIR algorithm which is dramatically less sensitive to atmospheric uncertainty as well as the improvement in retrieval using the SWIR algorithm in eliminating the underestimation of reflectances due to bright pixel contamination.

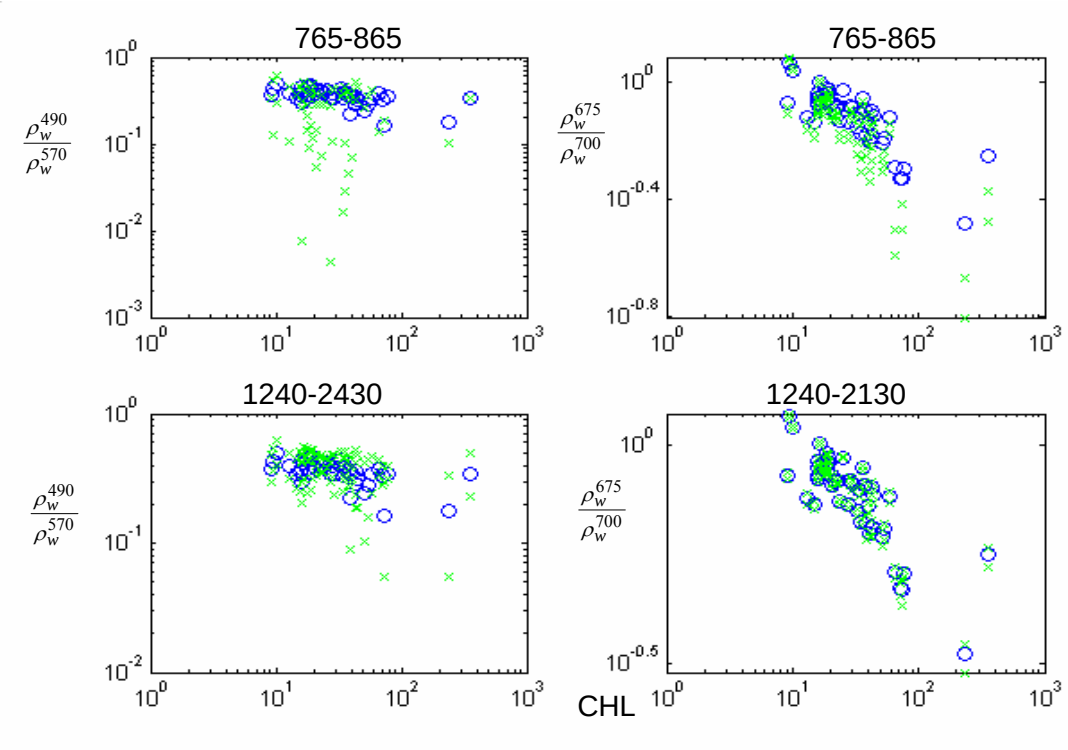

Figure 6.13 Effect of atmospheric retrieval algorithm and CHL band ratio algorithm on retrieval of CHL. (x=surface measurement, o=retrieved results from LUT)

References Chapter 6

[1] GORDON, H. R., and WANG, M., 1994, Retrieval of water-leaving radiance and aerosol optical thickness over the oceans with SeaWiFS: A preliminary algorithm. Applied Optics, 33, 443–452.

[2] Stumpf, R. P., R. A. Arnone, R. W. Gould, P. M. Martinolich, and V. Ransibrahmanakul (2003), A Partially Coupled Ocean-Atmosphere Model for Retrieval of Water-Leaving Radiance From SeaWiFS in Coastal Waters, SeaWiFS Postlaunch Tech. Rep. Ser., vol. 22, NASA Tech. Memo. 2003-206892, edited by S. B. Hooker and E. R. Firestone, pp. 51– 59, NASA Goddard Space Flight Cent., Greenbelt, Md.

[3] Wang, M., and W. Shi (2005), Estimation of ocean contribution at the MODIS near-infrared wavelengths along the east coast of the U.S.: Two case studies, Geophys. Res. Lett.,32, L13606, doi:10.1029/2005GL022917

[4] Franz, B.A., P.J. Werdell, G. Meister, E.J. Kwiatkowska, S.W. Bailey, Z. Ahmad, and C.R. McClain (2006). MODIS Land Bands for Ocean Remote Sensing Applications, Proc. Ocean Optics XVIII, Montreal, Canada, 9-13 October 2006.

[5] P. F. Levelt, E.Hilsenrath, G. W. L. Gijsbertus H. J. van den Oord, P.n K. Bhartia, J.Tamminen, J. F. de Haan, and J. P. Veefkind, “Science Objectives of the Ozone Monitoring Instrument”, IEEE Transactions Geoscience and Rem. Sens. 44, 1199-1208 (2006)

[6] Werdell, P.J. and S.W. Bailey, 2005: An improved in situ data set for bio-optical algorithm development and ocean color satellite validation. Remote Sensing of Environment , 98 , 122-140.

[7] NASA bio-Optical Marine Algorithm Dataset (NOMAD) http://seabass.gsfc.nasa.gov/cgi-bin/nomad.cgi

[8] Wang, M., K. D. Knobelspiesse, and C. R. McClain (2005), Study of the Sea-Viewing Wide Field-of-View Sensor (SeaWiFS) aerosol optical property data over ocean in combination with the ocean color products, J. Geophys. Res., 110, D10S06, doi:10.1029/2004JD004950.

[9] Shettle, E. P., and R. W. Fenn (1979), Models for the aerosols of the lower atmosphere and the effects of humidity variations on their optical properties, Rep. AFGL-TR-79-0214, U.S. Air Force Geophys. Lab., Hanscom AFB, Mass.

[10] Omar, A. H., J. G. Won, et al. "Development of global aerosol models using cluster analysis of Aerosol Robotic Networrk (AERONET) measurements." JGR-Atmos. 110 (2005)

[11] Lyapustin, A. I. "Radiative transfer code SHARM for atmospheric and terrestrial applications," Appl. Opt. 44, 7764-7772 (2005)

[12] Earth Probe Total Ozone Mapping Spectrometer (TOMS) Data Products User's Guide. NASA Technical Publication 1998-206895. ftp://toms.gsfc.nasa.gov/pub/eptoms/EARTHPROBE_USERGUIDE.PDF

[13] IOCCG Report Number 1, (1998). Minimum Requirements for an Operational, Ocean-Colour Sensor for the Open Ocean. Published by the International Ocean-Colour Coordinating Group (IOCCG)

[14] L A. Remer, D. Tanre and Y. Kaufman, "Algorithm For Remote Sensing Of Tropospheric Aerosol From Modis: Collection 5" ATBD-02 Document http://modis.gsfc.nasa.gov/data/atbd/atbd_mod02.pdf

[15] Werdell, P.J., and S.W. Bailey, 2002: The SeaWiFS Bio-optical Archive and Storage System (SeaBASS): Current architecture and implementation. NASA Tech. Memo. 2002-211617 , G.S. Fargion and C.R. McClain, Eds., NASA Goddard Space Flight Center, Greenbelt, Maryland, 45 pp.

Chapter 7 Alternative Approach for Correcting Ocean Color Reflectance for Absorbing Aerosols.

7.1 Formulation of Problem

Knowledge of aerosol properties is crucial to atmospheric correction over the oceans. One of the most difficult problems encountered when doing atmospheric correction over coastal waters is the presence of absorbing aerosols offshore from urban areas.

The SeaDAS atmospheric correction algorithm relies on 12 aerosol models to estimate the aerosol radiance contribution to the top-of-atmosphere (TOA) signal [1]. It also uses two NIR bands to determine the most appropriate aerosol model. However, absorbing aerosols are not easily distinguished from non-absorbing aerosols in the NIR. All of the existing models in the SeaDAS aerosol model suite are non-absorbing or weakly-absorbing. If an absorbing aerosol is present, the aerosol component will be incorrectly estimated, resulting often in negative reflectances particularly in the blue portion of the spectrum and overestimation of chlorophyll concentration.

These absorbing aerosols absorb strongly in the blue and UV wavelengths and cannot be accurately corrected using the dark pixel assumption for longer wavelengths. Following the approach of Ransibrahmanakul and Stumpf [2] the method to correct for the effect of absorbing aerosols on contaminated water leaving reflectance assumes the following:

1) The current water reflectance is potentially contaminated by the presence of absorbing aerosols which will have the affect of reducing the retrieved water leaving signal below the true value

2) The contaminated signal can be decomposed into two components:

$$R_{con}(\lambda) = R_{\mathrm{mod}}(\lambda) - R_{aa}(\lambda) \qquad (7.1)$$

where $R_{con}(\lambda)$ is the potentially contaminated reflectance output from the current atmospheric correction algorithm, $R_{aa}(\lambda)$ is a measure of the absorbing aerosol effect, and $R_{\mathrm{mod}}(\lambda)$ is a conservative estimate of the true reflectance estimated from inherent optical properties obtained at longer wavelengths and bio-optical optical models. The term $R_{aa}(\lambda)$ is analogous to the difference between $R_{con}(\lambda)$ and field reflectance.

3) The spectral shape of $R_{aa}(\lambda)$ is approximated from field and satellite match-ups.

The match-ups suggest that the spectral shape of $\frac{R_{aa}(\lambda)}{R_{aa}(412)}$ resembles:

$\frac{R_{aa}(\lambda)}{R_{aa}(412)} = \left[\frac{412}{\lambda}\right]^n$, n ranges between 6 and 8.

4) $R_{aa}(670) \approx 0$ because the effect of absorbing aerosols decreases rapidly as wavelength increases.

7.2 Correction Procedure

$R_{\mathrm{mod}}(412)$ is estimated by first estimating three components of the absorption term.

$R_{con}(412)$ is replaced by $R_{\mathrm{mod}}(412)$ only when $R_{\mathrm{mod}}(412) > R_{con}(412)$ (7.2)

the procedure for estimating absorption due to detritus begins with estimating total absorption and backscattering coefficients from $R_{\mathrm{mod}}(670)$ based on the inherent optical properties [3].

$$R_{\mathrm{mod}}(\lambda) = \frac{Y \times b_b(\lambda)}{b_b(\lambda) + a_W(\lambda) + a_\phi(\lambda) + a_d(\lambda)} \tag{7.3}$$

where Y is a constant, $a_W(\lambda)$, $a_\phi(\lambda)$ and $a_d(\lambda)$ are absorption coefficients due to water, phytoplankton, and detritus; and total absorption $a_t(\lambda)$ is defined as:

$$a_t(\lambda) = a_w(\lambda) + a_\phi(\lambda) + a_d(\lambda) \tag{7.4}$$

in clear water where there is little CDOM and TSS equation (7.3) can be simplified because $b_b(\lambda)$ is much less than $a_t(\lambda)$ [4]

$$R_{\mathrm{mod}}(\lambda) = \frac{Y.b_b(\lambda)}{a_t(\lambda)} \tag{7.5}$$

the values of $a_W(\lambda)$ can be found in the literature [5]

$a_\phi(\lambda)$ can be estimated from chlorophyll concentration [6]

$$a_\phi(675) = \left[0.0176.C\right]^{0.97}$$

$$a_\phi(\lambda) = f_0(\lambda).a_\phi(675).\exp\left\langle f_1(\lambda).\tanh\left[f_2(\lambda).\ln\left(\frac{a_\phi(675)}{f_3(\lambda)}\right)\right]\right\rangle \tag{7.6}$$

where C is chlorophyll concentration and $f_0(\lambda), f_1(\lambda), f_2(\lambda), f_3(\lambda)$ are wavelength dependent constants.

If absorbing aerosol is present, $R_{con}(\lambda)$ and C will be underestimated and overestimated, respectively.

To determine $a_d(\lambda)$ equation (7.5) is written twice, as a numerator with one wavelength and a denominator with another.

$$\frac{a_t(510)}{a_t(670)} = \frac{R_{\mathrm{mod}}(670)}{R_{\mathrm{mod}}(510)} \cdot \frac{b_b(510)}{b_b(670)}$$
$$\frac{a_t(555)}{a_t(670)} = \frac{R_{\mathrm{mod}}(670)}{R_{\mathrm{mod}}(555)} \cdot \frac{b_b(555)}{b_b(670)} \qquad (7.7)$$

the values $\frac{b_b(\lambda_1)}{b_b(\lambda_2)}$ can be determined by this spectral relationship [7]

$$b_b(\lambda) = \frac{(-0.00113\lambda + 1.62517)}{0.86807} \cdot \frac{R_{\mathrm{mod}}(670) \cdot a_w(670)}{0.051}$$
$$\frac{b_b(\lambda_1)}{b_b(\lambda_2)} = \frac{(-0.00113\lambda_1 + 1.62517)}{(-0.00113\lambda_2 + 1.62517)} \qquad (7.8)$$

to determine the values for $\frac{a_t(510)}{a_t(670)}$ *and* $\frac{a_t(555)}{a_t(670)}$

assume $\frac{R_{\mathrm{mod}}(670)}{R_{\mathrm{mod}}(510)} \approx \frac{R_{con}(670)}{R_{con}(510)}$ *and* $\frac{R_{\mathrm{mod}}(670)}{R_{\mathrm{mod}}(555)} \approx \frac{R_{con}(670)}{R_{con}(555)}$

the values for $\frac{a_t(510)}{a_t(670)}$ *and* $\frac{a_t(555)}{a_t(670)}$

can be written as part of equation (7.4) to determine $\frac{a_d(510)}{a_d(555)}$

$$\frac{a_d(510)}{a_d(555)} = \frac{a_t(670) \cdot \frac{a_t(510)}{a_t(670)} - a_\phi(510) - a_w(510)}{a_t(670) \cdot \frac{a_t(555)}{a_t(670)} - a_\phi(555) - a_w(555)} \qquad (7.9)$$

the remaining unknown, $a_t(670)$ is assumed to be $a_w(670) + a_\phi(670)$ because detritus absorbs weakly at 670nm.

To measure how realistic the results is, $\frac{a_d(510)}{a_d(555)}$ is expressed in a different form [8] independent of equation (7.9)

$$\frac{a_d(\lambda)}{a_d(555)} = \exp[-S(\lambda - 555)] \qquad (7.10)$$

where S describes the spectral rate of decay of $a_d(\lambda)$ as wavelength increases.

The term $a_d(412)$ is estimated analytically via equation (7.11) if the estimated S falls between 0.008 and 0.025 nm^{-1}

$$a_d(555) = a_t(670) \cdot \left[\frac{a_t(555)}{a_t(670)}\right] - a_\phi(555) - a_w(555)$$

$$\frac{a_d(412)}{a_d(555)} = \exp\left[-S(412-555)\right] \tag{7.11}$$

$$a_d(412) = \left\langle a_t(670) \cdot \left[\frac{a_t(555)}{a_t(670)}\right] - a_\phi(555) - a_w(555) \right\rangle \cdot \left\langle \exp\left[-S(412-555)\right] \right\rangle$$

otherwise, if S is outside of this range, $a_d(412)$ is interpolated from the nearest neighbor derived from equation (7.11). Once an image of $a_d(412)$ is filled, $R_{\mathrm{mod}}(412)$ is determined by writing equation (7.5) twice, as a numerator with one wavelength and a denominator with another:

$$R_{\mathrm{mod}}(412) = R_{con}(670) \cdot \frac{[a_w(670) + a_\phi(670)]}{[a_w(412) + a_\phi(412) + a_d(412)]} \cdot \frac{b_b(412)}{b_b(670)} \tag{7.12}$$

Only if $R_{\mathrm{mod}}(412) >= R_{con}(412)$ will $R_{con}(\lambda)$ be replaced by $R_{\mathrm{mod}}(\lambda)$ as follows:

$$R_{\mathrm{mod}}(\lambda) = R_{con}(\lambda) + \left[R_{\mathrm{mod}}(412) - R_{con}(412)\right] \times \left[\frac{412}{\lambda}\right]^6 \tag{7.13}$$

7.3 Assessment of Bio-Optical Estimator Performance

In order to apply this method, a necessary requirement is that the estimator should always underestimate the water leaving signal. If this property is not satisfied, the correction procedure will attempt to adjust for cases when no absorbing aerosols are present resulting in the generation of errors due to an incorrect classification of

aerosols by misinterpretation. To begin, we have implemented the bio-optical estimator on the NOMAD database remote sensing reflectance spectra.

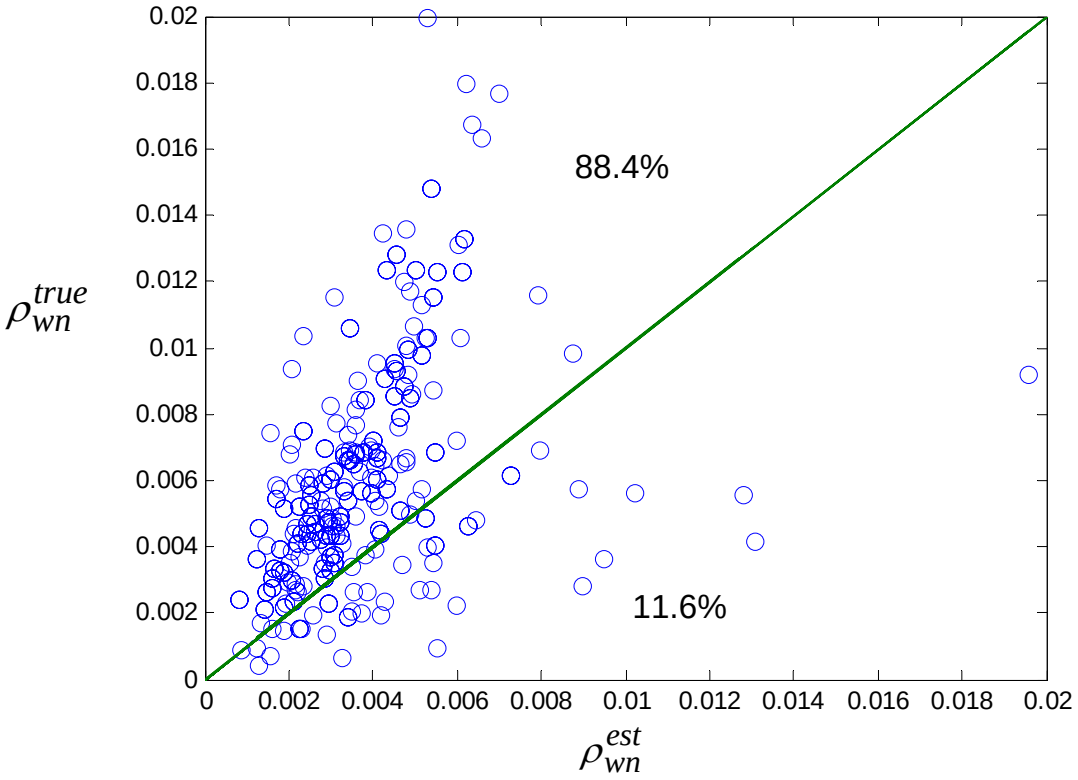

Fig. 7.1 Intercomparison of measurements to bio-optical estimator to verify that the bio-optical estimator in general underestimates the water leaving signal at 412nm

The results are given in figure 7.1 and show that the estimator does in general underestimate the water leaving signal although we observe a significant spread of the estimator which will affect the compensation effectiveness. While these measurements were taken in turbid coastal waters, it is important to assess the performance on other water quality types. Instead of using in situ measurements however, we prefer to assess the estimator based on well controlled simulated datasets where we can control the conditions of the water body. These synthetic measurements were obtained using Hydrolight to obtain synthetic spectra which can

be used for testing purposes. The main bio-optical model is similar to the Lee datasets with a CHL spread from $0.1 < CHL < 100$, a much higher mineral spread and more phytoplankton specific absorption models which are plotted in figure 7.2.

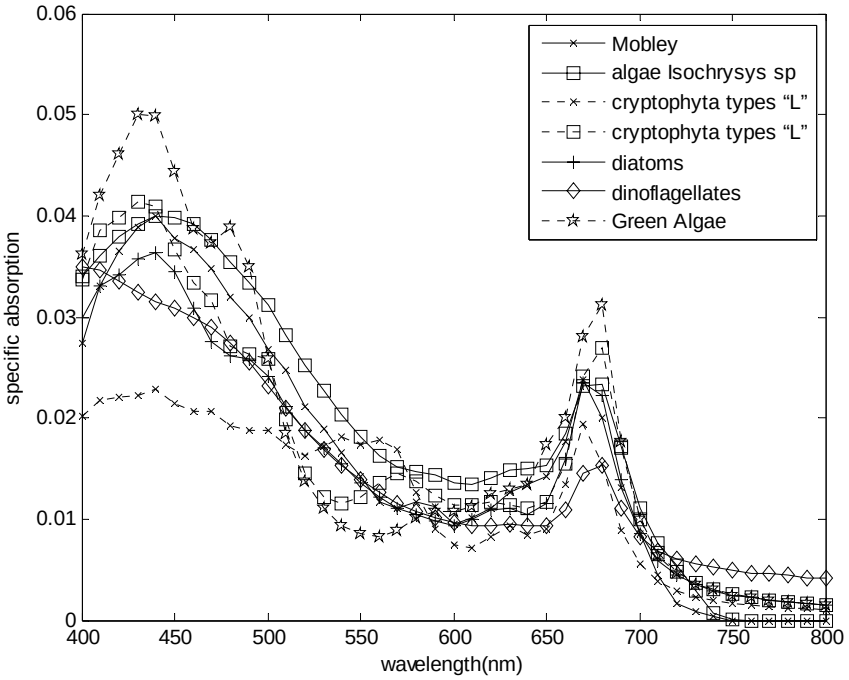

Fig. 7.2 Various Model Specific Phytoplankton Absorptions

From our radiative transfer database, we plot in figures 7.3a and 7.3b the performance of the bio-optical estimator for both low mineral (.01~1mg/l) case and the high mineral (2~100mg/l) case for all 7 specific absorption models. We note in particular for the high mineral case that the estimator is nearly always underestimating the water leaving signal independent of the specific absorption.

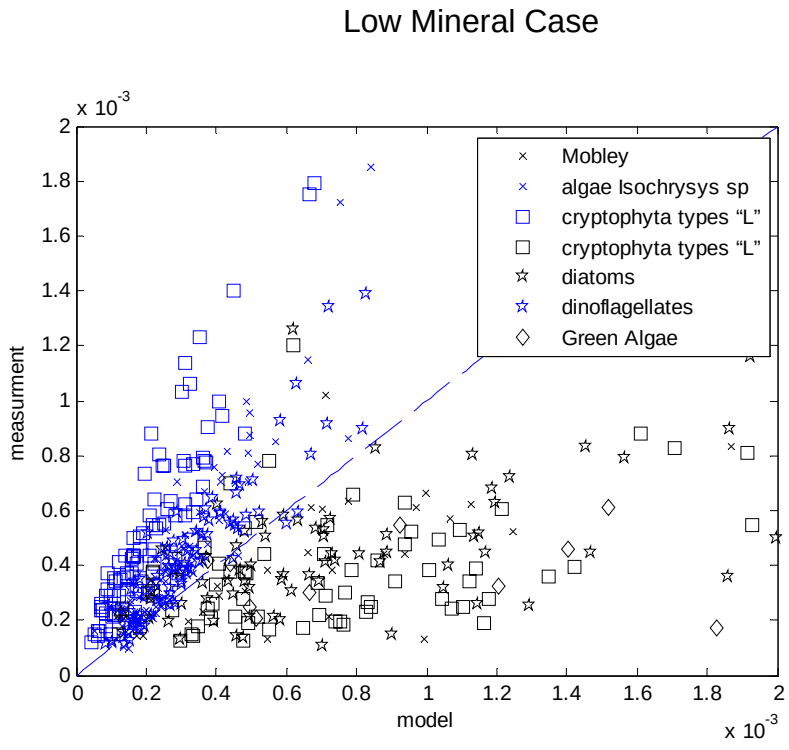

Figure 7.3a Intercomparison of synthetic datasets to bio-optical estimator for different specific absorption classes a) low mineral case

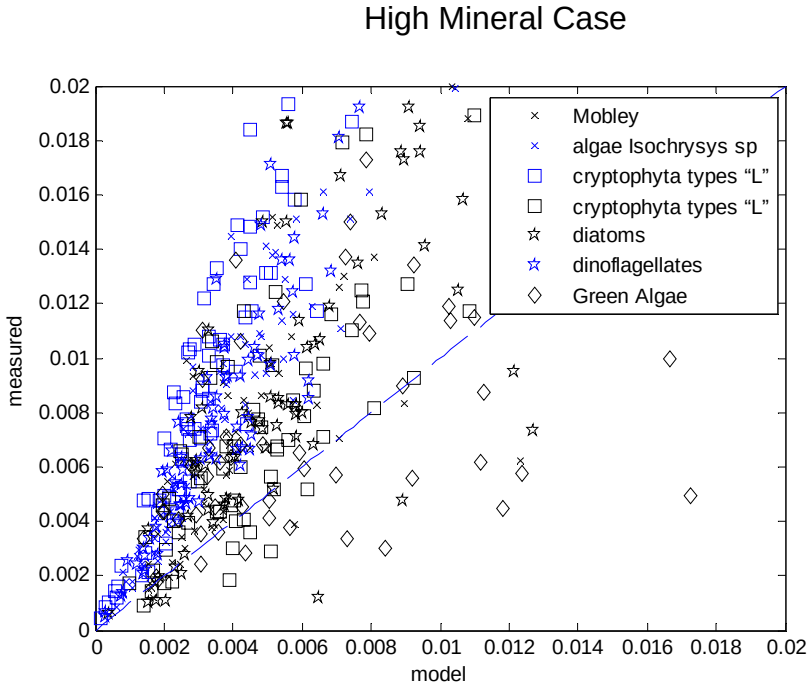

Figure 7.3b Intercomparison of synthetic datasets to bio-optical estimator for different specific absorption classes b) high mineral case.

On the other hand, in the low mineral case, we note that the estimator can either underestimate or overestimate the water leaving signal and the behavior depends primarily on the phytoplankton species.

7.4 Preliminary results testing Ransibrahmanakul and Stumpf's approach.

The above results indicate that in general a strong absorption feature should be able to be classified and dramatically improved since the bio-optical estimator uncertainty is less than the contamination feature. This is clearly illustrated in figure 7.4. for a case where the absorption feature is so large that it drives the retrieval of the water leaving reflectance negative. In this case, the ability of the algorithm to correct for absorbing aerosols is dramatic with an overall improvement of about 90%. It is interesting to note however that the errors in the correction are fairly uniform spectrally compared to the error at 412nm which is due solely to the error in the bio-optical estimator.

This error cannot be eliminated since it is based on the necessary criteria that the water leaving signal as predicted by the estimator should be less than the true value so the off-set at 412 is a necessary consequence.

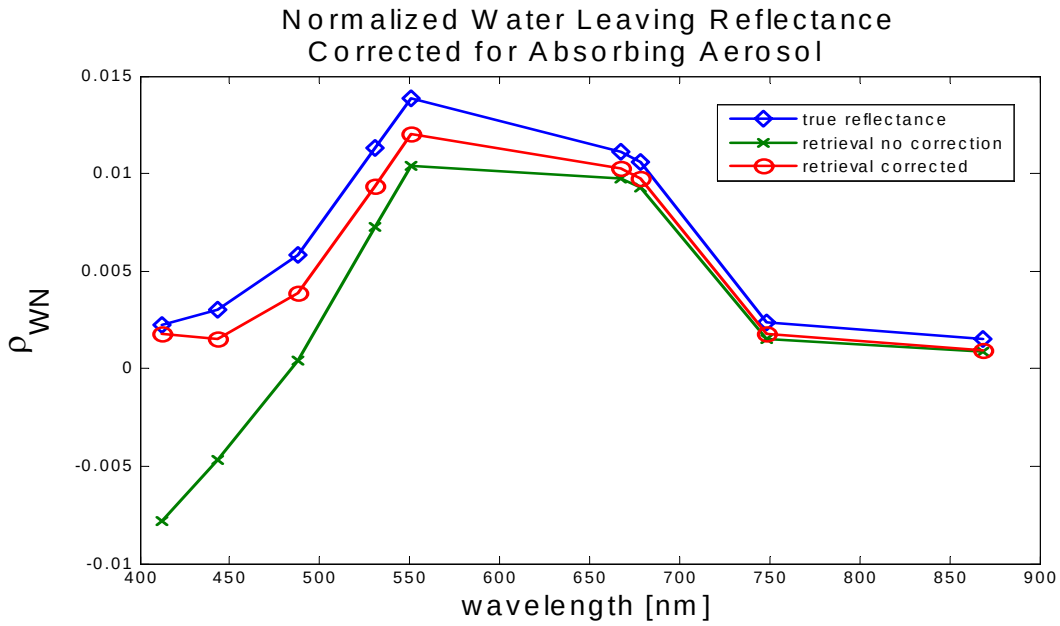

Figure 7.4 Reflectance spectra corrected for absorbing aerosols using Stumpf's algorithm.

Therefore, the bio-optical estimator can be thought of as a constraint (although biased) which can be used in much the same way as the threshold estimator. In this case, the approach need not be limited to absorbing aerosol contamination but can correct for other sources of errors such as an underestimation of the true epsilon (ε) parameter. This is illustrated in figure 7.5 where a large angstrom atmosphere from the AERONET database was used. In this case, the correction is reversed and of the

form $\Delta R(\lambda) = -\Delta R(412)\left(\frac{\lambda}{412}\right)^{-n}$ (7.14)

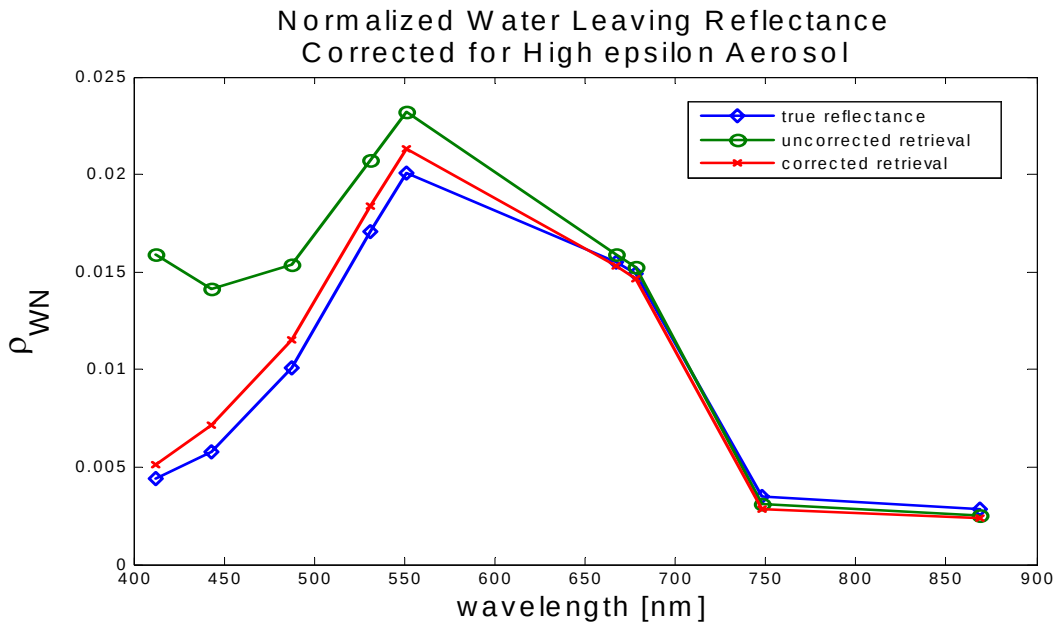

Figure 7.5 Reflectance spectra corrected for high ε aerosols using Bio-optical correction algorithm.

To more clearly show the robustness of the correction, we first performed a conventional SWIR correction to the TOA reflectances which were obtained by overlaying insitu (46 stations) water leaving reflectances with a high ε atmosphere which resulted in a set of "contaminated" retrieved water leaving reflectances which significantly over predict the 412 water leaving reflectance. To this set, we performed the correction discussed above. The results are presented in figure 7.6 as retrieval error frequency histograms at 443, 488 and 551 nm. The blue trace represents the uncertainty obtained by processing within the SeaDAS database which results in a nearly constant water leaving signal uncertainty over all stations. However, when the Bio-Optical correction is applied, the retrieval errors are greatly reduced for almost all cases.

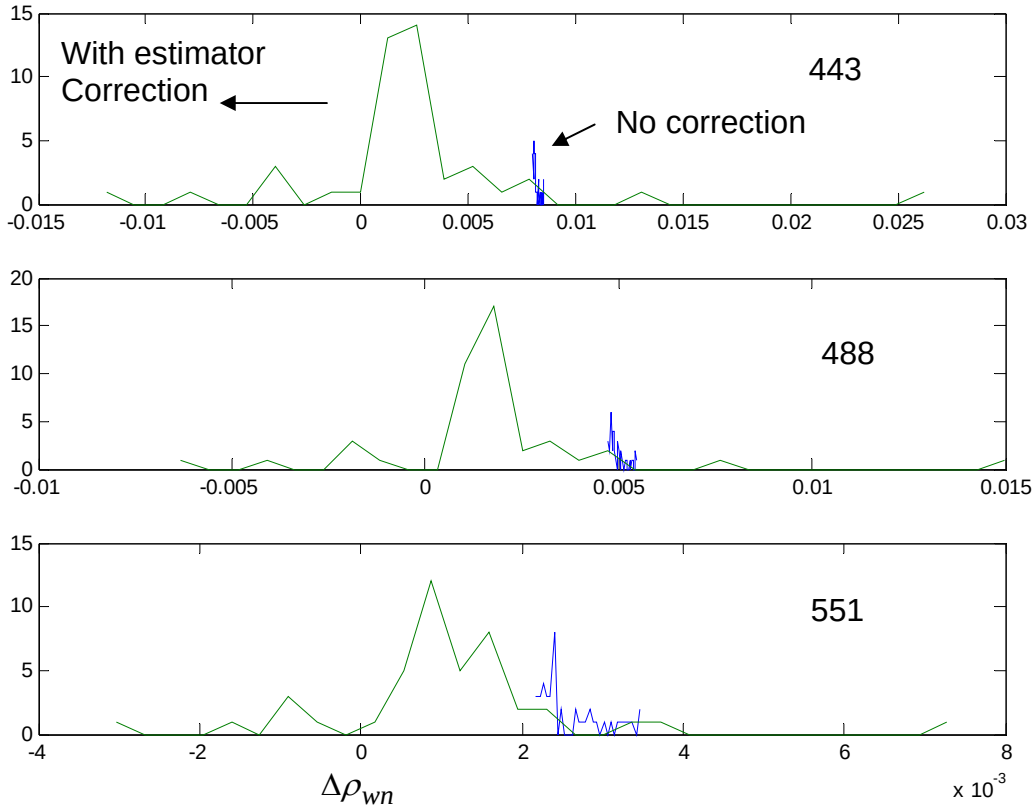

Fig. 7.6 retrieval error frequency histograms at 443, 488 and 551 nm for high ε atmosphere (blue=contaminated SWIR retrieval, green=Bio-Optically corrected)

In the case of the threshold estimator, we found that for the 2σ confidence level, the uncertainty in the estimator is equal to the estimator itself so if the bio-optical estimator can predict the 412 signal with less error, we could replace the threshold condition with the bio-optical estimator as the constraint. In the next section, this possibility is explored.

7.5 Assessment of bio-optical model estimator

In our previous analysis, the rough normalized water leaving reflectance estimator which was used $.005 - \Delta\rho_{wn} \le \rho_{wn}(412) \le .005 + \Delta\rho_{wn}$ was obtained by statistical data mining from the NOMAD database. However, this approach makes no use of the possible bio-optical connections which may exist between normalized water leaving reflectance at 412nm and the longer VIS channels. Connecting these quantities through a robust bio-optical algorithm may significantly improve the uncertainty level due to errors in water leaving reflectance for the 412nm aerosol path reflectance retrieval.

To assess this possibility, we utilize a bio-optical model [2] for the empirical estimation of the water leaving radiance which depends on CHL concentration and water reflectances (i.e.) $\overline{\rho_{wn}(412)} = F[ChL, \rho_{wn}(510), \rho_{wn}(555), \rho_{wn}(670)]$ and study how the bio-optical estimator spread compares to the threshold. In figure 7.7, we plot the cumulative distributions for the residuals between the estimator and the measured reflectance for both the threshold estimator and the bio-optical estimator. We first note that the threshold estimator outperforms the biased bio-optical estimator by a significant amount for the Chesapeake region. However, on a global scale (coastal + deep water), the threshold estimator is no longer useful and the bio-optical estimator can provide a better constraint although both estimators perform poorly in comparison to the Chesapeake results. In addition, we also plot the residuals for the case that the bio-optical estimator retrieval is modified to remove the bias by

subtracting the mean of the residuals. While this is not a reasonable approach in practice, it does provide a lower limit to the uncertainty that could be achieved. We note that even when the bio-optical estimator is externally corrected for bias, the uncertainty in the threshold estimator is still optimal especially beyond the 1σ confidence level. These observations clearly illustrate that the simple threshold estimator is most suited to providing a constraint on the 412nm atmospheric path reflectance.

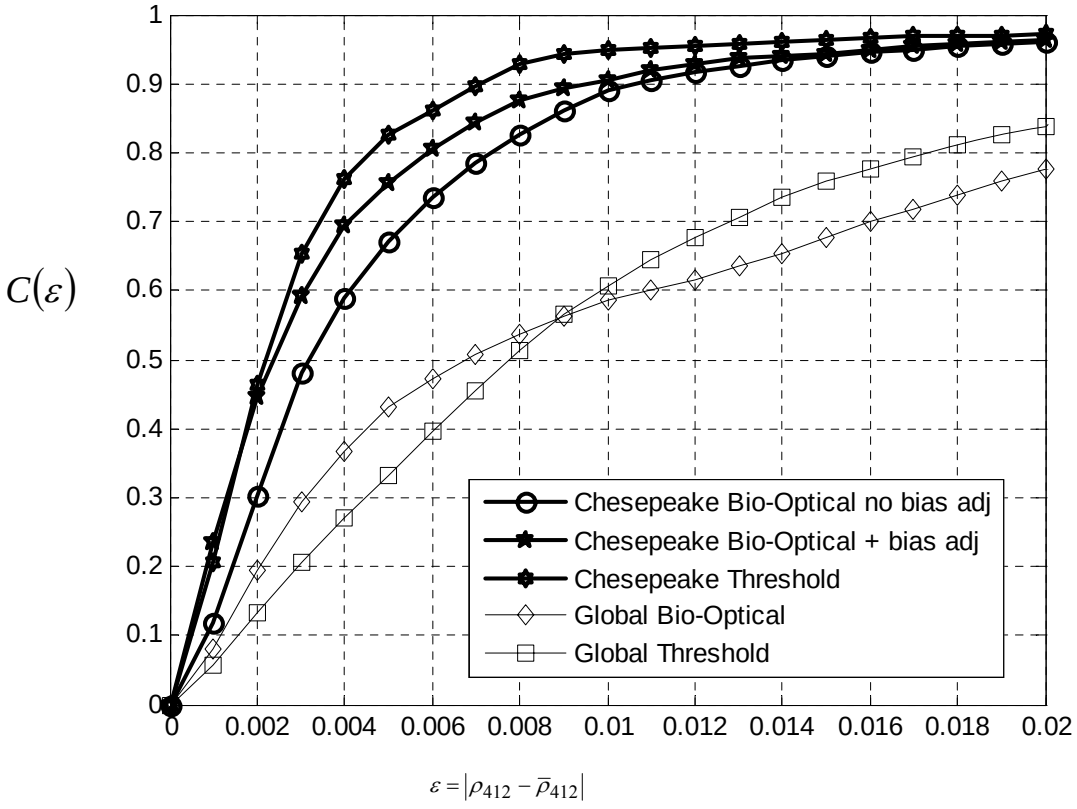

Fig. 7.7 Cumulative distribution of residual error for both the bio-optical estimator and the threshold estimator. Both Chesapeake and Global water statistics are given.

7.6 Conclusions

We found that the necessary property that the 412nm bio-optical estimator underestimates the water leaving signal is satisfied with a high degree of statistical probability ~90%. However, using synthetic data generated by hydrolight, we found that this property is only satisfied when the mineral concentration is sufficiently high which is quite intuitive since the presence of mineral particles will drive the true signal higher at low wavelengths. For low minerals, we find that the estimator can either underestimate or overestimate the water leaving signal and the behavior is driven by the phytoplankton specific absorption model.

We also found that the threshold estimator outperforms the biased bio-optical estimator by a significant amount for the Chesapeake region. However, on a global scale (coastal + deep water), the threshold estimator is no longer useful and the bio-optical estimator can provide a better constraint although both estimators perform poorly in comparison to the Chesapeake results. In addition, we also attempted to improve the bio-optical estimator by eliminating the bias. While this is not a reasonable approach in practice, it does provide a lower limit to the uncertainty that could be achieved. We noted that even when the bio-optical estimator is externally corrected for bias, the uncertainty in the threshold estimator was still optimal especially beyond the 1σ confidence level. These observations clearly illustrate that the simple threshold estimator is most suited to providing a constraint on the 412nm atmospheric path reflectance.

Therefore, we can conclude that the use of the bio-optical estimator will not be an improvement and the most useful approach to constrain atmospheric retrieval for the Chesapeake region is to use the simple statistically derived estimator to eliminate the water leaving reflectance contamination on the 412 reflectance signal.

References Chapter 7

[1] Wang, M. (2000), The SeaWiFS Atmospheric Correction Algorithm Updates, SeaWiFS Postlaunch Tech. Rep. Ser., vol. 9, NASA Tech. Memo. 2000-206892, edited by S. B. Hooker and E. R. Firestone, pp. 57–63, NASA Goddard Space Flight Cent., Greenbelt, MD.

[2] Ransibrahmanakul, V. and R. P. Stumpf, 'Correcting ocean colour reflectance for absorbing aerosols", International Journal of Remote Sensing , 27, 1759 - 1774 , 2006

[3] Gordon,H.R., BROWN,O.B. and JACOBS,M.M., 1975, Computed relationships between the inherent and apparent optical properties of a flat homogeneous ocean. Applied Optics, 14**,** pp. 417-427.

[4] CHEN, C., SHI, P. and ZHAN,H., 2003, A local algorithm for estimation of yellow substance (gelbstoff) in coastal waters from SeaWiFS data: Pearl River estuary, China. International Journal of Remote Sensing, 24, pp. 1171-1176.

[5] POPE, R.M. and FRY, E.S., 1997, Absorption spectrum (380-700nm) of pure water, II, integrating cavity measurements. Applied Optics, 36, pp. 8710-8723.

[6] CARDER,K.L., CHEN, F.R. and CANNIZZARO, J.P., 2002, MODIS Algorithm Theoretical Basis Documents (Ocean), ATBD-MOD-19:Case 2 Chlorophyll_a algorithm and Case 2 Absorption Coefficient Algorithm, http://modis.gsfc.nasa.gov/data/atbd/ ocean_atbd.html, Vers. 6.

[7] GOULD, R.W., ARNONE,R.A. and MARTINOLICH, P.M., 1999, Spectral dependence of the scattering coefficient in Case-1 and Case-2 waters. Applied Optics, 38, pp. 2377-2383.

[8] BRICAUD,A., MOREL,A. and PREUR,L., 1981, Absorption by dissolved organic matter in the sea (yellow substance) in the UV and visible domains. Limnology and Oceanography, 26, pp. 43-53.

8. Concluding Remarks

8.1 Thesis Summary

The research presented in this thesis is a description of our efforts to improve on coastal remote sensing. The main results which have formed the two articles which are to be submitted include:

1) A detailed incomparison of the NIR and SWIR retrieval methods where it was found that SWIR retrieval method provides a 25% improvement of water leaving reflectance over the NIR algorithm using 90% bright pixel compensation.

2) The performance of the NIR algorithm becomes significantly worse when a more representative set of atmospheres are used in the inversion scheme. In addition, we found that the NIR water leaving estimators used by SeaDAS can provide at best 90% compensation for bright pixel contamination and the iterative scheme actually leads to larger errors when atmospheres not contained within the traditional atmospheric LUT are present.

3) We have found that by using the 412nm channel which has an extremely small outgoing reflectance due to the increased absorption of CHL and CDOM as an additional sensing channel, an improvement in water leaving retrieval can be gained.

4) When using the conventional SeaDAS atmospheric LUT, it was found that the constraints imposed by the additional 412nm channel does not improve the retrieval. However, when the generalized LUT composed of atmospheres from both SeaDAS and AERONET, a significant improvement in water leaving retrieval is obtained.

5) The above conclusion leads to the result that while the additional constraint is not needed for atmospheres contained within the spectral variability of the existing LUT, the constraint is extremely valuable both as a flag to indicate a non-traditional atmosphere and as a way of retrieving the water leaving reflectance using the more extensive database

8.2 Scholarly Publications and Presentations

8.2.1 Publications in Submission Process

- Vargas, M., Oo, M., Gilerson, A., Gross, B., Moshary, F., Ahmed, S. "Improved Robustness of atmospheric correction for highly productive coastal waters using the SWIR retrieval algorithm together with water leaving reflectance constraints at 412nm"

- Vargas, M., Oo, M., Gilerson, A., Gross, B., Moshary, F., Ahmed, S. "Assessment and extension of empirical correction of absorbing aerosol contamination to fine particulate aerosols."

8.2.2 Presentations and Proceedings

- Vargas, M., Gross, B., Moshary, F., Ahmed, S. "Effects of Atmospheric Retrieval Uncertainty on Different Band Ratio and Hyperspectral Algorithms". Proc. NASA Ocean Color Research Team Meeting 2006. April 11-13, 2006 Newport, RI

- Vargas, M., Gross, B., Moshary, F., Ahmed, S , “Atmospheric Correction Approaches in Coastal Waters: Chesapeake Study”, NOAA-CREST Symposium (Mayaguez) 2006

- Vargas, M., Gross, B., Moshary, F., Ahmed, S , “Hyperspectral Sensing of Coastal Waters”, : Einstein in the City (New York) 2005

- Vargas, M., Gross, B., Moshary, F., Ahmed, S , “Hyperspectral Sensing of Coastal Waters The GOES-R Coastal Water Imager”, : NOAA-CREST Symposium (Hampton VA) 2004

- Vargas, M., Gross, B., Moshary, F., Ahmed, S , “Stability of an Iterative Multiwavelength Lidar Scheme”, SPIE Annual Meeting (SanDiego) 2003

Bibliography

[1] Srokosz, M.A. Biological Oceanography by Remote Sensing. Encyclopedia of Analytical Chemistry. R.A. Meyers (Ed.) pp. 8506–8533, 2000

[2] Jeffrey, S. w., & Vesk,M. (1997). Introduction to marine phytoplankton and their pigment signatures. In Phytoplankton Pigments in Oceanography: Guidelines to Modern Methods, ed. S. W. Jeffrey, R. F. C. Mantoura & S. W. Wright, pp. 37-84. Paris: UNESCO Publishing.

[3] Gordon, H. R. and M. Wang. ,"Retrieval of water-leaving radiance and aerosol optical thickness over the oceans with SeaWiFS: A preliminary algorithm". Applied Optics, 33, 443–452. (1994)

[4] Darecki, M., and D. Stramski. "An evaluation of MODIS and SeaWiFS bio-optical algorithms in the Baltic Sea". Remote Sensing of Environment, 89, 326-350. (2004)

[5] K. G. Ruddick, F. Ovidio, and M. Rijkeboer, "Atmospheric Correction of SeaWiFS Imagery for Turbid Coastal and Inland Waters," Appl. Opt. 39, 897-912 (2000)

[6] Lavender, S. J., Pinkerton, M. H., Moore, G. F., Aiken, J. & Blondeau-Patissier, D. "Modification to the atmospheric correction of SeaWiFS ocean colour images over turbid waters", Continental Shelf Research, 25, 539-555, 2005.

[7] Hu Chuanmin, Carder Kendall L, Muller Karger, Frank E. Atomospheric Correction of SeaWiFS Imagery over Turbid Coastal Waters: A practical method. Remote sensing of Environment, , 74, 195-206. (2000)

[8] Stumpf, R. P., R. A. Arnone, R. W. Gould, P. M. Martinolich, and V. Ransibrahmanakul (2003), A Partially Coupled Ocean-Atmosphere Model for Retrieval of Water-Leaving Radiance From SeaWiFS in Coastal Waters, SeaWiFS Postlaunch Tech. Rep. Ser., vol. 22, NASA Tech. Memo. 2003-206892, edited by S. B. Hooker and E. R. Firestone, pp. 51– 59, NASA Goddard Space Flight Cent., Greenbelt, Md.

[9] D. A. Siegel, M. Wang, S. Maritorena, and W. Robinson, "Atmospheric Correction of Satellite Ocean Color Imagery: The Black Pixel Assumption," Appl. Opt. 39, 3582-3591 (2000)

[10] M. Wang and W. Shi "Estimation of ocean contribution at the MODIS near-infrared wavelengths along the east coast of the U.S.: Two case studies" Geophys. Res. Lett, 32, L13606, doi:10.1029/2005GL022917, (2005)

[11] V. Ransibrahmanakul and R. P. Stumpf, 'Correcting ocean colour reflectance for absorbing aerosols", International Journal of Remote Sensing , 27, 1759 - 1774 , 2006

[12] HE Xianqiang, PAN Delu, MAO Zhihua "Atmospheric correction of SeaWiFS imagery for turbid coastal and inland waters" Acta Oceanologica Sinica,Vol. 23, No. 4, p.609-615, (2004)

[13] R. C. Levy, L. A. Remer, J. V. Martins, and Y. J. Kaufman," Evaluation of the MODIS Aerosol Retrievals over Ocean and Land during CLAMS", J. Atmos. Sci., 62**,** 974–992. (2005)

Chapter 2

[1] Morel, A., & Prieur, L. (1977). Analysis of variations in ocean color. Limnol. Oceanogr.,22, 709-722.

[2] Mobley C. D., "Light and Water: Radiative Transfer in Natural Waters", Academic Press, New York, 1994

[3] Pope, R. M. and Fry, E. S. (1997). Absorption spectrum (380 - 700 nm) of pure water: II. Integrating cavity measurements. Appl. Optics 36**:** 8710-8723

[4] Bricaud, A., Babin, M., Morel, A., and Claustre, H. (1995). Variability in the chlorophyll-specific absorption coefficients of natural phytoplankton: Analysis and parameterization. J. Geophys. Res. 100: 13321-13332.

[5] Fischer, J., and Fell, F. (1999). Simulation of MERIS measurements above selected ocean waters. Int. J. Remote Sensing 20: 1787-1807.

[6] Wang, M., A sensitivity study of the SeaWiFS atmospheric correction algorithm: Effects of spectral band variations, Remote Sens. Environ., 67, 348– 359, 1999.

[7] Robinson, I. S. (1985). Satellite Oceanography. Chichester, UK: Ellis Horwood.

[8] Wang, M., 2002, The Rayleigh lookup tables for the SeaWiFS data processing: Accounting for the effects of ocean surface roughness. International Journal Remote Sensing, 23, 2693–2702.

[9] Gordon, H. R., & Clark, D. K. (1981). Clear water radiances for atmospheric correction of coastal zone color scanner imagery. Appl. Opt., 20, 4175-4180.

[10] Gordon, H. R. and M. Wang., "Retrieval of water-leaving radiance and aerosol optical thickness over the oceans with SeaWiFS: A preliminary algorithm". Applied Optics, 33, 443–452. (1994)
[11] Siegel, D. A., Wang, M., Maritorena, S., & Robinson, W. (2000). Atmospheric correction of satellite ocean color imagery: the black pixel assumption. Appl. Opt., 39, 3582-3591.

[12] Chomko, R. and Gordon, H. R. (1998). Atmospheric correction of ocean color imagery: use of the Junge power-law aerosol size distribution with variable refractive index to handle aerosol absorption. Appl. Optics 37**:** 5560-5572.

[13] Li, L., H. Fukushima, R. Frouin, B. G. Mitchell, M.-X. He, I. Uno, T. Takamura, and S. Ohta, Influence of submicron absorptive aerosol on Sea-viewing Wide Field-of-view Sensor (SeaWiFS)-derived marine reflectance during Aerosol Characterization Experiment (ACE)-Asia, J. Geophys. Res., 108(D15), 4472, doi:10.1029/2002JD002776, 2003.

[14] Fukushima, H., and M. Toratani (1997), Asian dust aerosol: Optical effect on satellite ocean color signal and a scheme of its correction, J. Geophys. Res., 102(D14), 17,119–17,130.

[15] V. Ransibrahmanakul and R. P. Stumpf, 'Correcting ocean colour reflectance for absorbing aerosols", International Journal of Remote Sensing , 27, 1759 - 1774 , 2006

Chapter 3

[1] Gordon, H. R. and Morel, A. (1983). Remote Assessment of Ocean Color for Interpretation of Satellite Visible Imagery. A Review, Lecture Notes on Coastal and Estuarine Studies, R. T. Barber, N. K. Mooers, M. J. Bowman and B. Zeitzschel (eds.), Springer-Verlag, New York, 114 p.

[2] Acker J G, Vasilkov A, Nadeau D, Kuring N (2004) Use of SeaWiFS ocean color data to estimate neritic sediment mass transport from carbonate platforms for two hurricane-forced events, CORAL REEFS 23: (1) 39-47

[3] Lee Zhongping, Kendall L. Carder, Curtis D. Mobley, Robert G. Steward, and Jennifer S. Patch. Hyperspectral remote sensing for shallow waters: 2. Deriving bottom depths and water properties by optimization. Applied Optics 38, 3831-3843 (1999)

[4] Garver, S. A., and D. A. Siegel (1997), Inherent optical property inversion of ocean color spectra and its biogeochemical interpretation 1. Time series from the Sargasso Sea, J. Geophys. Res., 102(C8), 18,607–18,626.

[5] O'Reilly, J. E., S. Maritorena, B. G. Mitchell, D. A. Siegel, K. L. Carder, S. A. Garver, M. Kahru, and C. R. McClain (1998), Ocean color chlorophyll algorithms for SeaWiFS, J. Geophys. Res., 103, 24,937–24,953.

[6] Liew S. C., Aik Song Chia, Kim Hwa Lim and Leong Keong Kwoh. Modeling the reflectance spectra of tropical coastal waters. SPIE Proc. 4488B – Ocean Color Remote Sensing and Applications Part of SPIE's International Symposium on Optical Science and Technology, 29 July to 3 August 2001, San Diego, California, USA.

[7] Morel A, "Optical properties of oceanic Case I waters, revisited," Ocean Optics XIII, SPIE Proc. 2963, pp. 108-114, 1996.

[8] Roesler, C. S., and M. J. Perry (1995), In situ phytoplankton absorption, fluorescence emission, and particulate backscattering spectra determined from reflectance, J. Geophys. Res., 100(C7), 13,279–13,294.

[9] Burenkov VI, Vasilkov AP, Stephantsev LA (1995) Retrieval of spectral inherent optical properties of seawater from the spectral reflectance. Oceanology 25:49–54

[10] D.K. Clarke, MODIS Algorithm Theroretical Basis Document, Bio-Optical Algorithms – Case 1 Waters, version 1.2, http://modis.gsfc.nasa.gov/data/atbd/atbd_mod18.pdf, 1997.

[11] K.L. Carder, F.R. Chen, Z.P. Lee and S.K. Hawes, "Semi-analytic moderate-resolution imaging spectrometer algorithms for chlorophyll-a and absorption with bio-optical domains based on nitrate depletion temperatures," Journal of Geophysical Research, vol. 104, pp. 5403-5421, 1999.

[12] IOCCG. Ocean-Colour Algorithms. http://www.ioccg.org/groups/OCAG_data.html

[13] Darecki M and Stramski D 2004 An evaluation of MODIS and SeaWiFS bio-optical algorithms in the Baltic Sea Remote Sens. Environ. 89 326–50

[14] Siegel D. A., M. Wang, S. Maritorena, and W. Robinson, "Atmospheric Correction of Satellite Ocean Color Imagery: The Black Pixel Assumption ," Appl. Opt. 39, 3582-3591 (2000)

[15] Dall'Olmo G. and Gitelson A., Effect of the variability of bio-optical parameters on the remote estimation of chlorophyll-a concentration in turbid productive waters: experimental results. Applied Optics 44, 422-6338 (2005)

[16] IOCCG Ocean Color Algorithm Working Group. June 2003 Models, parameters, and approaches that used to generate wide range of absorption and backscattering spectra. http://www.ioccg.org/groups/lee_data.pdf

[17] Wetlabs instrument manual

[18] Ruddick, K. G., H. J. Gons, M. Rijkeboer, and G. Tilstone, "Optical Remote Sensing of Chlorophyll a in Case 2 Waters by Use of an Adaptive Two-Band Algorithm with Optimal Error Properties ," Appl. Opt. 40, 3575-3585 (2001)

Chapter 4

[1] Mobley, C. D., Light and Water, 592, Academic Press, San Diego, CA, 1994.

[2] Bissett W. P,, Sharon DeBra, Mubin Kadiwala, David D. R. Kohler, Curtis Mobley, Robert G. Steward, Alan Weidemann, Curtiss O. Davis, Jeff Lillycrop, Robert Pope. Development, Validation, and Fusion of High Resolution Active and Passive Optical Imagery. Signal Processing, Sensor Fusion, and Target Recognition XIV, edited by Ivan Kadar, Proc. of SPIE Vol. 5809 (SPIE, Bellingham, WA, 2005)

[3] Lyzenga, D. R. 1981. Remote sensing of bottom reflectance and water attenuation parameter in shallow water using aircraft and Landsat data. Int. J. Remote Sens. 2: 71.

[4] Philpot, W. D. 1988. Bathymetric mapping with passive multispectral imagery. Appl. Opt. 28: 1569–1578.

[5] Lee, Z., K. L. Carder, R. G. Steward, T. G. Peacock, C. O. Davis, And J. L. Mueller. 1997. Remote sensing reflectance and inherent optical properties of oceanic waters derived from above-water measurements. In S. G. Ackleson [ed.], Ocean optics XIII. Proc. SPIE 2963: 160–166.

[6] Holden, H., and E. Ledrew. 1998. Monitoring the health of coral reefs. Backscatter: Aquat. Inf. Technol. 9(3): 28–31.

[7] Lee, Z.P. and Carder, K.L., 2002. Effects of spectral band numbers on the retrieval of water column and bottom properties from ocean color data. Applied Optics, 41(12): 2191-2201.

[8] Louchard, E., Reid, R., Stephens, F., Davis, C., Leathers, R. and Downes, T., 2003. Optical remote sensing of benthic habitats and bathymetry in coastal environments at Lee Stocking Island, Bahamas: A comparative spectral classification approach. Limnol. Oceanogr., 48(1, part 2): 511-521.

[9] Stumpf, R., Holderied, K. and Sinclair, M., Mapping Coral Reef Bathymetry With High-Resolution, Multispectral Satellite Imagery, Seventh International Conference on Remote Sensing for Marine and Coastal Environments, Miami, (2002)

[10] Lee, Z., Carder, K.L., Mobley, C.D., Steward, R.G. and Patch, J.S., 1998. Hyperspectral remote sensing for shallow waters. 1. A semianalytical model. Applied Optics, vol. 37(no. 27): 6329-6338.

[11] Lee, Z., Carder, K.L., Mobley, C.D., Steward, R.G. and Patch, J.S., 1999. Hyperspectral remote sensing for shallow waters: 2. Deriving bottom depths and water properties by optimization. Applied Optics, 38(18): 3831-3843.

[12] Pope, R., and E. Fry, Absorption spectrum (380 - 700 nm) of pure waters: II. Integrating cavity measurements, Applied Optics, 36, 8710-8723, 1997.

[13] Morel, A., Optical properties of pure water and pure sea water, in Optical aspects of oceanography, edited by N.G. Jerlov, and Nielsen, E. S., pp. 1-24, Academic, New York, 1974.

[14] Roesler, C.S., M.J. Perry, and K.L. Carder, Modeling in situ phytoplankton absorption from total absorption spectra in productive inland marine waters, Limnol. Oceanogr., 34, 1510-1523, 1989.

[15] Bricaud, A., M. Babin, A. Morel, and H. Claustre, Variability in the chlorophyll-specific absorption coefficients of naturnal phytoplankton: Analysis and parameterization, J. Geophy. Res., 100, 13321-13332, 1995.

[16] Bukata, R.P., J.H. Jerome, K.Y. Kondratyev, and D.V. Pozdnyakov, Optical Properties and Remote Sensing of Inland and Coastal Waters, CRC Press, Boca Raton, FL, 1995.

[17] Stramski, D., A. Bricaud, and A. Morel, Modeling the inherent optical properties of the ocean based on the detailed composition of the planktonic community, Applied Optics, 40, 2929-2945, 2001.

[18] Roesler, C.S., and E. Boss, Spectral beam attenuation coefficient retrieved from ocean color inversion, Geophys. Res. Lett., 30 (9), 1468, 2003.

Chapter 5

[1] Siegel D. A., M. Wang, S. Maritorena, and W. Robinson, "Atmospheric Correction of Satellite Ocean Color Imagery: The Black Pixel Assumption," Appl. Opt. 39, 3582-3591 (2000)

[2] Stumpf, R. P., R. A. Arnone, R. W. Gould, P. M. Martinolich, and V. Ransibrahmanakul (2003), A Partially Coupled Ocean-Atmosphere Model for Retrieval of Water-Leaving Radiance From SeaWiFS in Coastal Waters, SeaWiFS Postlaunch Tech. Rep. Ser., vol. 22, NASA Tech. Memo. 2003-206892, edited by S. B. Hooker and E. R. Firestone, pp. 51– 59, NASA Goddard Space Flight Cent., Greenbelt, Md.

[3] Wang, M., 2002, The Rayleigh lookup tables for the SeaWiFS data processing: Accounting for the effects of ocean surface roughness. International Journal Remote Sensing, 23, 2693–2702.

[4] Wang M. and W. Shi "Estimation of ocean contribution at the MODIS near-infrared wavelengths along the east coast of the U.S.: Two case studies" Geophys. Res. Lett, 32, L13606, doi:10.1029/2005GL022917, (2005)

[5] Franz, B.A., P.J. Werdell, G. Meister, E.J. Kwiatkowska, S.W. Bailey, Z. Ahmad, and C.R. McClain (2006). MODIS Land Bands for Ocean Remote Sensing Applications, Proc. Ocean Optics XVIII, Montreal, Canada, 9-13 October 2006.

Chapter 6

[1] GORDON, H. R., and WANG, M., 1994, Retrieval of water-leaving radiance and aerosol optical thickness over the oceans with SeaWiFS: A preliminary algorithm. Applied Optics, 33, 443–452.

[2] Stumpf, R. P., R. A. Arnone, R. W. Gould, P. M. Martinolich, and V. Ransibrahmanakul (2003), A Partially Coupled Ocean-Atmosphere Model for Retrieval of Water-Leaving Radiance From SeaWiFS in Coastal Waters, SeaWiFS Postlaunch Tech. Rep. Ser., vol. 22, NASA Tech. Memo. 2003-206892, edited by S. B. Hooker and E. R. Firestone, pp. 51– 59, NASA Goddard Space Flight Cent., Greenbelt, Md.

[3] Wang, M., and W. Shi (2005), Estimation of ocean contribution at the MODIS near-infrared wavelengths along the east coast of the U.S.: Two case studies, Geophys. Res. Lett., 32, L13606, doi:10.1029/2005GL022917

[4] Franz, B.A., P.J. Werdell, G. Meister, E.J. Kwiatkowska, S.W. Bailey, Z. Ahmad, and C.R. McClain (2006). MODIS Land Bands for Ocean Remote Sensing Applications, Proc. Ocean Optics XVIII, Montreal, Canada, 9-13 October 2006.

[5] P. F. Levelt, E.Hilsenrath, G. W. L. Gijsbertus H. J. van den Oord, P.n K. Bhartia, J.Tamminen, J. F. de Haan, and J. P. Veefkind, "Science Objectives of the Ozone Monitoring Instrument", IEEE Transactions Geoscience and Rem. Sens. 44, 1199-1208 (2006)

[6] Werdell, P.J. and S.W. Bailey, 2005: An improved in situ data set for bio-optical algorithm development and ocean color satellite validation. Remote Sensing of Environment, 98 , 122-140.

[7] NASA bio-Optical Marine Algorithm Dataset (NOMAD)
http://seabass.gsfc.nasa.gov/cgi-bin/nomad.cgi

[8] Wang, M., K. D. Knobelspiesse, and C. R. McClain (2005), Study of the Sea-Viewing Wide Field-of-View Sensor (SeaWiFS) aerosol optical property data over ocean in combination with the ocean color products, J. Geophys. Res., 110, D10S06, doi:10.1029/2004JD004950.

[9] Shettle, E. P., and R. W. Fenn (1979), Models for the aerosols of the lower atmosphere and the effects of humidity variations on their optical properties, Rep. AFGL-TR-79-0214, U.S. Air Force Geophys. Lab., Hanscom AFB, Mass.

[10] Omar, A. H., J. G. Won, et al. "Development of global aerosol models using cluster analysis of Aerosol Robotic Networrk (AERONET) measurements." JGR-Atmos. 110 (2005)

[11] Lyapustin, A. I. "Radiative transfer code SHARM for atmospheric and terrestrial applications," Appl. Opt. 44, 7764-7772 (2005)

[12] Earth Probe Total Ozone Mapping Spectrometer (TOMS) Data Products User's Guide. NASA Technical Publication 1998-206895.
ftp://toms.gsfc.nasa.gov/pub/eptoms/EARTHPROBE_USERGUIDE.PDF

[13] IOCCG Report Number 1, (1998). Minimum Requirements for an Operational, Ocean-Colour Sensor for the Open Ocean. Published by the International Ocean-Colour Coordinating Group (IOCCG)
[14] L A. Remer, D. Tanre and Y. Kaufman, “Algorithm For Remote Sensing Of Tropospheric Aerosol From Modis: Collection 5” ATBD-02 Document
http://modis.gsfc.nasa.gov/data/atbd/atbd_mod02.pdf

[15] Werdell, P.J., and S.W. Bailey, 2002: The SeaWiFS Bio-optical Archive and Storage System (SeaBASS): Current architecture and implementation. NASA Tech. Memo. 2002-211617 , G.S. Fargion and C.R. McClain, Eds., NASA Goddard Space Flight Center, Greenbelt, Maryland, 45 pp.

Chapter 7

[1] Wang, M. (2000), The SeaWiFS Atmospheric Correction Algorithm Updates, SeaWiFS Postlaunch Tech. Rep. Ser., vol. 9, NASA Tech. Memo. 2000-206892, edited by S. B. Hooker and E. R. Firestone, pp. 57–63, NASA Goddard Space Flight Cent., Greenbelt, MD.

[2] Ransibrahmanakul, V. and R. P. Stumpf, 'Correcting ocean colour reflectance for absorbing aerosols", International Journal of Remote Sensing , 27, 1759 - 1774 , 2006

[3] Gordon,H.R., BROWN,O.B. and JACOBS,M.M., 1975, Computed relationships between the inherent and apparent optical properties of a flat homogeneous ocean. Applied Optics, 14**,** pp. 417-427.

[4] CHEN, C., SHI, P. and ZHAN,H., 2003, A local algorithm for estimation of yellow substance (gelbstoff) in coastal waters from SeaWiFS data: Pearl River estuary, China. International Journal of Remote Sensing, 24, pp. 1171-1176.

[5] POPE, R.M. and FRY, E.S., 1997, Absorption spectrum (380-700nm) of pure water, II, integrating cavity measurements. Applied Optics, 36, pp. 8710-8723.

[6] CARDER, K. L., CHEN, F.R. and CANNIZZARO, J.P., 2002, MODIS Algorithm Theoretical Basis Documents (Ocean), ATBD-MOD-19:Case 2 Chlorophyll_a algorithm and Case 2 Absorption Coefficient Algorithm, http://modis.gsfc.nasa.gov/data/atbd/ ocean_atbd.html, Vers. 6.

[7] GOULD, R.W., ARNONE, R. A. and MARTINOLICH, P.M., 1999, Spectral dependence of the scattering coefficient in Case-1 and Case-2 waters. Applied Optics, 38, pp. 2377-2383.

[8] BRICAUD, A., MOREL, A. and PREUR,L., 1981, Absorption by dissolved organic matter in the sea (yellow substance) in the UV and visible domains. Limnology and Oceanography, 26, pp. 43-53.